

## **INFORMATION TO USERS**

**This manuscript has been reproduced from the microfilm master. UMI films the text directly from the original or copy submitted. Thus, some thesis and dissertation copies are in typewriter face, while others may be from any type of computer printer.**

**The quality of this reproduction is dependent upon the quality of the copy submitted. Broken or indistinct print, colored or poor quality illustrations and photographs, print bleedthrough, substandard margins, and improper alignment can adversely affect reproduction.**

**In the unlikely event that the author did not send UMI a complete manuscript and there are missing pages, these will be noted. Also, if unauthorized copyright material had to be removed, a note will indicate the deletion.**

**Oversize materials (e.g., maps, drawings, charts) are reproduced by sectioning the original, beginning at the upper left-hand corner and continuing from left to right in equal sections with small overlaps.**

**Photographs included in the original manuscript have been reproduced xerographically in this copy. Higher quality 6" x 9" black and white photographic prints are available for any photographs or illustrations appearing in this copy for an additional charge. Contact UMI directly to order.**

**ProQuest Information and Learning  
300 North Zeeb Road, Ann Arbor, MI 48106-1346 USA  
800-521-0600**

**UMI<sup>®</sup>**



**SEAFLOOR GEOLOGY, DEGLACIAL HISTORY, AND EARLY POST-  
GLACIAL EVOLUTION OF EASTERN JUAN DE FUCA STRAIT**

**BY**

**ANTONY T. HEWITT**

**B.Sc. University of Victoria, 1994**

**M.Sc. University of Victoria, 1996**

**Submitted to the University of New Hampshire**

**in Partial Fulfillment of**

**the Requirements for the Degree of**

**Doctor of Philosophy**

**in**

**Earth Science**

**May, 2002**

**UMI Number: 3045326**

**UMI<sup>®</sup>**

---

**UMI Microform 3045326**

**Copyright 2002 by ProQuest Information and Learning Company.**

**All rights reserved. This microform edition is protected against  
unauthorized copying under Title 17, United States Code.**

---

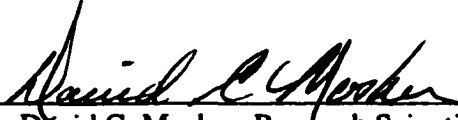
**ProQuest Information and Learning Company  
300 North Zeeb Road  
P.O. Box 1346  
Ann Arbor, MI 48106-1346**

**Ph.D. DISSERTATION**

This dissertation has been examined and approved.



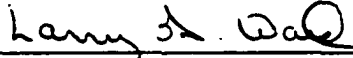
Dissertation Director, Dr. Larry A. Mayer, Professor, Ocean  
Engineering/Earth Sciences, UNH



Dr. David C. Mosher, Research Scientist, Geological Survey of Canada



Dr. Francis S. Birch, Professor, Earth Sciences, UNH



Dr. Larry G. Ward, Associate Research Professor, Earth Sciences, UNH



Dr. James V. Gardner, Senior Research Geologist, United States  
Geological Survey

April 03, 2002  
Date

## **ACKNOWLEDGEMENTS**

This research was supported by the United States Geological Survey (USGS) National Earthquake Hazards Reduction Program (NEHRP), Department of the Interior, under USGS award number 1434-HQ-96-GR-02726, and by the Geological Survey of Canada (GSC). The author also received support from the National Oceanic and Atmospheric Administration (NOAA) of the United States through its sponsorship of the Center for Coastal and Ocean Mapping at the University of New Hampshire (NOAA award number NA97OG0241 and CICEET award number NA07OR0351). The efforts of the officers, crew and scientific support staff of CCGS vessels, *John P. Tully*, *Revisor*, and *R. B. Young* are greatly appreciated. The author also wishes to thank Kim Conway for arranging the radiocarbon dating, Robert Kung for assistance with some of the maps, Glenda Rathwell for conducting the grain-size analyses, and Seismic Micro-technology, Inc., for their generous loan of the Kingdom Suite 2D/3D PAK seismic processing and interpretation software package.

## TABLE OF CONTENTS

AKNOWLEDGEMENTS .....	iii
LIST OF TABLES .....	vii
LIST OF FIGURES .....	viii
ABSTRACT .....	x

CHAPTER	PAGE
I. INTRODUCTION .....	1
Geologic Setting .....	4
Glacial History .....	5
Sealevel History .....	7
II. METHODS .....	10
Seismic Data .....	10
Bathymetric Data .....	12
Sediment Cores .....	13
III. BATHYMETRY AND GEOMORPHOLOGY .....	18
Bathymetric Data .....	18
Geomorphology .....	27
IV. SEISMIC STRATIGRAPHY .....	39
Unit 1 .....	39
Unit 2 .....	43

Unit 3 .....	43
Unit 4 .....	53
Unconformities .....	54
Climoform Units .....	59
<b>V. LITHOSTRATIGRAPHY, SEDIMENTOLOGY, AND</b>	
<b>DISTRIBUTION OF NEAR-SURFACE GEOLOGIC UNITS .....</b>	<b>65</b>
Correlation of Cores to Seismic-Reflection Data .....	65
Lithology, Physical Properties, and Age .....	66
Units 1 and 2 .....	66
Unit 3 .....	66
Unit 4 .....	75
Distribution of Near-Surface Geologic Units .....	79
<b>VI. DISCUSSION .....</b>	<b>85</b>
Interpretation of Seismic-Geologic Units .....	85
Unit 1 .....	85
Unit 2 .....	85
Unit 3 .....	86
Unit 4 .....	89
Ice-Retreat History .....	91
Rate of Ice Retreat .....	95
Sealevel History .....	96
Erosional Unconformities .....	96
Climoform Units .....	102



Drowned Spits.....	104
Partially Isolated Low-Stand Basin.....	105
Drowned Fluvial Features .....	106
Sealevel Curve and Rates of Sealevel Change.....	110
VII.    SUMMARY AND CONCLUSIONS .....	117
REFERENCES .....	120
APPENDIX: ADDITIONAL PHYSICAL PROPERTIES BACKGROUND .....	129

## **LIST OF TABLES**

<b>Table 1. Cores and their assignment to seismic-geologic units, and 14C dates.....</b>	<b>15</b>
<b>Table 2. Average physical properties in cores from the main seismic units.....</b>	<b>76</b>

## LIST OF FIGURES

Figure 1. The study area.....	2
Figure 2. Core locations, seismic and multibeam surveys, and figure locations.....	11
Figure 3. Relationship between raw dates and corrected ages.....	17
Figure 4. Schematic diagram of sonar sounding geometry.....	19
Figure 5. Sun illuminated bathymetry of eastern Juan de Fuca Strait.....	21
Figure 6. Coverage and density of singlebeam hydrographic soundings.....	23
Figure 7. EM3000 and EM1002 multibeam bathymetry off Victoria.....	24
Figure 8. EM3000 multibeam bathymetry at Rocks.....	25
Figure 9. Contour bathymetric map of the study area.....	28
Figure 10. EM3000 multibeam bathymetry of Esquimalt and Victoria Harbours.....	30
Figure 11. 3D view of EM3000 multibeam bathymetry off Esquimalt.....	31
Figure 12. EM3000 multibeam data showing giant dunes off Victoria.....	33
Figure 13. Submerged “spit-like” features along the Olympic Peninsula.....	34
Figure 14. Bathymetric profiles off the Olympic Peninsula.....	36
Figure 15. Singlebeam bathymetry from the northeast corner of the study area.....	37
Figure 16. Singlebeam bathymetry near the entrance to Admiralty Inlet.....	38
Figure 17. Hunttec boomer profiles showing seismic-acoustic units.....	40
Figure 18. Airgun profile showing seismic-acoustic units.....	41
Figure 19. Airgun profile through McArthur and Lawson Banks.....	42
Figure 20. Hunttec boomer profile showing units 3a and 2.....	44
Figure 21. Hunttec boomer profile showing unit 3b and 2.....	45
Figure 22. Airgun profile near Constance Bank.....	46
Figure 23. Airgun profile through Eastern Bank.....	47
Figure 24. Airgun profile through Partridge Bank.....	49
Figure 25. Airgun profile through the unnamed bank.....	50
Figure 26. Airgun profile through Middle Bank.....	51
Figure 27. Airgun profile through Dallas Bank.....	52
Figure 28. Hunttec boomer profile showing unit4a, 3a, and 2.....	55
Figure 29. Seistec boomer profile showing terraces near Victoria.....	56
Figure 30. Hunttec boomer profile through the giant dunes off Victoria.....	57
Figure 31. Hunttec boomer profiles showing and unconformity in unit 3a.....	58
Figure 32. Airgun profile off Green Point.....	62
Figure 33. Airgun profile near Admiralty Inlet.....	63
Figure 34. Airgun profile near Admiralty Inlet.....	64
Figure 35. Average grain-size in the various geologic units.....	67
Figure 36. Core TUL96-12 and corresponding Hunttec profile.....	68
Figure 37. Core TUL96-08 and corresponding Hunttec profile.....	69
Figure 38. Core TUL96-09 and corresponding Hunttec profile.....	70
Figure 39. Core TUL97-16 and corresponding Hunttec profile.....	71
Figure 40. Core TUL96-07 and corresponding Hunttec profile.....	72
Figure 41. Core TUL96-02 and corresponding Hunttec profile.....	74
Figure 42. Core TUL96-04 and corresponding Hunttec profile.....	77
Figure 43. Core TUL97-12 and corresponding Hunttec profile.....	78
Figure 44. Seafloor geology in eastern Juan de Fuca Strait.....	80

Figure 45. Seafloor geology in the area of multibeam coverage off Victoria .....	82
Figure 46. Seafloor geology in the area of multibeam coverage off Race Rocks .....	84
Figure 47. Proposed stages during ice retreat and subsequent sealevel changes .....	92
Figure 48. The unconformity of Esquimalt Harbour .....	98
Figure 49. Cores that penetrate the unconformity off Victoria .....	99
Figure 50. Cores and a Huntex profile form a basin near Whidbey Island .....	107
Figure 51. Airgun profile through submerged river channel .....	109
Figure 52. Relative sealevel curve for eastern Juan de Fuca Strait .....	111
Figure 53. Two extreme stages of post-glacial sealevel in the study area .....	114

## **ABSTRACT**

### **SEAFLOOR GEOLOGY, DEGLACIAL HISTORY, AND EARLY POST-GLACIAL EVOLUTION OF EASTERN JUAN DE FUCA STRAIT**

by

**Antony T. Hewitt**

**University of New Hampshire, May, 2002**

Seismic-reflection data, bathymetric data, and sediment cores were used to map the seafloor geology of eastern Juan de Fuca Strait, and interpret the stratigraphy in terms of the latest deglacial episode and associated sealevel change. The surficial geologic units comprise bedrock (unit 1), ice-contact diamicton (unit 2), glacial-marine sediments (unit 3), and post-glacial sediments (unit 4). Bedrock crops out near Vancouver Island, and diamicton crops out in the numerous morainal banks. A series of banks running roughly north-south in the middle of the strait divides it into two areas based on the main surficial units; post-glacial sediments dominate to the east and glacial-marine sediments to the west. Subunits within the glacial-marine sediments suggest progression from an ice-proximal to ice-distal depositional environment during glacier retreat. There is currently little sediment input to the strait, so most modern sediments consist of reworked glacial deposits that occur in banks and coastal exposures.

The strait was deglaciated rapidly; in about 100 years at a rate of 475 m/yr. Ice retreat was probably episodic, however, with times of rapid calving retreat separated by periods when retreat paused on morainal banks.

After the period of maximum marine submergence following deglaciation, isostatic rebound caused relative sealevel to fall to a level lower than present. A number of drowned features indicate sealevel fell to 55 m below present sealevel (-55 m) by 11,280 yr B.P., then reached the low stand maximum of around -60 m by 10,720 yr B.P. During regression, sealevel fell 150.4 m at an average rate of 59.0 mm/yr; meanwhile the eustatic rise was 37.3 m, yielding an average rate of crustal uplift of 73.6 mm/yr. During the subsequent transgression, sealevel rose to a depth of -55 m by 10,630 yr B.P., then a depth of -44 m by 9,880 yr B.P., and -33 m by 8,910 yr B.P. by 10,700 yr B.P. most isostatic adjustment was complete and eustatic rise dominated, resulting in a gradual transgression toward the present. Relative sealevel rose 60.4 m during transgression at 5.6 mm/yr, while the eustatic sealevel rise was 61.4 m, giving an average rate of crustal uplift of less than 1 mm/yr.

## **CHAPTER I**

### **INTRODUCTION**

Juan de Fuca Strait is the principal marine connection between the Pacific Ocean and inner shelf waters of southern British Columbia and Washington (Fig. 1), and is a major international shipping route to two large cities, Vancouver and Seattle, and several smaller settlements situated around the borders of the Strait. A growing population and expanding industry and tourism in both countries will increase pressure on the Strait's usage. It has become increasingly important, therefore, to monitor the natural environment, including the seafloor geology. Knowledge of the geology is required for proper environmental protection and management of offshore resources, including potential mineral deposits (e.g. aggregate), fish habitat, and installation of offshore cables and pipelines. Seismicity along crustal faults may pose a significant hazard, especially since earthquakes in the marine environment can generate tsunamis, impacting coastal communities and facilities.

There have been few previous investigations into the seafloor geology of Juan de Fuca Strait (Anderson, 1968; Mayers and Bennet, 1973; Linden and Schurrer, 1988; Dethier, et al, 1995). This is the first to focus on the eastern portion of the strait (Fig. 1). The study area will henceforth be referred to as eastern Juan de Fuca Strait. The objective is to map the seafloor geology and study the stratigraphy in order to understand the deglacial and sealevel history. The main near-surface geologic units will be characterized in terms of their seismic-reflection character, lithology, physical properties,

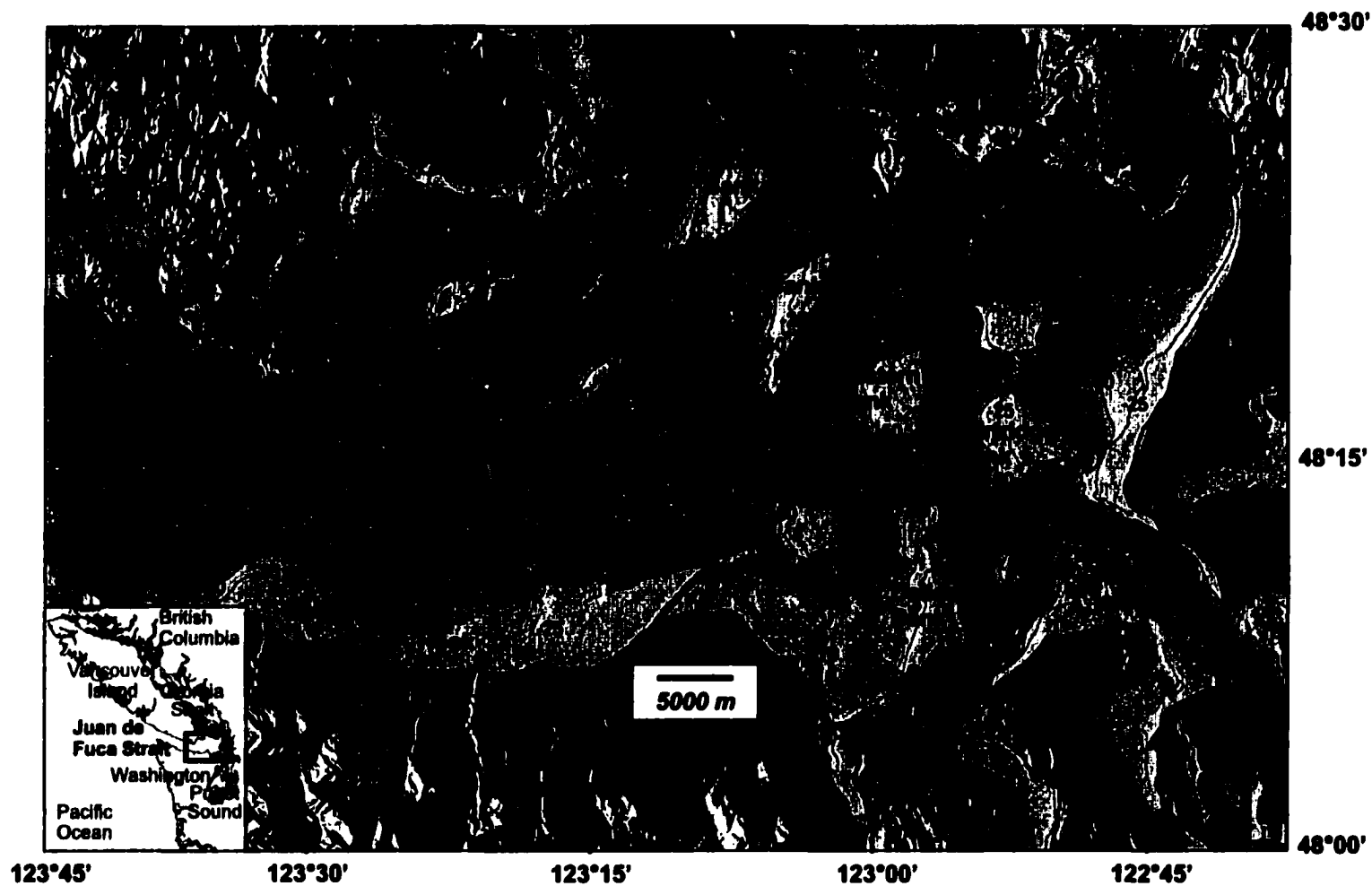


**Figure 1.** Map of the study area in eastern Juan de Fuca strait, showing places referred to in the text. Selected topographic and bathymetric contours are in meters. The study area is about 80 km west-east, and 55 km north-south.



age, and then the distribution of these units will be mapped based on high-resolution seismic-reflection records and bathymetric data. The mapping effort, along with new radiocarbon dates, will complement interpretation of the late Pleistocene sequence stratigraphy and lateral facies relationships (system tracks) in order to understand the latest glacial and deglacial episode and subsequent sealevel change.

Juan de Fuca Strait was the main conduit to the Pacific for late Pleistocene glaciers flowing from the mainland in southern British Columbia and Washington, but compared with surrounding land areas and Puget Sound, details of the straits deglacial history were less well known, including its complex post-glacial sealevel history. In particular, the magnitude and age of the low stand is a missing control point critical in establishing an accurate sealevel history for this region, and separating the eustatic, isostatic, and neotectonic contributions to sealevel change. Obtaining this information about the low stand bares directly on assessment of the seismic hazard in southern British Columbia and Washington State. The eastern strait was deeply buried by ice during the last glaciation, and once ice retreated, some of the isostatic readjustment would have occurred along crustal faults as earthquakes. In the marine environment, such earthquakes have the potential to be particularly destructive because of the danger of tsunamis. Earthquake frequency was probably greater during the early Holocene than at present, as this is when most of the isostatic adjustment occurred (Thorson, 1996). In order to use the geologic record of past earthquakes as an indication of future frequency requires knowledge of when the crust had recovered from ice loading. The elevation and timing of high and low sealevel stands is also important, since this allows quantification

of the total amount and rates of vertical motion, both critical parameters in models of crustal dynamics.

### **Geologic Setting**

Juan de Fuca Strait lies within the structurally complex continental margin of the Pacific Northwest, where subduction of the Juan de Fuca Plate occurs beneath North America. Within this setting, the strait is part of a linear topographic depression (Puget Sound, Eastern Juan de Fuca Strait, and Georgia Strait) bounded by Vancouver Island and the Olympic Mountains to the west and the Cascade Range volcanic arc to the east. Juan de Fuca Strait has been a marine embayment since its formation, a result of crustal compression and folding during the Eocene (Mayers and Bennet, 1973). Since then, tectonic processes, igneous intrusion, erosion, and deposition of clastic sediments have modified its morphology. The regional geology has been summarized by Johnson *et al.* (2001b), but in brief, the pre-Quaternary geology consists of pre-Tertiary meta-sediments and igneous rocks, middle-Eocene submarine volcanics, Oligocene and Pliocene nearshore marine sedimentary rocks, and Eocene-Oligocene gabbros. The strait occurs over a major northwest-trending crustal boundary between basement rocks of the pre-Tertiary Cascades province to the northeast and the Eocene Coast Range province to the southwest. The province southwest of this boundary is part of a forearc sliver consisting of Eocene volcanic basement and overlying sedimentary rocks. Major crustal faults trending through the study area include the Southern Whidbey Island fault, the Leech River fault, and the Devils Mountain Fault. These faults are potentially active (Mosher *et al.*, 1997; Johnson *et al.*, 2001a).

The bathymetry of the strait is quite variable as a result of the many shallow banks and intervening deep troughs. These were formed from glacial erosion and deposition during the late Quaternary, when the strait was occupied several times by lobes of continental ice. The Quaternary sequence consists of glacial and interglacial deposits that are locally as thick as 1,100 m (Johnson *et al.*, 2001c). The uppermost section of the sequence is the product of retreating glaciers of the last glaciaton, which left a thick sequence of ice-contact and glacial-marine sediments. Previous investigations of these sediments in the western strait (Anderson, 1968; Mayers and Bennet, 1973), in the approaches to Esquimalt Harbour (Linden and Schurrer, 1988), and on Whidbey Island (Domack, 1983), each identified similar lithologic units: post-glacial mud and sand overlying one or more units of glacial-marine mud. The glacial-marine sediments, in turn, overlie either ice contact sediments of the last glaciation, or in rare cases when this is absent, older Quaternary sediments or pre-Quaternary basement rocks. Currently, there are only a few small rivers flowing into eastern Juan de Fuca Strait. As a consequence, there is relatively little modern-day sediment input.

### **Glacial History**

During the Pleistocene, eastern Juan de Fuca Strait was occupied several times by lobes of continental ice. Blunt *et al.* (1987) and Easterbrook (1992, 1994) described several distinct glacial drift units on land. These units comprise till, outwash, and glaciomarine deposits of the Double Bluff and Westlynn Drifts (~250,000-120,000 yr B.P.), and the Possession, Semiahoo, and Dashwood Drifts (~80,000-60,000 yr B.P.). Associated interglacial strata deposited in fluvial environments include the Whidbey and

Muir Point Formations (~120,000-80,000 yr B.P.) and the Olympia beds and Cowichan Head Formation (~60,000-30,000 yr B.P.).

Late Wisconsinan (Marine Isotope Stage 2) glaciation, known locally as the Fraser Stade glaciation, began after  $28,800 \pm 740$   $^{14}\text{C}$  yr B.P. (GSC-95) in British Columbia (Clague., 1981), when alpine glaciers advanced down mountain valleys and coalesced in the northern Strait of Georgia. From there, the ice cap began a slow southward expansion, reaching the vicinity of Victoria on Vancouver Island by 22,600  $^{14}\text{C}$  yr B.P. (Clague *et al.*, 1980), where the advance stalled and large quantities of proglacial outwash were deposited (Clague, 1977). After  $16,000 \pm 180$  to  $16,100 \pm 150$   $^{14}\text{C}$  yr B.P. (GSC-4355 and GSC-4363; Clague *et al.*, 1988), the Vashon stade began and ice advanced westward and southward as the Juan de Fuca and Puget Lobes, respectively (Armstrong *et al.*, 1965; Mullineaux *et al.*, 1965; Armstrong and Clague, 1977; Hicock *et al.*, 1982; Easterbrook, 1992; Porter and Swanson, 1998). Ice reached the northern Puget Lowland ( $48^\circ\text{N}$ ) at around 15,000  $^{14}\text{C}$  yr B.P. (several dates in Porter and Swanson, 1998). There are no dates closely constraining the time when ice was at its terminal position in the Puget Lowland, but based on the average advance rate, it arrived at its terminal position at about 14,150  $^{14}\text{C}$  yr B.P. (Porter and Swanson, 1998). The Juan de Fuca Lobe reached the shelf edge through Juan de Fuca Strait (Herzer and Bornhold, 1982) shortly before  $14,460 \pm 200$   $^{14}\text{C}$  yr B.P. (Y-2452; Huesser, 1973). Estimates of ice thickness at the glacial maximum are 1500 m near Victoria, 800 m at the western end of the Juan de Fuca Strait, and 1000 m near Seattle (Alley and Chatwin, 1979; Thorson, 1989).

The Puget Lobe probably remained at its maximum limit for 100 years or so before it began retreating (Porter and Swanson, 1998). By  $13,600 \pm 280$  to  $13,700 \pm 150$   $^{14}\text{C}$  yr B.P. (QL-4065 and QL-4067), it had receded to a position near Seattle (Porter and Swanson, 1998). Deglaciation of the Juan de Fuca Lobe is not nearly so well known, but it seems to have begun around  $14,460 \pm 200$   $^{14}\text{C}$  yr B.P. (Y-2452; Huessner, 1973) and retreated rapidly, reaching Whidbey Island by  $13,595 \pm 145$   $^{14}\text{C}$  yr B.P. (Dethier *et al.*, 1995). When the retreating Juan de Fuca Lobe reached Admiralty Inlet, ice blocking the entrance to Puget Sound was removed, allowing marine incursion and accelerated destruction of the remainder of the Puget Lobe (Thorson, 1980). At approximately the same time that the Puget Lowlands and adjacent areas were inundated, glaciers calved rapidly northward toward the San Juan Islands and had receded to the international boundary, north of the study area, by  $13,000$   $^{14}\text{C}$  yr B.P. (Armstrong, 1981).

### **Sealevel History**

In eastern Juan de Fuca Strait, the relationship between glacio-isostatic depression, postglacial rebound, and eustatic sealevel change is complex, and likely further complicated by neotectonic activity. The region has undergone two transgressions separated by a regression since the last deglaciation. Evidence for high stands is found in land exposures of former marine sediments deposited when the crust was still isostatically depressed shortly after ice retreated. The marine limit during the initial transgression appears to have been fairly uniform from west to east, but increases northward from +50 m along the Olympic Peninsula to +90 m near Victoria (Dethier *et al.*, 1995; Huntley *et al.*, 2001); a result of the thicker ice cover in the north. The period

of maximum submergence in the Victoria area, of +90 m, occurred at  $13,270 \pm 60$   $^{14}\text{C}$  yr B.P. (Huntley *et al.*, 2001). Isostatic rebound then caused sealevels to fall, eventually reaching a level the same as today at  $11,700 \pm 170$   $^{14}\text{C}$  yr B.P. (I-3675; Clague *et al.*, 1982), but sealevel continued to fall since eustatic sealevel was still lower than present, resulting in emergence of areas now underwater.

Near Ediz Hook, submerged shoreline features have been observed at -30 m (U.S. Army Corps of Engineers, 1976), and on southern Vancouver Island, there are many features that suggest at least 10-15 m lowering. These features are discussed in Mathews *et al.* (1970) and Clague *et al.* (1982), and summarized below:

1. Subaerially leached shells and oxidized marine sediments in Esquimalt Harbor at -9 m.
2. Drowned post-glacial river mouth at Ladysmith 80 km north of Victoria at -10m.
3. Drowned post-glacial river mouths at Metchosin 25 km west of Victoria at -10 m.
4. Unconformities and wave-cut terraces formed below the modern level of wave erosion are seen in seismic-reflection profiles at -9 to -15 m in numerous bays and inlets on southern Vancouver Island.

There are no dates from the above features, and previous to this study, there are only a few published dates that constrain sealevel in the area. In Portage Inlet, Victoria, a peat layer at -6.1 m is found between marine sediments. The sequence consists of

glacial-marine clay grading upward into glacial-lacustrine clays, overlain by peat, then marine sediments of non-glacial origin. The glacial lacustrine clay dates to  $11,700 \pm 170$   $^{14}\text{C}$  yr B.P. (I-3675). Dates within the peat layer are  $9250 \pm 140$   $^{14}\text{C}$  yr B.P. (I-3676) near its base and  $5470 \pm 115$   $^{14}\text{C}$  yr B.P. (I-3673) near the top, suggesting Portage Inlet was subareal between these dates. Eustatic rise eventually submerged Portage Inlet again after  $5470 \pm 120$   $^{14}\text{C}$  yr B.P. as sealevel rose toward the present level (Clague *et al.*, 1982). Oceanographic conditions and a depositional environment similar to the present were probably established by this time throughout the strait.

The evidence discussed above does not unequivocally indicate the greatest depth of the low stand, for which the only evidence was (before this report) an erosional unconformity in glacial-marine sediments off Esquimalt that was traced to a depth of -55 m, and dated between  $9670 \pm 140$   $^{14}\text{C}$  yr B.P. and  $10,650 \pm 230$   $^{14}\text{C}$  yr B.P. (RIDDL-265 and RIDDL-258, respectively; Linden and Schurrer, 1988). It was suggested this unconformity is a result of shallow water erosion (Linden and Schurrer, 1988), but without supporting evidence for the regional continuity of the unconformity, the claim for a low stand of this magnitude has not been accepted, generally. The magnitude and age of this low stand is a critical control point in establishing an accurate sealevel history for this region, and for separating the eustatic, isostatic, and neotectonic contributions to sealevel change.

## **CHAPTER II**

### **METHODS**

#### **Seismic Data**

High-resolution seismic-reflection profiles were collected using Hunttec and IKB™ Seistec boomer systems (Hutchins *et al.*, 1976; Simpkin and Davis, 1993), and an airgun single-channel system described in Mosher *et al.* (1998). A total of 2169 km of Hunttec profiles were collected in 1996 and 1997 (Mosher and Johnson, 2001), and several hundred kilometers of Seistec data were collected along the Victoria waterfront (Mosher and Bornhold, 1995). During the 1997 survey, around 800 km of single-channel airgun seismic-reflection data were simultaneously collected with Hunttec boomer operations. Survey track-lines are shown in Figure 2.

The Hunttec system uses a deep-towed boomer source with a frequency bandwidth of 0.5 to 6.0 kHz. The Hunttec tow fish contains an internal receiving array designed for acquiring high frequencies and yields a vertical resolution of about 0.10 m. The system also was fitted with a 20-element external receiving array, which, through channel summation, has a higher signal to noise ratio for lower frequencies and, therefore, yields better subbottom penetration, but poorer resolution (approximately 0.25 m). The Seistec system uses a surface-towed boomer source with a frequency bandwidth of 1.0 to 10.0 kHz and an internal receiving array that can resolve layering to better than 0.10 m. The single-channel source employed two 1.64 L (10 in<sup>3</sup>) airguns suspended in a frame, 0.5 m apart and towed at a depth of 0.5 m, 15 m behind the ship. The source frequency



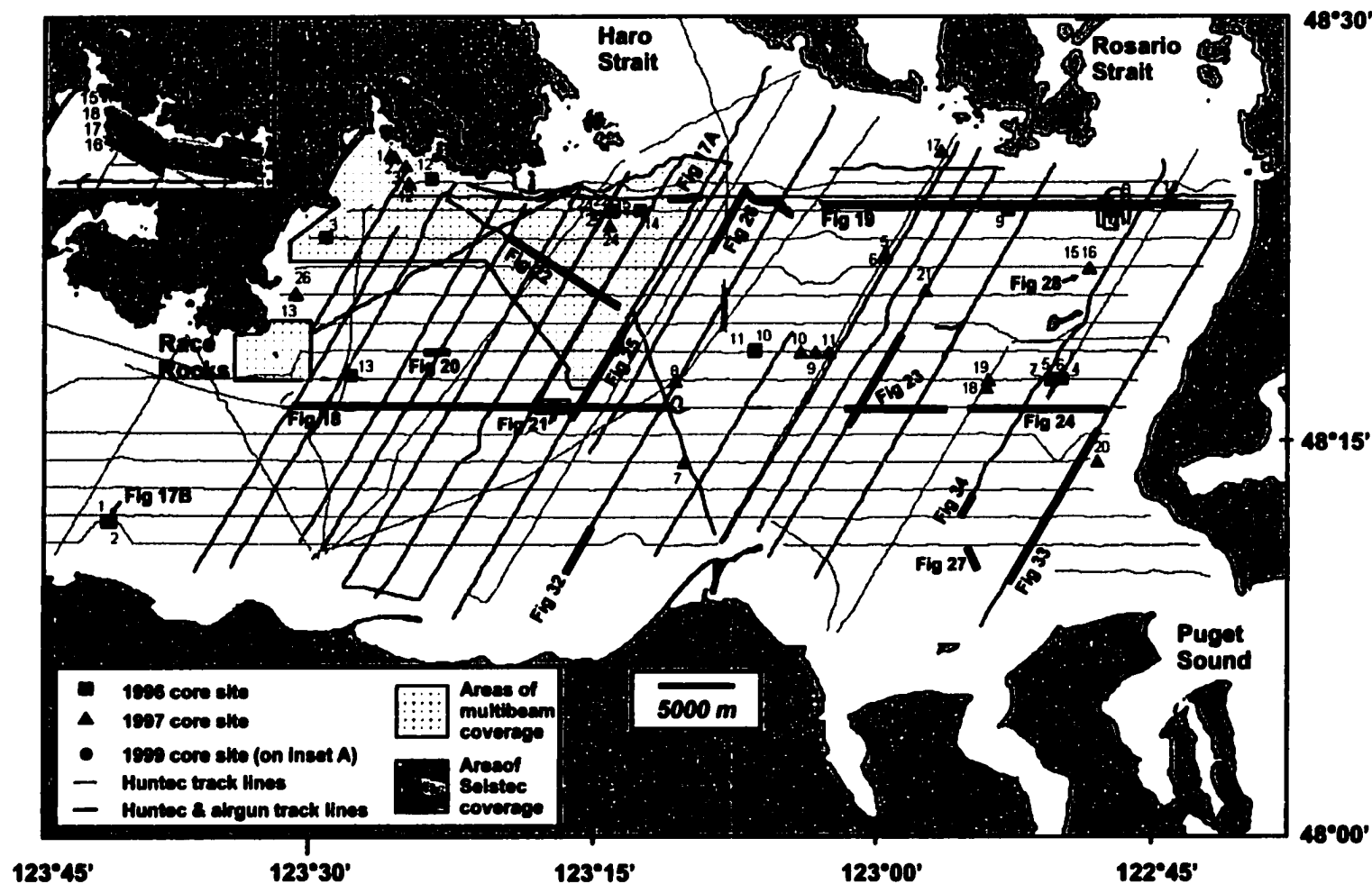


Figure 2. Core locations, seismic survey tracklines, and location of multibeam sonar surveys in the study area. The small inset maps in the left corner indicates the location of the 1999 cores and the area where Seistec data was collected. The location of selected figures are indicated by thick lines.

spectrum spans 1.4 kHz. Two different streamer receiving arrays were used: (1) A Benthos array, having 50 hydrophones with 0.15 m spacing, towed just below the surface, 30 m behind the ship; and (2), a Teledyne array, having 25 hydrophones separated by 1 m, towed at 3-m depth, 50 m behind the ship. The two receiving arrays provide different imaging characteristics. The Benthos array is designed for high frequency acquisition. The Teledyne array is longer, sums more channels, and is designed to acquire lower frequencies and image deeper into the subsurface. Seismic profiles imaged from the data acquired with the Benthos array proved the most useful, although in some profiles prominent water-bottom multiples obscure subsurface details. Vertical resolution with the Benthos array is better than 0.5 m.

Seismic data were processed and imaged using Kingdom Suite 2D/3D PAK from Seismic-Microtechnology, Inc. On seismic imagery, depths to seafloor are from bathymetric data, and depths to sub-seafloor reflections are based on measurements of average sound velocity in the sediment (see following section on sediments cores), or where these measurements are unavailable, a velocity of 1500 m/s was assumed. All depths are expressed in meters below present sealevel.

### **Bathymetric Data**

Over 600,000 single-beam bathymetry soundings were provided by the Canadian Hydrographic Service (CHS) and National Oceanic and Atmospheric Administration (NOAA) of the United States. In addition, several multibeam sonar surveys were conducted off southern Vancouver Island using Simrad EM3000 and EM1002 systems. The surveys were conducted by the CHS, the Geological Survey of Canada, and the

Department of National Defense. The EM3000 is mounted on the *H/V Revisor*, and the EM1002 is mounted on the CCGS *R.B. Young*. The EM3000 is a high frequency (300 kHz) system designed for mapping in shallow water (< 150 m). It has 127 beams per ping in an angular sector of up to 130 degrees, and can map a swath as wide as 4 times the water depth. The EM1002 operates at frequencies of 98 kHz for the inner swath (nadir  $\pm 50^\circ$ ) and 93 kHz for the outer swath ( $> 50^\circ$ ), and is designed for mapping in water up to 1000-m deep. It has 111 beams per ping in an angular sector of up to 150 degrees and is capable of mapping a swath of up to 7.5 times the water depth.

### **Sediment Cores**

Coring targets were selected to provide stratigraphic information and to investigate targets identified from seismic-reflection data. A total of 36 cores were collected using a Benthos™ piston corer or an Aymers-MacLean™ vibro-corer. Their locations are shown on Figure 2. After recovery, all cores were sealed and kept in refrigerated storage. Cores were later split, described and measured for the following physical properties: (1) particle grain-size was measured using a Sedigraph™ (X-ray absorption) for the fine fraction (<63  $\mu\text{m}$ ), and by settling tower (particle settling velocity) for the sand fraction (>63  $\mu\text{m}$  and <2 mm), and by sieve for grains larger than 2 mm. Samples for grain-size analysis were taken at intervals of ~20 cm in selected cores that are considered representative of the various seismic-geologic units; (2) magnetic susceptibility was measured at 5-cm intervals, using a 6-cm-wide, 10.5-cm diameter whole-core coil sensor from Sapphire Instruments™; (3), micro-resistivity was measured at an interval of 5 cm, with a 4-pin Wenner array probe. The pins were 4-mm long and

separated by 2 mm; (4) the velocity of sound in the sediment was measured with an IKB Technologies™ digital sound velocimeter that uses a pair of transducers, separated by ~7 cm and inserted longitudinally into the core. These data were acquired at an interval of 10 cm; (5) undrained shear strength was measured with a motorized Wykeham-Farrance™ miniature shear vane, at 20-cm intervals; (6) wet bulk density and dry bulk density were measured on constant volume samples (~10 cm<sup>3</sup>) at an interval of 10 cm. Additional information on physical properties measurements is given in Appendix A.

A total of 40 samples were removed from the cores, identified, and submitted to Laurence Livermore National Laboratory for AMS radiocarbon dating (Table 1). Marine Mollusc shells were used as the source of carbon, except in two instances where a piece of wood and a fish bone were used. If whole shells existed, they were selected for dating as they were more likely to represent an in situ, undisturbed sample. More typically, however, reworked shell fragments were all that were available. The ages reported in Table 1 are in radiocarbon years determined using the conventions of Stuiver and Polach (1977). To account for differences between atmospheric and ocean carbon reservoirs, there are two suitable corrections for marine shell dates from eastern Juan de Fuca Strait. Robinson and Thompson (1981) determined a reservoir correction of  $-801 \pm 23$  yr from samples collected in Sooke, and a correction of  $-798 \pm 50$  yr was determined for a single wood/shell pair from Saanich Inlet (Bornhold *et al.*, 1998). Since these two corrections are similar, the correction of  $801 \pm 23$  yr is adopted since it minimizes error. Reservoir corrected ages were converted to calendar years B.P. using CALIB 4.3 (Stuiver *et al.*, 1998) (Table 1; Figure 3).

Table 1. Cores, their assignment to seismic-geologic units (see text), and AMS radiocarbon dates along with their reservoir corrected and calendar age equivalents. Table is continued on following page.

Core Number	Longitude (o)	Latitude (o)	Water Depth (m)	Core Length (m)	Sample Number	Depth in core (cm)	Raw <sup>14</sup> C Age* (Yr-B.P.)	+/- Error (Yr-B.P.)	Corrected** <sup>14</sup> C Age (Yr-B.P.)	Calendar age range Max. - Min. (Yr-B.P.)	Material Dated	Unit
TUL96B-01	-122.67772	48.19557	131.0	1.21	-	-	-	-	-	-	-	4a
TUL96B-02	-123.67477	48.19542	137.5	1.64	-	-	-	-	-	-	-	3a/3b
TUL96B-03	-123.48792	48.36683	71.3	3.76	58672	20	1720	40	919	953 - 749	shell	4a
TUL96B-03	-123.48792	48.36683	71.3	3.76	58673	360	11900	50	11099	13158 - 12861	shell	3a
TUL96B-04	-122.83417	48.28350	118.9	3.63	58674	63	1190	40	389	502 - 328	shell	4a
TUL96B-04	-122.83417	48.28350	118.9	3.63	58675	319	8310	50	7509	846 - 8257	shell	4a
TUL96B-05	-122.83677	48.28313	120.7	5.83	58676	63	8580	40	7779	8883 - 8529	shell	4a
TUL96B-05	-122.83677	48.28313	120.7	5.83	58677	210	10630	50	9829	11591 - 10843	shell	4a
TUL96B-05	-122.83677	48.28313	120.7	5.83	58678	373	10780	50	9979	11698 - 10867	shell	4a
TUL96B-06	-122.83895	48.28305	122.5	5.65	58679	85	10690	50	9869	11625 - 10855	shell	4a
TUL96B-06	-122.83895	48.28305	122.5	5.65	58680	479	10930	50	10129	12074 - 10887	shell	4a
TUL96B-07	-122.84350	48.28283	124.4	3.47	58681	64	13390	60	12589	15523 - 14172	shell	3a
TUL96B-08	-122.78783	48.38317	82.0	4.03	-	-	-	-	-	-	-	4a
TUL96B-09	-122.88107	48.38343	93.0	3.70	-	-	-	-	-	-	-	4a
TUL96B-10	-123.10567	48.30013	87	0.19	-	-	-	-	-	-	-	4a
TUL96B-11	-123.10670	48.29973	88.0	0.26	-	-	-	-	-	-	-	4a
TUL96B-12	-123.39400	48.40133	64.8	2.03	-	-	-	-	-	-	-	4a
TUL96B-13	-123.46425	48.28478	158.0	0.10	-	-	-	-	-	-	-	3b
TUL96B-14	-123.20867	48.38333	72.0	2.04	-	-	-	-	-	-	-	3b
TUL96B-15	-123.23217	48.38283	97.0	0.10	-	-	-	-	-	-	-	4b
TUL97B-01	-123.42975	48.41652	36.1	2.63	-	-	-	-	-	-	-	4a
TUL97B-02	-123.42630	48.41535	41.7	2.36	58682	31	190	40	190	190	wood	4a
TUL97B-02	-123.42630	48.41535	41.7	2.36	58683	45	1090	40	289	459 - 268	shell	4a
TUL97B-02	-123.42630	48.41535	41.7	2.36	58685	96	10640	50	9839	11595 - 10845	shell	4a
TUL97B-02	-123.42630	48.41535	41.7	2.36	58684	224	9880	50	9079	10545 - 9833	shell	4a
TUL97B-03	-123.41665	48.40980	51.0	3.70	-	-	-	-	-	-	-	4a/3a
TUL97B-04	-122.78883	48.38283	85.7	4.48	58686	13	3660	40	2859	3223 - 2940	shell	3a
TUL97B-05	-122.99042	48.35807	153.6	5.13	58688	114	10630	40	9829	11588 - 10845	shell	4b/4a
TUL97B-05	-122.99042	48.35807	153.6	5.13	58687	123	10950	50	10149	12080 - 10889	shell	4a
TUL97B-05	-122.99042	48.35807	153.6	5.13	58689	205	13230	50	12429	15395 - 14113	shell	3a
TUL97B-06	-122.99117	48.35623	153.3	3.19	-	-	-	-	-	-	-	4a
TUL97B-07	-123.16820	48.23322	155.7	1.65	58690	31	13250	50	12449	15411 - 14120	shell	3a
TUL97B-08	-123.17573	48.28287	121.6	3.47	58691	33	4320	50	3519	4049 - 3743	shell	4b

\* Raw <sup>14</sup>C ages were determined using the Libby half life of 5568 years and following the conventions of Stuiver and Polach (1977).

\*\* Corrected <sup>14</sup>C ages were determined using the reservoir correction of -801 +/- 23 years (Thomson, 1981).

\*\*\* Calendar age was determined using CALIB 4.3 (Stuiver, et al., 1998) and employs the reservoir correction of -801 +/- 23 years.

Table 1. Continued

Core Number	Longitude (°)	Latitude (°)	Water Depth (m)	Core Length (m)	Sample Number	Depth in core (cm)	Raw <sup>14</sup> C Age* (Yr.B.P.)	+/- Error (Yr.B.P.)	Corrected** <sup>14</sup> C Age (Yr.B.P.)	Calendar age range Max. - Min. (Yr.B.P. <sup>3</sup> )	Material Dated	Unit
TUL97B-09	-123.05173	48.29973	156.5	4.57	58693	93	12670	50	11869	14047 - 13437	shell	3a
TUL97B-09	-123.05173	48.29973	156.5	4.57	58692	133	13250	50	12449	15411 - 14120	fish bone	3a
TUL97B-10	-123.03968	48.29998	101.0	0.59	-	-	-	-	-	-	-	2
TUL97B-11	-123.03968	48.29993	173.7	0.10	58694	182	13470	60	12689	15603 - 14203	shell	3a
TUL97B-12	-123.41362	48.39950	58.0	3.73	58695	246	10720	60	9919	11663 - 10858	shell	4a/3a
TUL97B-12	-123.41362	48.39950	58.0	3.73	58696	325	13690	50	12869	15849 - 14381	shell	3a
TUL97B-13	-123.51308	48.33342	96.0	0.93	-	-	-	-	-	-	-	4a
TUL97B-14	-122.73705	48.39185	73.3	0.86	-	-	-	-	-	-	-	4b
TUL97B-15	-122.80896	48.34887	104.9	4.83	-	-	-	-	-	-	-	4a
TUL97B-16	-122.80795	48.34905	103.6	5.11	58697	43	2510	50	1709	1823 - 1548	shell	4a
TUL97B-16	-122.80795	48.34905	103.6	5.11	58698	179	11910	50	11109	13160 - 12865	shell	3a
TUL97B-16	-122.80795	48.34905	103.6	5.11	58699	182	13030	50	12229	15222 - 13708	shell	3a
TUL97B-16	-122.80795	48.34905	103.6	5.11	58700	342	13150	50	12349	15330 - 14085	shell	3a
TUL97B-16	-122.80795	48.34905	103.6	5.11	58701	504	13500	50	12699	15630 - 14213	shell	3a
TUL97B-17	-122.94027	48.41822	94.9	1.10	-	0	-	-	-	-	-	4a
TUL97B-18	-122.90070	48.27907	114.8	3.37	58702	61	9340	50	8539	9818 - 9093	shell	4a
TUL97B-18	-122.90070	48.27907	114.8	3.37	58703	206	9530	50	8729	9962 - 9495	shell	4a
TUL97B-18	-122.90070	48.27907	114.8	3.37	58704	320	9840	50	9039	10539 - 9823	shell	4a
TUL97B-19	-122.89848	48.28373	107.0	0.54	-	-	-	-	-	-	-	4a
TUL97B-20	-122.80155	48.23363	72.0	0.69	-	-	-	-	-	-	-	3b
TUL97B-21	-122.95393	48.33597	132.5	3.83	58705	221	10580	50	9779	11576 - 10828	shell	4a
TUL97B-22	-123.23278	48.38305	75.7	0.10	-	-	-	-	-	-	-	4b
TUL97B-23	-123.51300	48.33355	94.6	1.31	-	-	-	-	-	-	-	4b
TUL97B-24	-123.23375	48.38288	73.0	0.10	-	-	-	-	-	-	-	4b
TUL97B-25	-123.68498	48.37483	98.6	1.53	-	-	-	-	-	-	-	4b
TUL97B-26	-123.23287	48.38285	76.6	0.10	-	-	-	-	-	-	-	4a
TUL99-15	-123.43000	48.41960	30.7	2.17	62767	213	8910	50	8109	9312 - 8854	shell	4a
TUL99-16	-123.42200	48.40880	48.7	1.69	62768	164	3600	50	2799	3165 - 2844	shell	4a
TUL99-17	-123.42500	48.41240	48.0	2.05	62531	44	5020	50	4219	4952 - 4727	shell	4a
TUL99-17	-123.42500	48.41240	48.0	2.05	62532	77	6480	50	5659	6614 - 6351	shell	4a
TUL99-18	-123.42700	48.41540	41.2	2.93	62533	55	8490	50	7689	8722 - 8404	shell	4a
TUL99-18	-123.42700	48.41540	41.2	2.93	62534	132	13370	50	12569	15503 - 14166	shell	3a

\* Raw <sup>14</sup>C ages were determined using the Libby half life of 5568 years and following the conventions of Stuiver and Polach (1977).

\*\* Corrected <sup>14</sup>C ages were determined using the reservoir correction of -801 +/- 23 years (Thomson, 1981).

\*\*\* Calendar age was determined using CALIB 4.3 (Stuiver, et al., 1998) and employs the reservoir correction of -801 +/- 23 years.

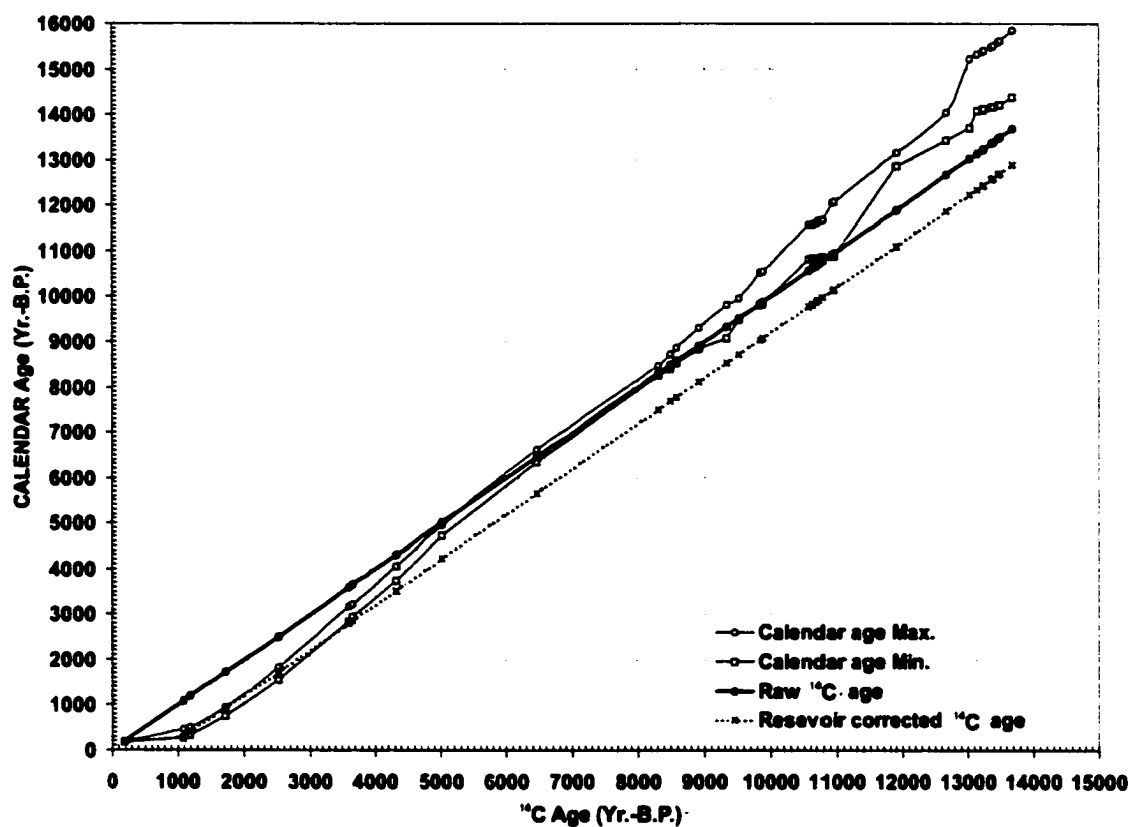


Figure 3. Relationship between raw  $^{14}\text{C}$  age (dark line), reservoir corrected  $^{14}\text{C}$  age ( $-801 \pm 23$  years; Robinson and Thomson, 1981) (dashed line), and the possible range in calendar age (light lines), calculated using CALIB 4.3 (Stuiver et al., 1998).

## **CHAPTER III**

### **BATHYMETRY AND GEOMORPHOLOGY**

#### **Bathymetry**

Data resolution is of importance to scientists using bathymetric data to interpret seafloor geomorphology, because spatial resolution determines the scale of features that can be detected. Vertical resolution of a bathymetric sonar is determined by the sonar pulse length (shorter pulse lengths yield better resolution), bottom detection technique, and corrections for vessel motion and water velocity structure. Vertical resolution is typically better than 1% of the water depth, but horizontal resolution is not nearly as good. Horizontal resolution is governed by the area ensonified (the sonar footprint) on the seafloor, and by the sounding density (soundings/area). For singlebeam sounders the area ensonified is a function of beam width and transducer height above the seafloor (Fig. 4). For multibeam sounders, the footprint is a function of beam width (in both across track and along track directions), water depth, and the receive-beam angle with respect to the seafloor (grazing angle). The footprint size of oblique soundings increases away from nadir. Therefore, resolution is at a maximum for nadir beams in shallow water and deteriorates with decreasing grazing angle and increasing water depth. Generally speaking, features smaller than the area ensonified will not be detected. However, with multibeam systems that use phase bottom detection, the across track resolution can be improved to about the equivalent of the along track resolution (Hughes Clarke, 1998c). Sounders like the EM3000 and EM1002 have the potential to ensonify 100% of the



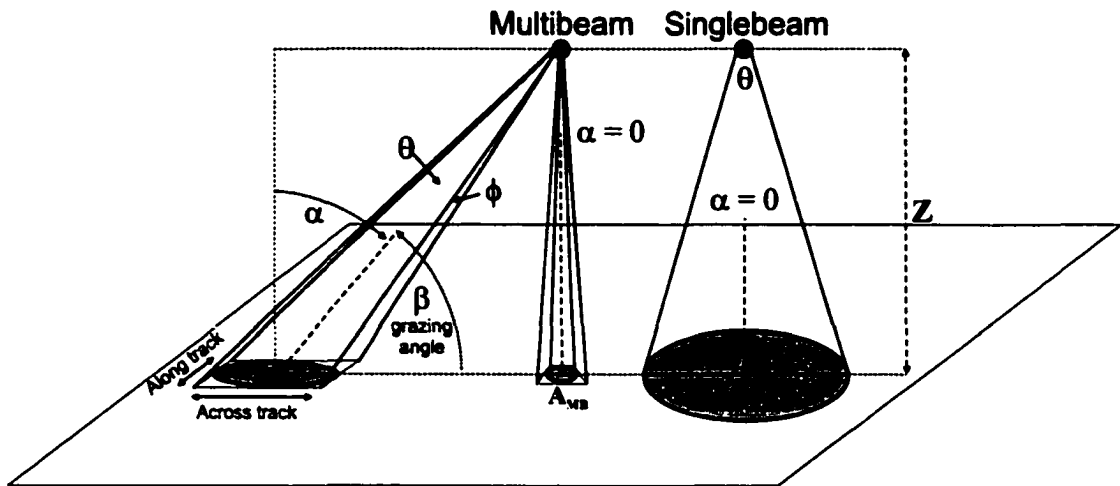


Figure 4. Schematic representation (not to scale) of sonar geometry and the seafloor area ensonified during a sounding (shaded areas on diagram). For singlebeam sonars at nadir ( $\alpha=0$ ), the area ensonified is a circle:  $A_{sb} = \pi[Z \tan (\theta/2)]^2$ . At oblique incident angles ( $\alpha > 0$ ), or if the seafloor is sloped, the energy will be spread over a larger area resulting in poorer horizontal resolution. This is the case with multibeam sonars, and the area ensonified is an ellipse:  $A_{mb} = \pi[Z/\cos(\alpha)] \tan (\phi/2) \tan (\theta/2) / \sin (\beta)$ .

seafloor in a wide swath several times the water depth, and their narrow receive-beam widths (1.5° for the EM3000 and 2.4° for the EM1000) allow them to resolve seabed features with horizontal scales of 3-10% the water depth (Hughes Clarke, 1998a, 1998b, 1998c). Singlebeam sounders typically have beam widths many times wider (5-25°), resulting in much poorer resolution, and usually much smaller percentages of the seafloor are ensonified, depending on survey requirements.

Maximum horizontal resolution is inherent in sonar design, but bathymetric data is frequently presented as a surface rendered from a digital elevation model (DEM) based on the soundings (Fig. 5). In practice, the actual resolution obtained depends on the size of the DEM elements, or else the equivalent pixel dimensions of the viewed image, whichever is larger.

When constructing a DEM, a regular grid of depth values is created based on interpolation of the original soundings to estimate depth values at grid nodes. There are numerous interpolation techniques; here the point data were first built into a TIN (Triangular irregular network) data structure. Then an inverse distance weighted averaging algorithm was run over the TIN to produce a grid with a regular cell interval. The depth assigned to a specific grid node using the inverse distance method is a weighted average of a given number of nearest soundings (nearest neighbors); the general formula is (Burrough, 1986):

$$Z_G = \frac{\sum_{i=0}^{i=n} (z_i / d_i^p)}{\sum_{i=0}^{i=n} (1 / d_i^p)}$$

Where, ( $Z_G$ ) is the calculated depth at the grid node location, ( $Z_i$ ) is the depth of point ( $i$ ), ( $d_i$ ) is the distance from this point to the grid node, and ( $p$ ) is the weighting exponent, which determines how much emphasis is to be placed on the nearer points.

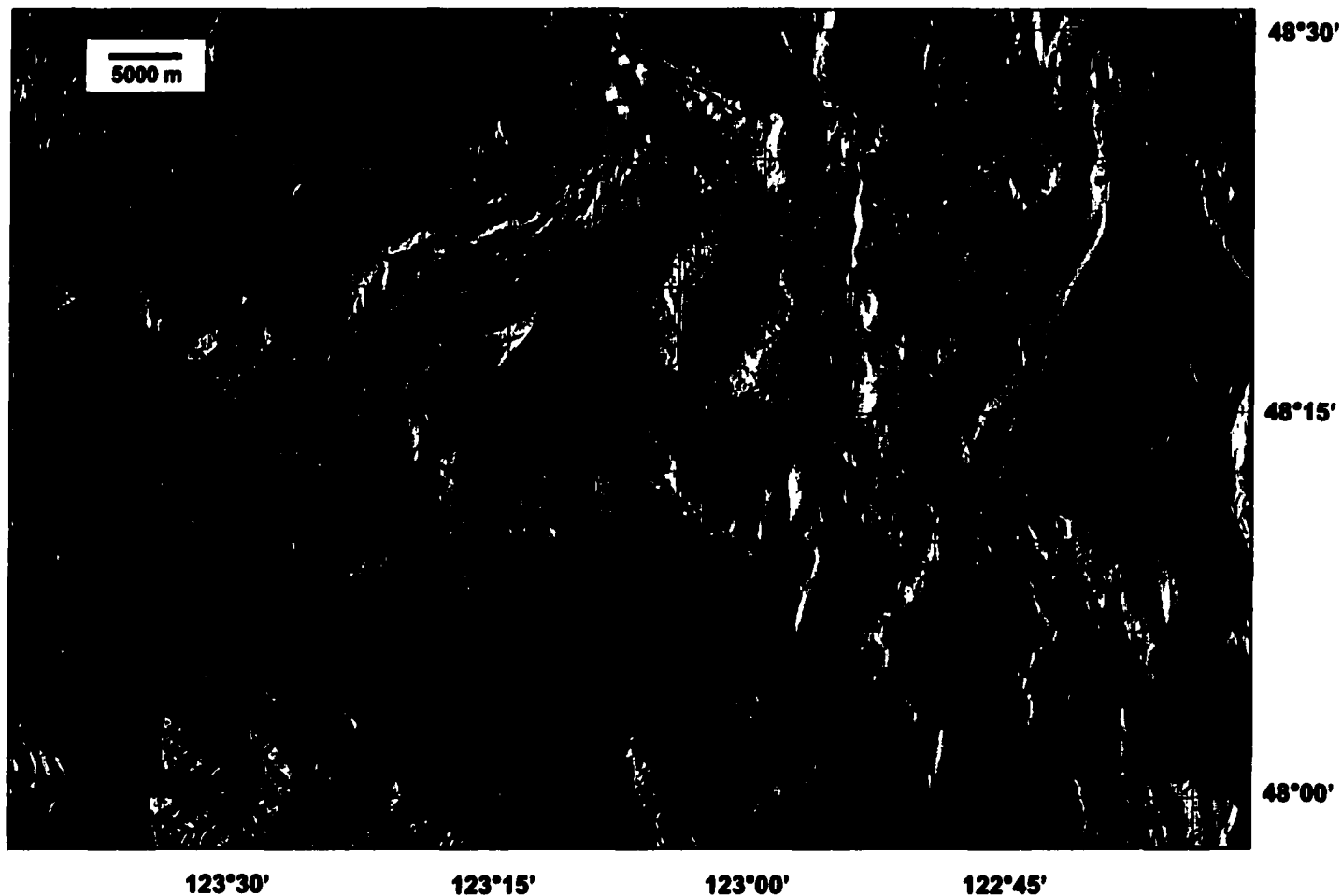


**Figure 5.** Sun-illuminated bathymetry of the eastern Juan de Fuca Strait. Solid black borders surround areas where imagery generated from the multibeam data has been superimposed on singlebeam imagery. Dashed black borders surround areas where the only digitized soundings available were acquired during the seismic surveys.

Soundings farther from a grid node are valued less than those closer to it. The four nearest neighbors were used to determine the interpolated cell value. Horizontal resolution is, therefore, limited to an area equivalent to the grid node spacing (grid cell size) determined by the user. There is little benefit in choosing a cell size smaller than the maximum horizontal resolution of multibeam sonars, or in the case of singlebeam sounders, a cell size smaller than the distance between soundings.

In the singlebeam data from eastern Juan de Fuca Strait, the area of greatest sounding density occurs in Esquimalt Harbour, where there is one sounding every 10 m in some areas. In the middle of the strait, soundings are as far apart as 150 m, and in the western strait, they are 300 m apart or more. Figure 6 shows the location of digitized singlebeam soundings and their relative density. Using a small cell size (<10 m) over the entire study area creates a large data set that can be difficult to manipulate, and in most areas of the strait, it is not warranted since sounding density is quite sparse. Another consideration is the pixel resolution of images generated. The equivalent pixel dimensions of a 21.59 x 27.94 cm (8.5" x 11") image (2550 x 3300 pixels; 300 dpi) of the entire study area are about 25 m per side; so, if a grid cell size smaller than 25 m is used, the resolution will not be honored in the final imagery. Therefore, a 25 m grid cell size was chosen as it provided an acceptable compromise between maintaining horizontal resolution and ease of data presentation in publications. In Figure 1, the multibeam data were combined with the singlebeam data and gridded at 25 m. Separate, larger scale maps were created for smaller subregions where there is multibeam coverage.

Presently, within the study area, multibeam sonar data are available only along the Victoria waterfront and off Race Rocks (Fig. 7 and 8). EM3000 data were gridded at 2 m



Figure 6. Coverage and relative density of digitized singlebeam hydrographic soundings currently available in the study area.

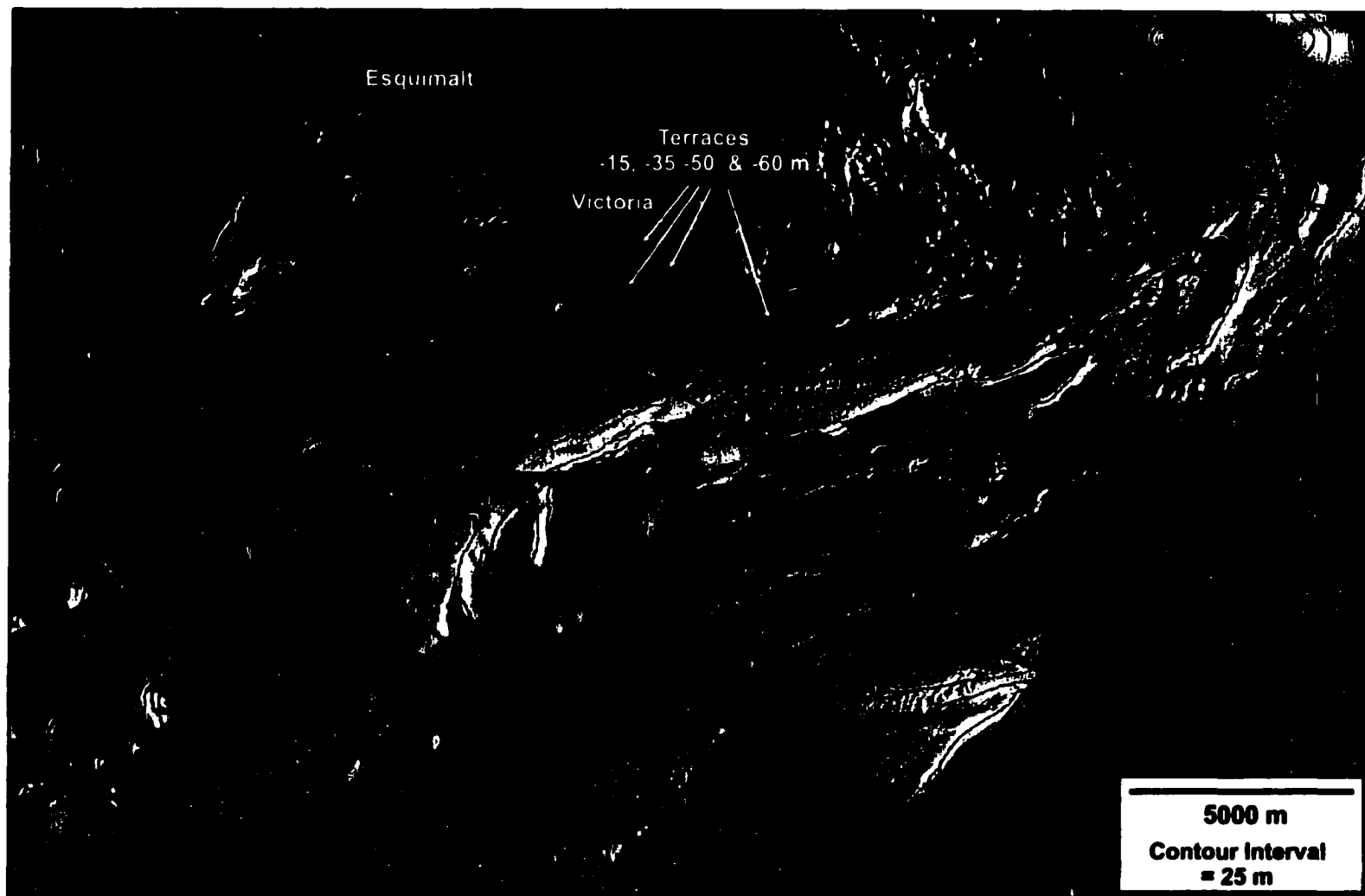


Figure 7. Image of merged EM3000 and EM1002 multibeam bathymetry gridded at 5 m (area surrounded by black border), superimposed on singlebeam hydrographic data. The location of Figure 22 and “terraces” are shown (see discussion).



**Figure 8. EM3000 multibeam bathymetry at Race Rocks gridded at 2 m (location is indicated on Figure. 2), showing an example of highly fractured sea floor that occurs in localities off southern Vancouver Island. The blank areas in the middle of the outcrop are locations where rocks reach the sea surface.**

and EM1002 data were gridded at 5 m. The multibeam data provide a scale of resolution, impossible to achieve using standard singlebeam techniques, and reveal features, anthropogenic and natural, that otherwise would not have been observed. Still, there are limitations in spatial resolution (discussed above) and possible data artifacts.

Common artifacts in multibeam data result from imperfect corrections for tides, ship motion, and sound-ray refraction (Hughes-Clarke *et al.*, 1996). Tide information normally is acquired from tide measuring stations in the survey area, or are predicted by extrapolation between more distant stations. If tide corrections are imperfect, it can result in a “step” between two adjacent lines. Ship location and motions (heave, roll, pitch, and yaw) are monitored by an inertial motion sensor integrated with two DGPS receivers and used to correct for changes in the ships position and orientation during a sounding. If these corrections are imperfect, they can result in both a horizontal and vertical displacement of the apparent ray strike point, and therefore, an error in depth measurement. Heave results in a change in the altitude of the sonar above the bottom, which can cause a change in the size of the foot print and notable undulations on the seafloor. Roll will cause swath coverage to oscillate from side to side resulting in displaced depth measurements. Pitch will cause the along track beam spacing to become variable, which can cause gaps or overlap between successive swaths. Yaw results in rotational displacement of the swath axis, and is most pronounced in the outer beams where it can produce gaps and overlap.

The most common artifacts in multibeam data result from sound ray refraction. Sound rays travel through the water column according to Snell’s Law, and since the water column is not of uniform sound speed structure, they will be refracted (bent) away



from their original trajectory. If unaccounted for, refraction can cause an error in the measured oblique range to the seafloor (incorrect sounding position) and, hence, an incorrect depth estimate. In practice, a correction, called the refraction solution, is applied based on some knowledge of the water's sound velocity profile or SVP (usually measured periodically during a survey) and the beam angle, which is then used to trace the ray's path to the seafloor. In reality refraction solutions are imperfect because the water's physical properties (temperature, salinity, and pressure) can change both spatially and temporally during a survey, causing a corresponding change in the SVP. The refraction error increases away from nadir, such that the effect is most noticeable along the outer edges of a swath. These errors can be seen quite readily on a flat seafloor, but can be much harder to detect on a rough seafloor. For example, in the western half of Figure 7, where the seafloor is relatively flat, the parallel lines running west-east, in the along track direction, are a result of refraction error. These lines are not apparent in the eastern half of the image, where the seafloor is more irregular.

### **Geomorphology**

The present-day seafloor relief in eastern Juan de Fuca Strait is characterized by many shallow banks and intervening deep troughs, where water depths reach up to 250 m (Fig. 9). The most conspicuous features are the 10 large banks, which all have steep sides and relatively flat tops at less than 40 m below the sea surface. Several of banks have their steepest slope facing east, while their western slopes are more gradual. The exception is Constance Bank, where the seafloor shoals to about -60 m over a large flat area on the banks eastern side. Constance Bank, the unnamed bank in the middle of the

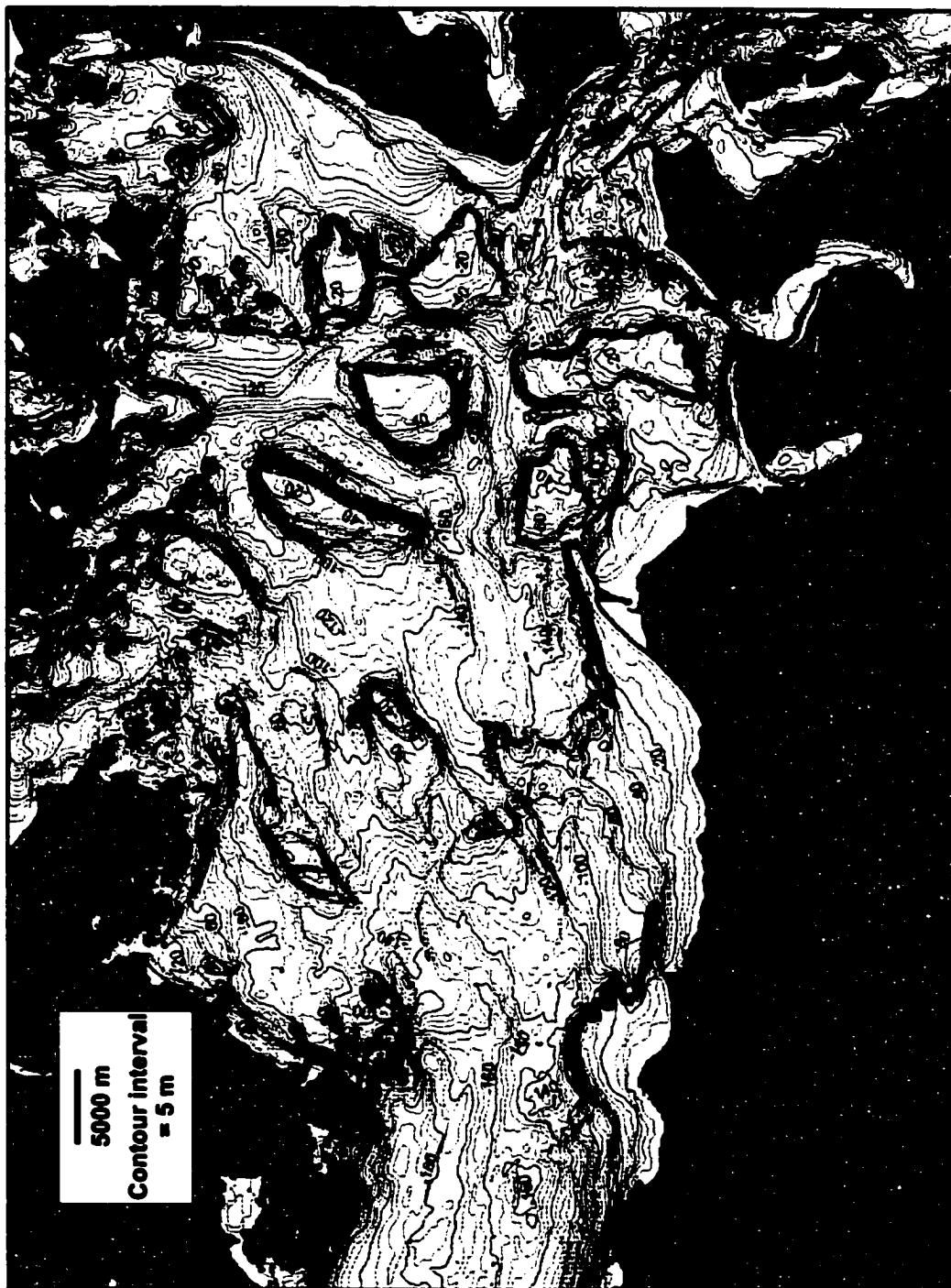


Figure 9. Bathymetric contour map, based on combined multibeam and singlebeam soundings.

strait, and the area of seafloor that extends north of Green Point create a roughly linear zone of relatively shallow water compared with the area immediately to the west and east. This feature has been referred to as the “Victoria-Green Point Sill” (Anderson, 1968). Although none of the banks were mapped in their entirety with multibeam sonar, several of the banks near Victoria were partially mapped. The superior resolution provided by the multibeam systems reveals that bank tops are not as flat and featureless as suggested in the singlebeam data. In some cases, there are linear ridges, depressions, and bedforms (Fig. 7).

In coastal areas along southern Vancouver Island, there are small areas of positive relief where the bathymetry is highly irregular. One of these areas, called Race Rocks, was mapped with the EM3000, which revealed an outcrop of highly fractured seafloor surrounded by smoother seafloor (Fig. 8). Similar, but smaller outcrops were mapped off Victoria with the EM3000 and EM1002 (Fig. 7), and in the vicinity of Trial Island and Discovery, more examples are seen in singlebeam data. Fracturing occurs at all scales resolvable by the various sonars. At Race Rocks, there are abundant small fractures measuring around 2-m long, and the largest fracture measures 130-m wide and extends 2770 m across the entire outcrop.

Both Esquimalt Harbour and Victoria Harbour have been mapped with the EM3000 (Fig. 10). The imagery clearly shows steep sided rectangular depressions that result from dredging.

along the Victoria waterfront, multibeam data also reveal a series of terraces at depths of around 15, 35, 50, and 65 m (Fig. 7). The continuity of these terraces can be traced westward into the Esquimalt offshore. The terraces become more subdued and

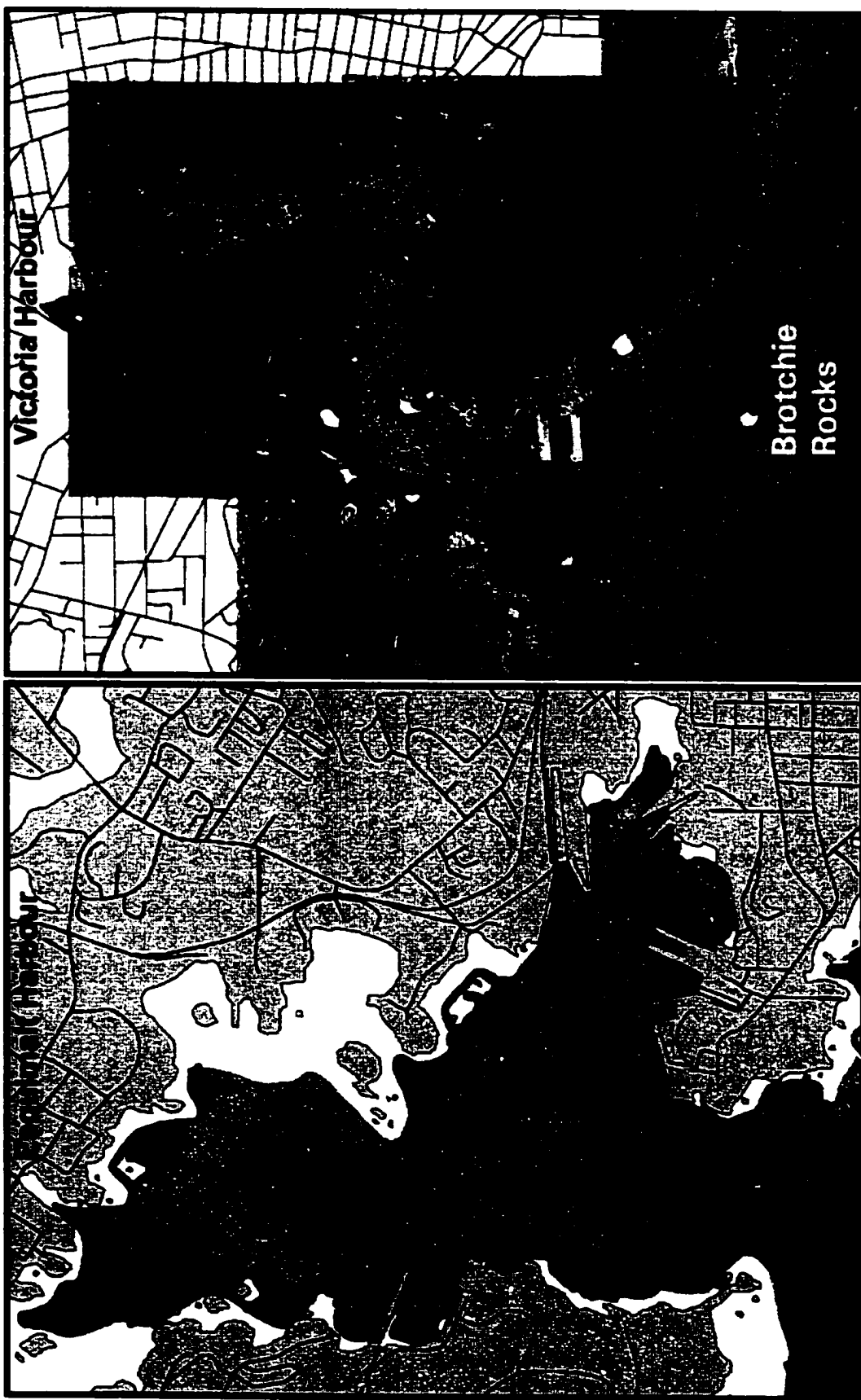


Figure 10. EM3000 multibeam bathymetry from Esquimalt Harbour and Victoria Harbour.

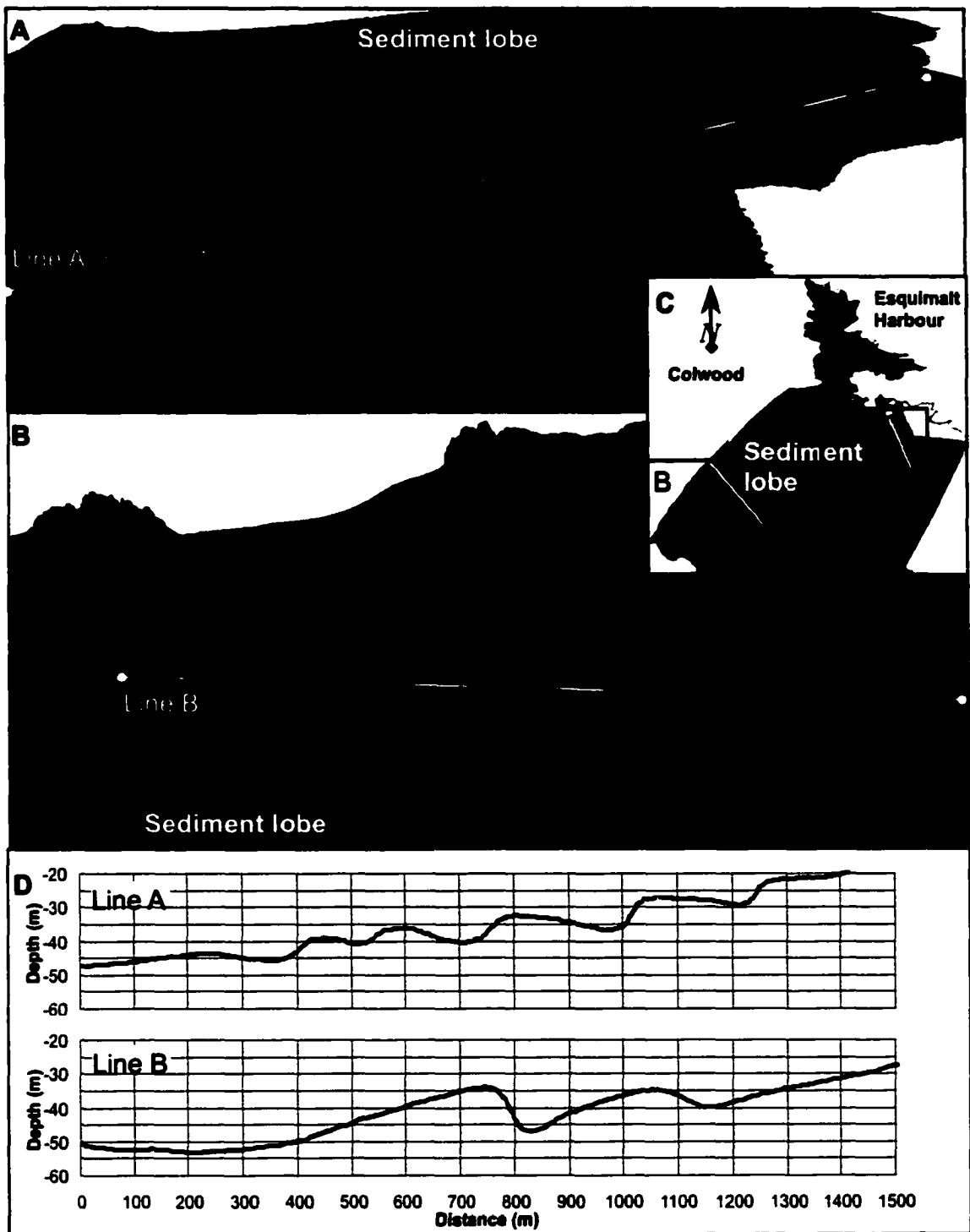


Figure. 11. EM3000 Multibeam bathymetry (vertical exaggeration is 6X) showing ridge features on either side of a sediment lobe that splays out onto the sea floor off Esquimalt Harbour. (C) Survey area, indicating regions (A) and (B), and orientation of profiles, line A and line B, shown in (D).

give way to a more gradual and continuous seafloor slope south of the entrance to Esquimalt Harbour, where a lobe of sediment appears to splay out onto the seafloor (Fig. 11). A peculiar feature of this lobe is the series of six curved ridges along its eastern margin. The ridges are asymmetric, dipping more steeply seaward ( $\sim 7^\circ$ ) and more gently landward ( $\sim 3^\circ$ ). Their width ranges from  $\sim 150$  m to 275 m, and their length is about 1300 m. The shallowest ridge crests at 20 m depth, and the rest are progressively deeper, with the deepest at 43 m. Two more ridges occur along the western side of the sediment lobe in water depths of 35 m (Fig. 11). Their asymmetry is reversed compared to those in the east, and they are straighter and larger, measuring 300 m and 600 m in width at their widest points, and taper to the east.

Multibeam data off Victoria reveal fields of large-scale bedforms that were not visible in the singlebeam data (Fig. 7). The giant dunes shown in Figure 12 are of particular interest. The dunes are located in a channel that has an average depth of about 90 m. The channel bottom is about 30 m deeper than the surrounding ocean floor. The dunes become progressively larger, and their crests straighter and longer toward the northeast. The smallest dunes discernable are about 1-m in high in 100 m of water, and the largest is 25-m high in 90 m of water (Mosher and Thomson, 2000).

There are several barrier-spits in eastern Juan de Fuca Strait; the two largest, Ediz Hook and Dungeness Spit, occur along the Olympic Peninsula (Fig. 13). Just offshore and to the west of Ediz Hook is a lobe-shaped platform of shallow seafloor that extends 4.5 km into the strait. Three protuberances with a similar bathymetric profile and width to Ediz Hook occur along the eastern edge of this platform (Fig. 13 & 14). They occur at

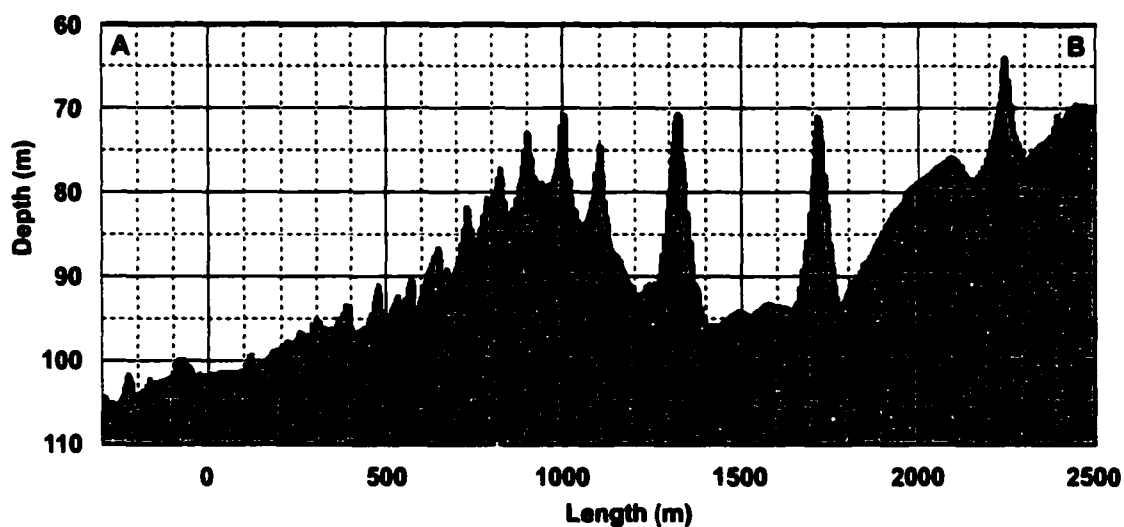
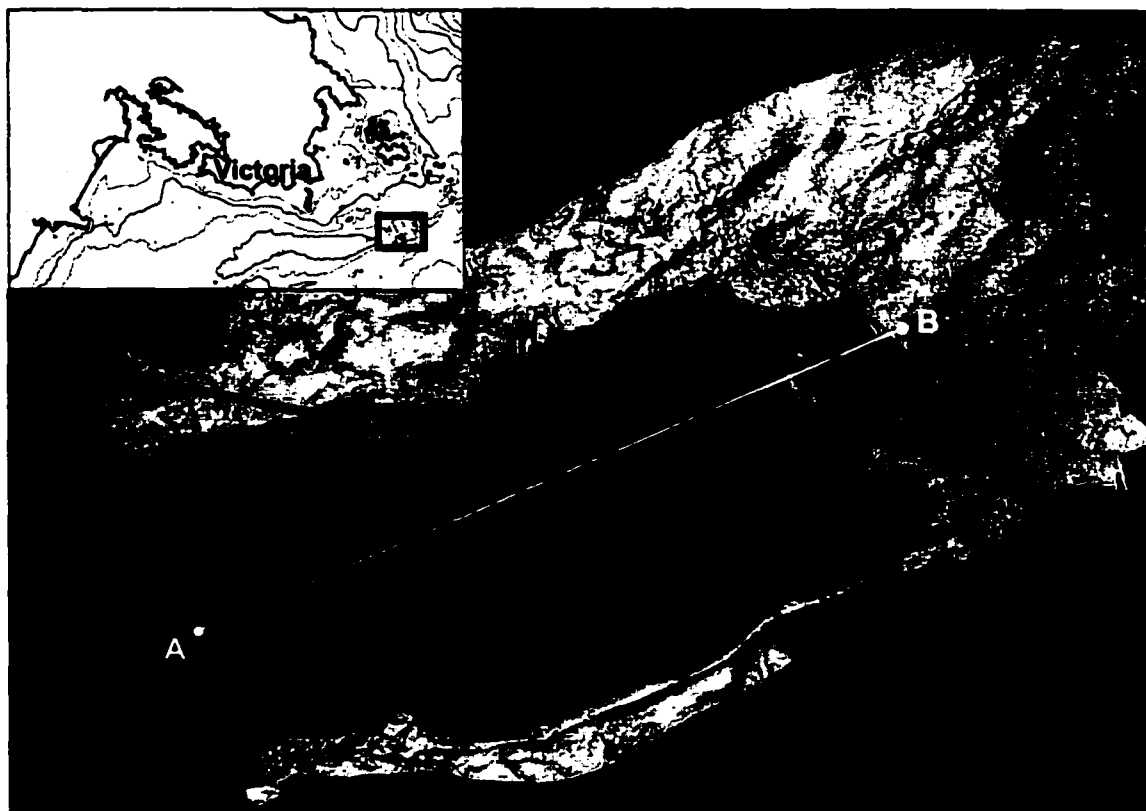


Figure. 12. EM3000 multibeam bathymetry, showing giant dunes in eastern Juan de Fuca Strait, off Victoria (location is shown in inset map at upper left). The lower panel is a bathymetric profile through points A and B.

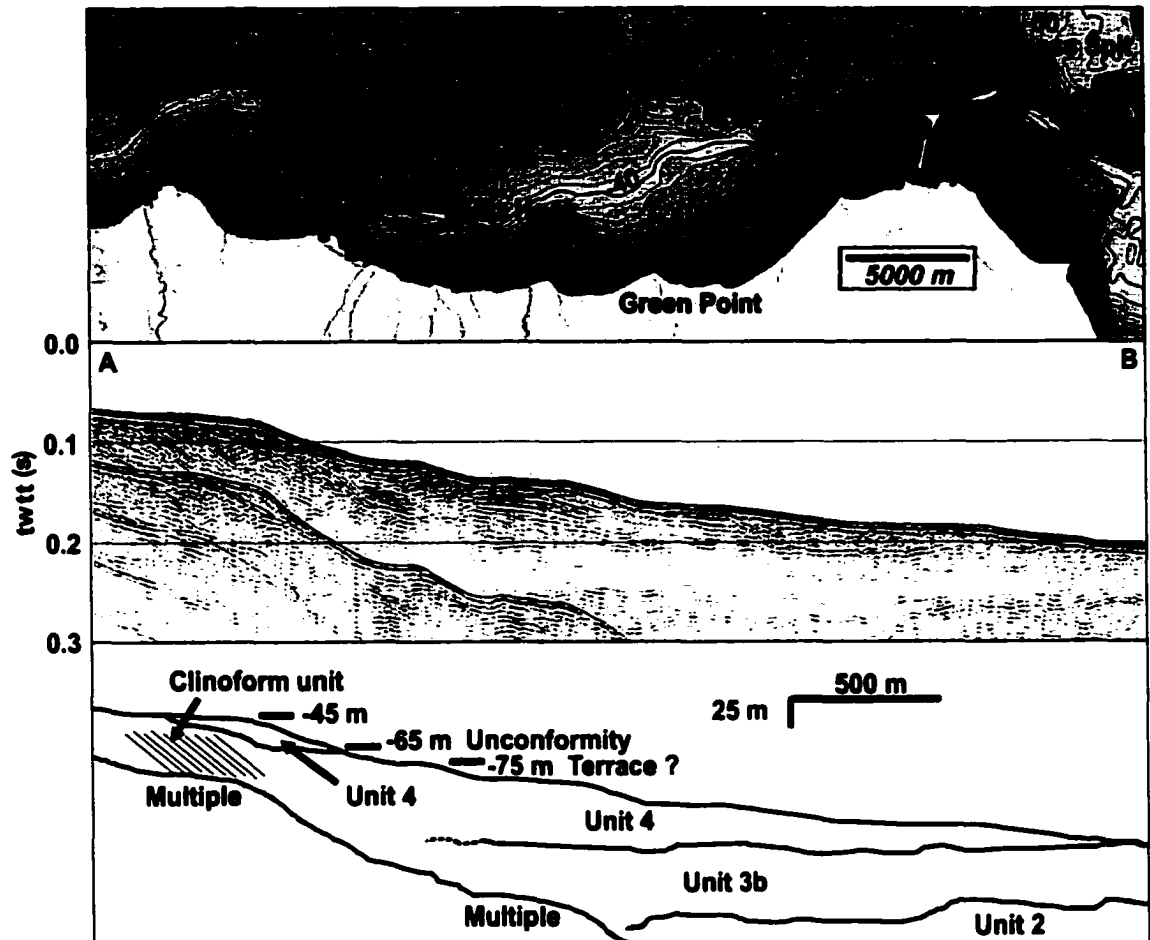


Figure. 13. The upper panel shows bathymetry along the Olympic Peninsula, and the depth of submerged “spit-like” protuberances offshore of present day spits, Ediz Hook and Dungeness Spit. Line A-B shows the location of the single-channel seismic profile in the lower panel. The profile shows clinoforms interpreted as submerged delta forsets prograded to, at least, -48 m depth.



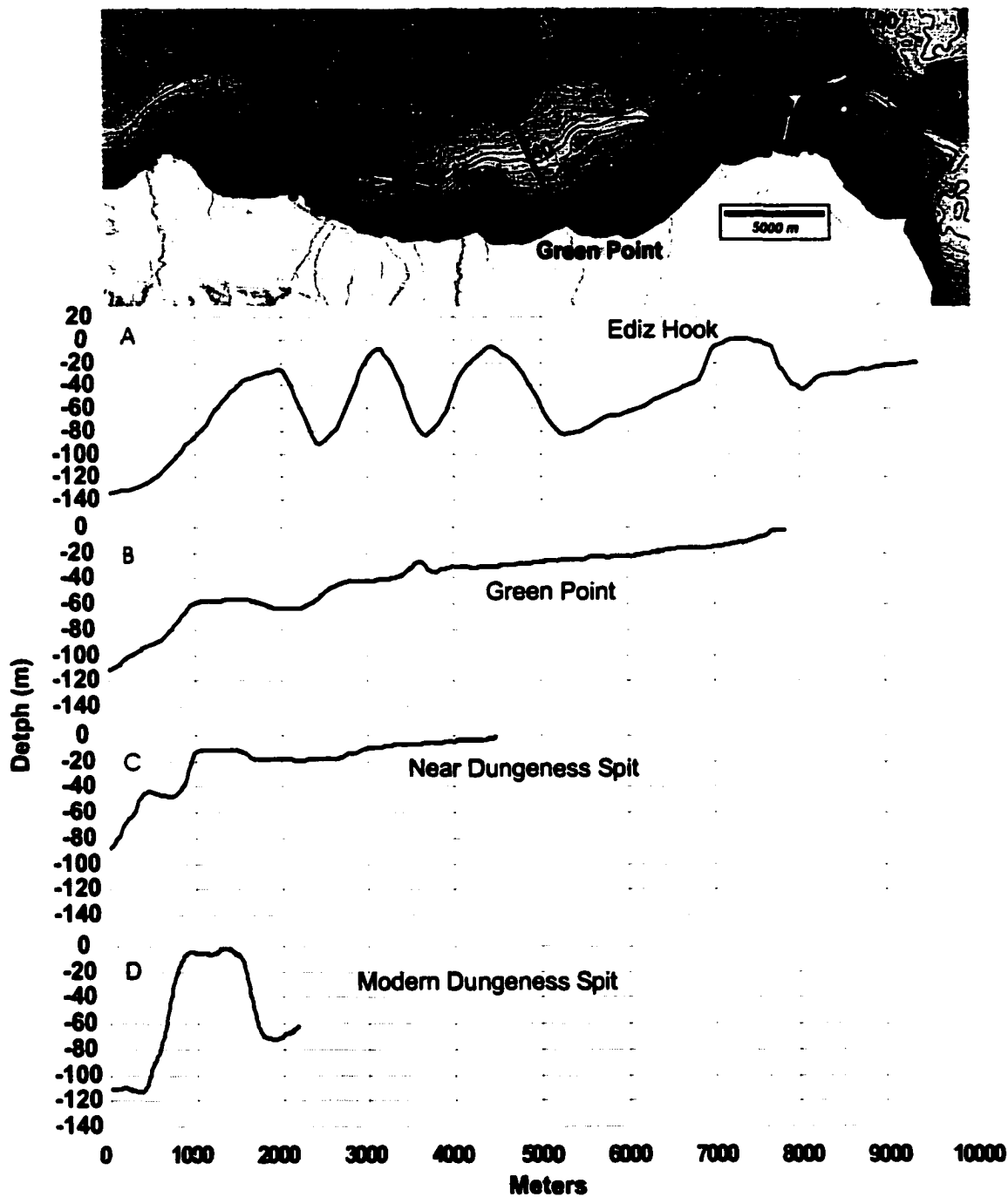


Figure 14. Bathymetric profiles offshore of the Olympic peninsula. The features represent: (A) Ediz Hook and a series of progressively deeper submerged features with similar morphology to the subareal spit; (B) A similar feature off Green Point at 58 m depth; (C) a submerged "spit-like" feature near Dungeness spit at 15 m depth; and (D), a bathymetric profile through modern Dungeness Spit.

depths of 6, 8, and 25 m. Off Dungeness Spit, the seafloor appears terraced at roughly the same depths as the terraces along the Victoria waterfront. A submerged feature at 15 m with a similar morphology to the subareal spit, is also noteworthy (Fig. 13). The bathymetric profile off Green Point shows a similar feature at 58 m (Fig. 14).

In the northeast corner of the study area, near Lopez Island, are two long, narrow (~1 km) ridges (Fig. 15). One of the ridges, known as McArthur Bank, is about 1 km wide and stretches for 12 km between Lopez Island and Smith Island. A “moat-like” depression (~10 m deep) runs parallel to the bank along its western side. The other ridge, known as Lawson Bank, is located in Rosario Strait, between Lopez Island and Whidbey Island. It is 11-km long and has a V-shaped plan. Another short ridge segment, 2.5-km long, joins Smith Island Bank and Partridge Bank.

The seafloor morphology of the Admiralty Inlet area appears somewhat different from the rest of the strait (Fig. 16). Bathymetric data reveal ridges and troughs, several kilometers long, giving it a channelized appearance. This terrain style ends to the north in the basin between Dallas Bank and Partridge Bank where two lobes of sediment appear to splay out onto the ocean floor, on either side of a small bathymetric high.



**Figure 15.** Singlebeam bathymetry from the northeast corner of the study area, showing linear ridge features, Lawson Bank and McArthur Bank. A smaller ridge joins Smith Island Bank and Partridge Bank. A “moat” and drift run parallel to McArthur Bank (see text and Figure 19).

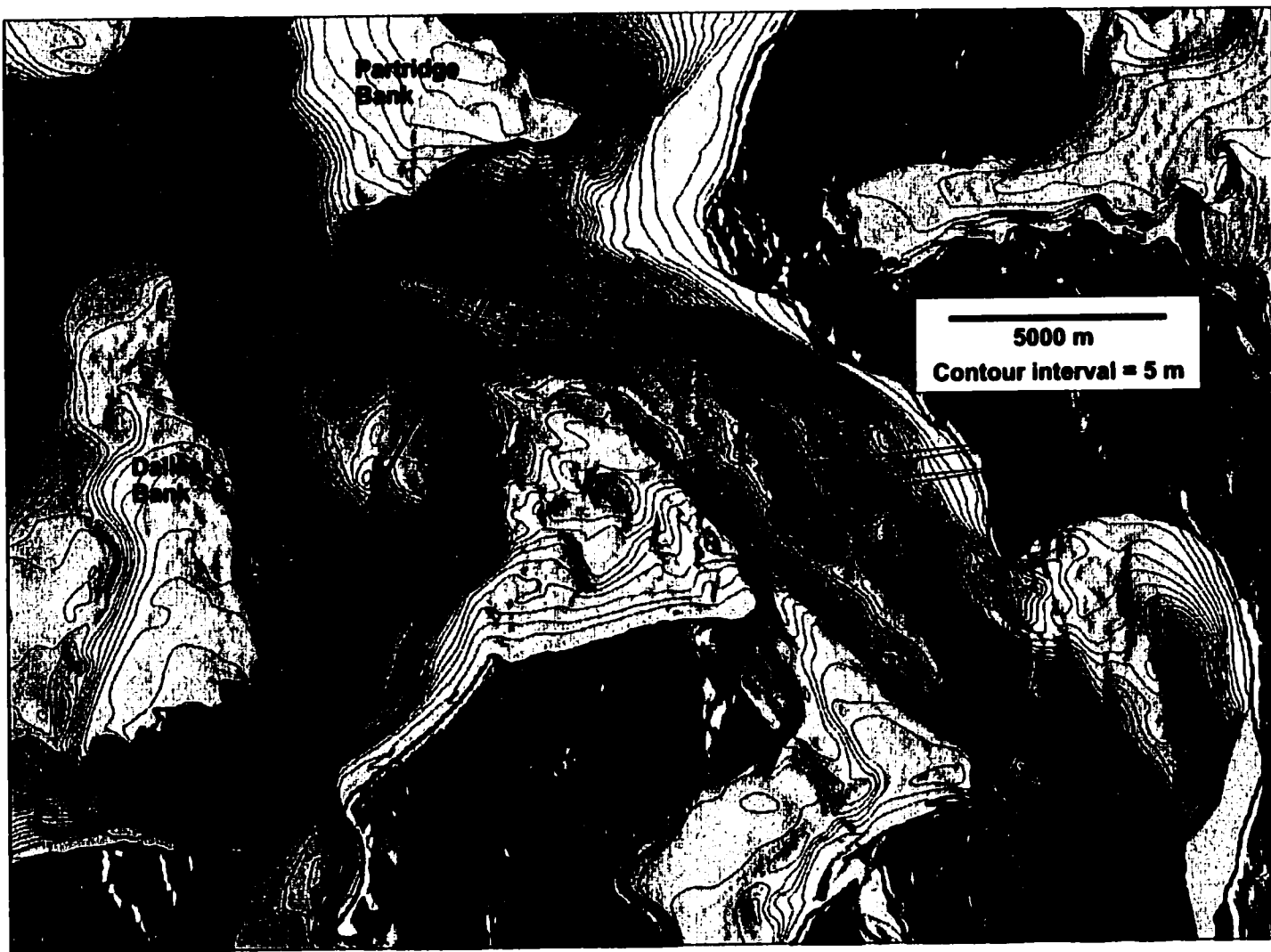


Figure. 16. Singlebeam bathymetry from Admiralty Inlet, showing a series of troughs and ridges aligned along the inlet's axis. The location of sediment lobes (see text) and the location of figures 32, 33 and 34 are indicated.

## **CHAPTER IV**

### **SEISMIC STRATIGRAPHY**

High-resolution seismic-reflection records from eastern Juan de Fuca Strait are characterized by four main seismic facies units. These units are defined as packages of reflections with similar characteristics (reflection architecture, amplitude, continuity, and spatial frequency) that distinguish one from another. Typically, the units are also separated from adjacent units by a regionally extensive reflection with high amplitude. The two seismic sources used in this study were boomers and airguns; the main differences between them being deeper penetration with the airguns, but poorer resolution compared with the boomer source. Generally speaking, the seismic-reflection character of the various units appears similar with both sources, so it was unnecessary to describe separate seismic facies units for each. These units are described in the following sections, and later sections will focus on features that are of particular relevance to the sealevel history.

#### **Unit 1**

Unit 1 is characterized by discontinuous, high-amplitude, hyperbolic reflections on the upper surface, and incoherent, but strong internal reflections, giving it a dark acoustic tone (Fig. 17-19). Neither the boomer nor airgun source penetrates deeply into unit 1, and the strong upper-surface reflections suggest high density and/or high velocity (hard) material. Unit 1 usually has a highly irregular topography, and dips steeply

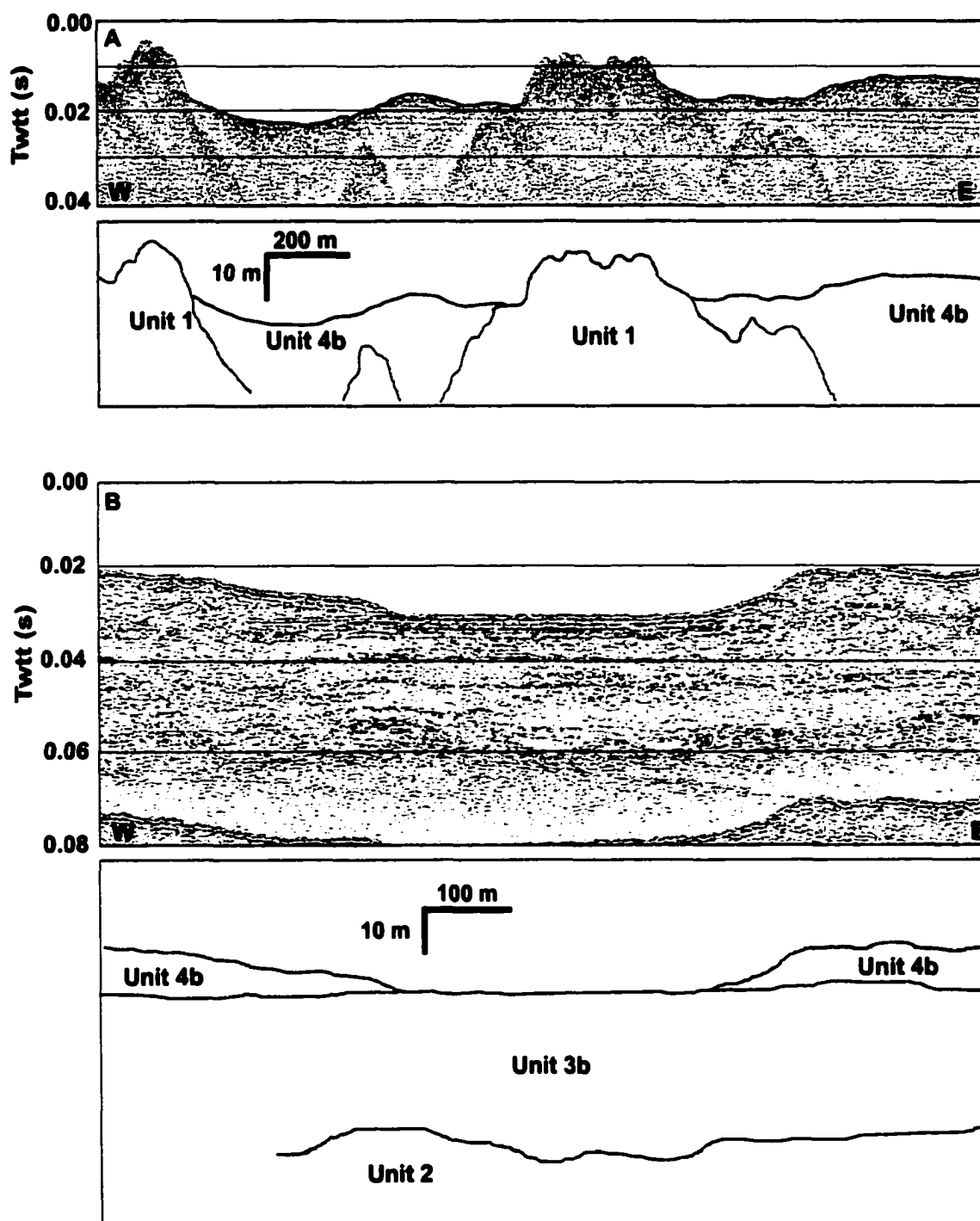


Figure 17. Hunttec boomer profiles; showing seismic units 1, 3b, and 4b. Water depth at the deepest point is 64 m in (A) and 138 m in (B). In this figure and all subsequent figures, the "W" and "E" in the lower left and right corners indicates the western and eastern end of the profile.

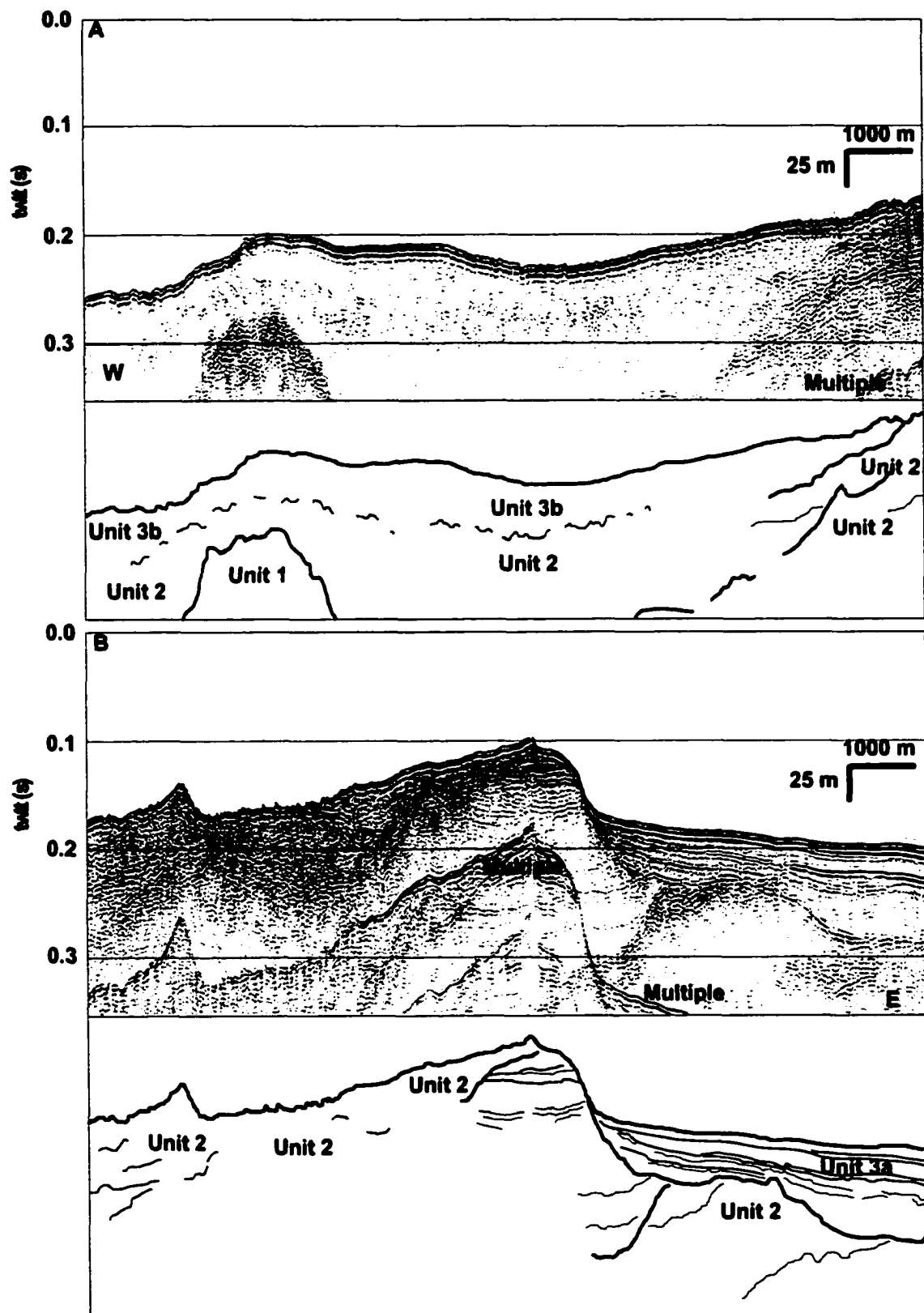


Figure 18. Airgun profile showing several of the main seismic units. (A) and (B) are contiguous.

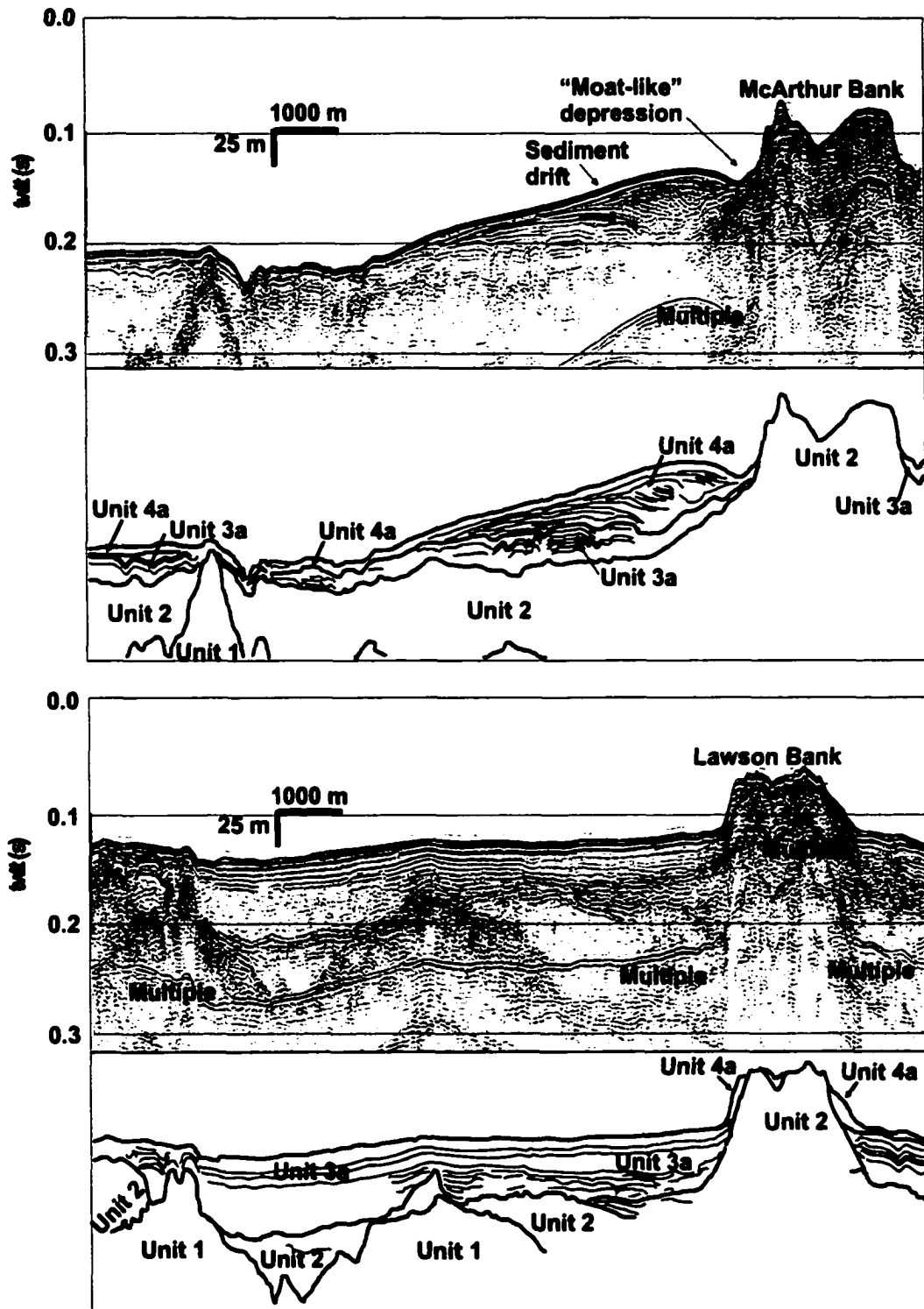


Figure 19. Airgun profile through McArthur Bank and the adjacent drift and "moat"-like depression (A), and Lawson Bank (B). (A) and (B) are contiguous.



into the subsurface. Within the study area, unit 1 is seen in seismic profiles from nearshore areas around southern Vancouver Island and San Juan Island.

## **Unit 2**

Unit 2 shows strong, semi-continuous reflections at bounding surfaces, and often displays an undulating or hummocky upper surface (Fig. 18-26). It has a dark acoustic tone in seismic imagery, but not as dark as unit 1, and internal reflections are incoherent to semi-coherent. Unit 2 is the most wide spread unit in the study area, but rarely crops out at the seafloor, except on the banks. Unit 2 usually forms the acoustic basement in Huntex records, except where unit 1 occurs, or where it has been buried by thick deposits of unit 3 or 4. The deeper penetration provided with the airguns reveals unit 2 to have a more complex internal structure than suggested by Huntex records, particularly on the banks (Fig. 22-27), where a collection of complex reflections dip at various orientations. In some locations, these reflections appear to truncate underlying reflections (suggesting and erosional unconformity), whereas in others areas, layered reflections appear more conformable. The airgun data reveal also several styles of clinoform deposits on banks and nearshore areas.

## **Unit 3**

Unit 3 overlies unit 2; offlapping it on bathymetric highs, draped over it on flat areas, and filling in local depressions on its surface (Fig. 18-27). The seismic character of unit 3 changes from east to west within the study area. In the east, it is referred to as unit 3a, where it can contain up to three distinct layers in boomer records (Fig. 20).

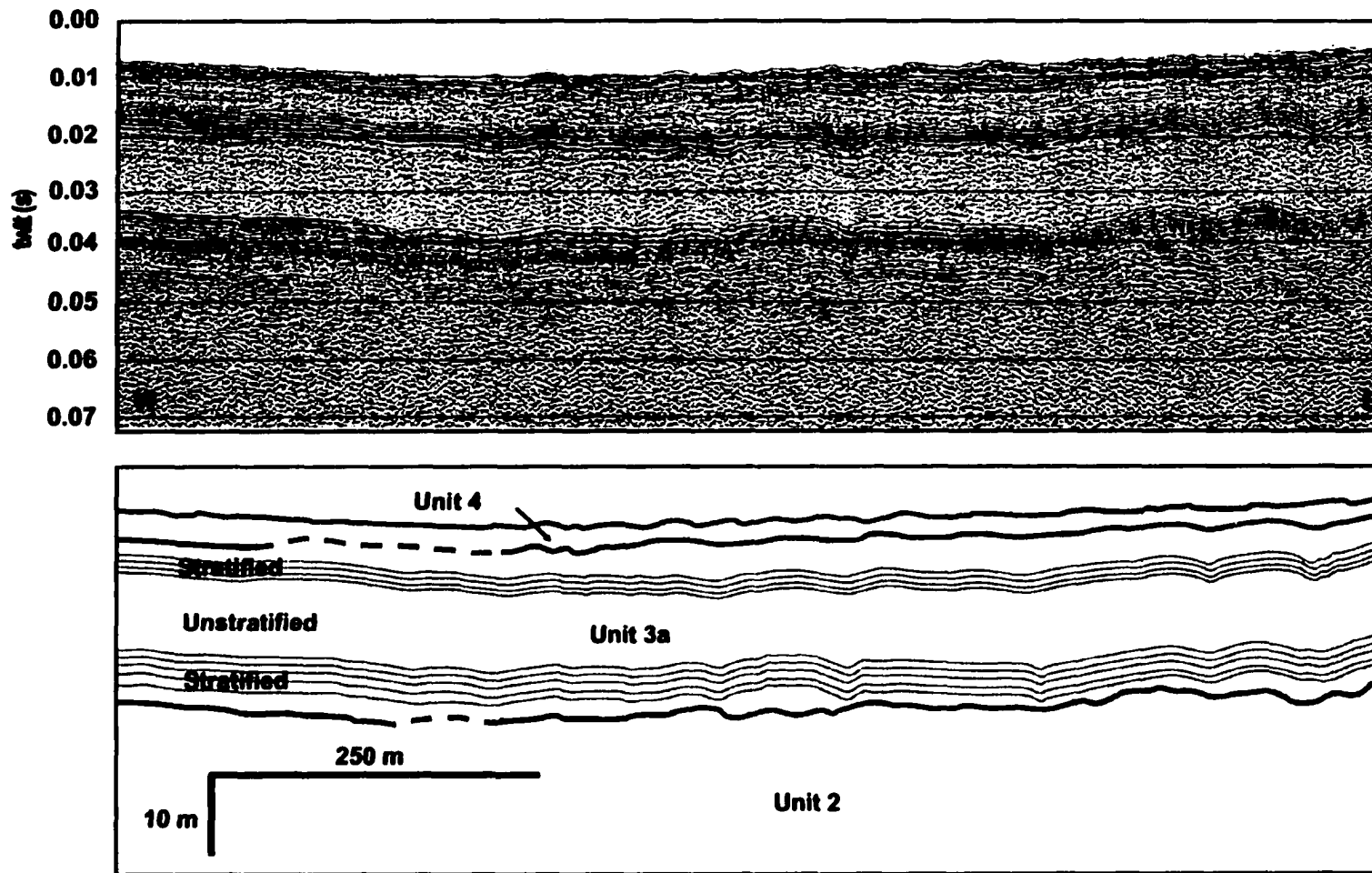
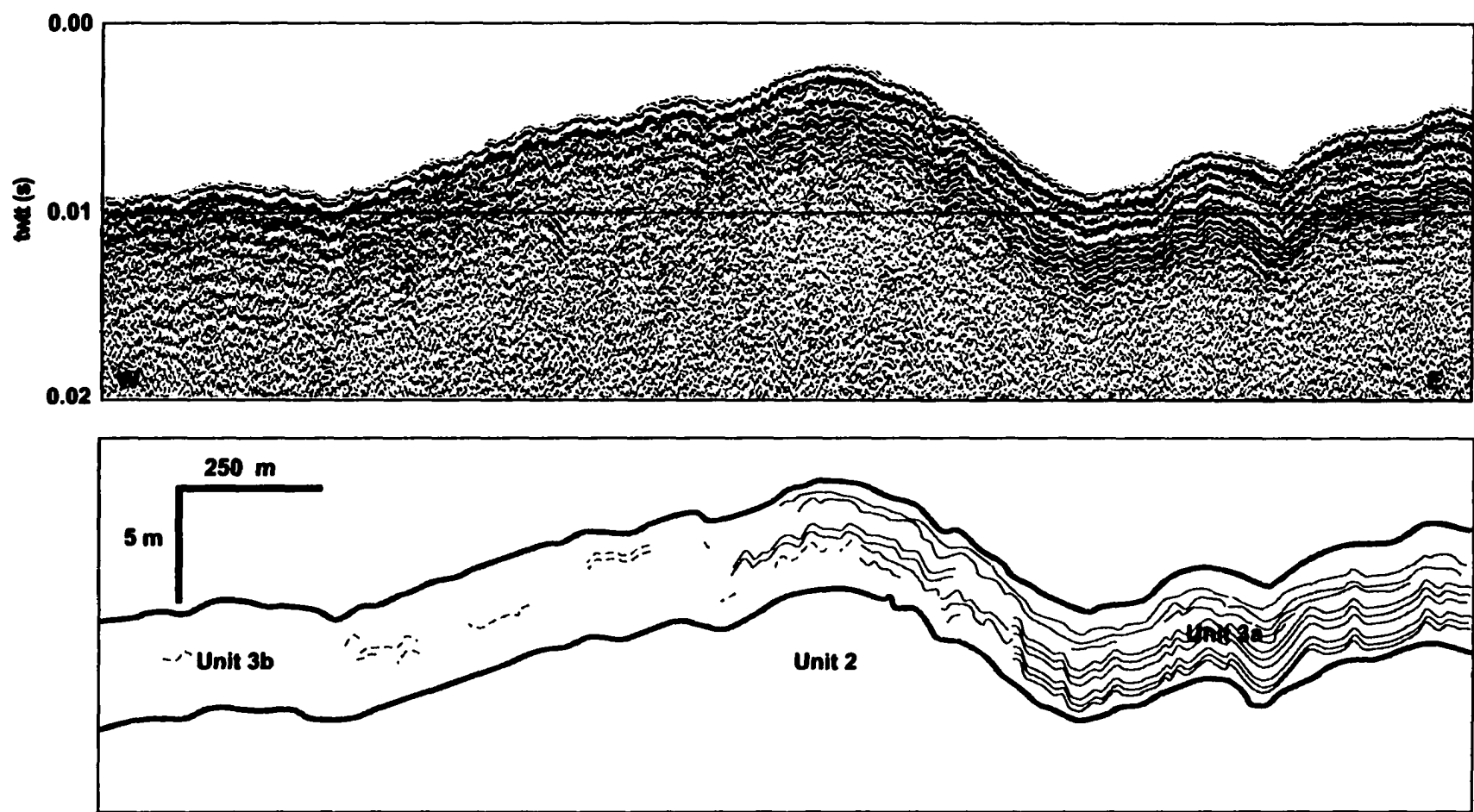


Figure 20. Hunttec boomer profile, showing the typical stratigraphy in the southeastern quadrant of the eastern Juan de Fuca Strait. Unit 3a shows three distinct layers: a lower stratified layer, a middle unstratified layer, and an upper stratified layer (see text for discussion). Unit 3a is capped by acoustically stratified sediments (unit 4), and underlain by unit 2, characterized by strong incoherent reflectors. Water depth at the deepest point in this profile is 137 m.



**Figure 21.** Hunttec boomer profile showing a region where the acoustic stratification that characterizes unit 3a gives way to poorly stratified sediments (unit 3b) in the west. Both units overlie unit 2. Water depth at the deepest point is 129 m.

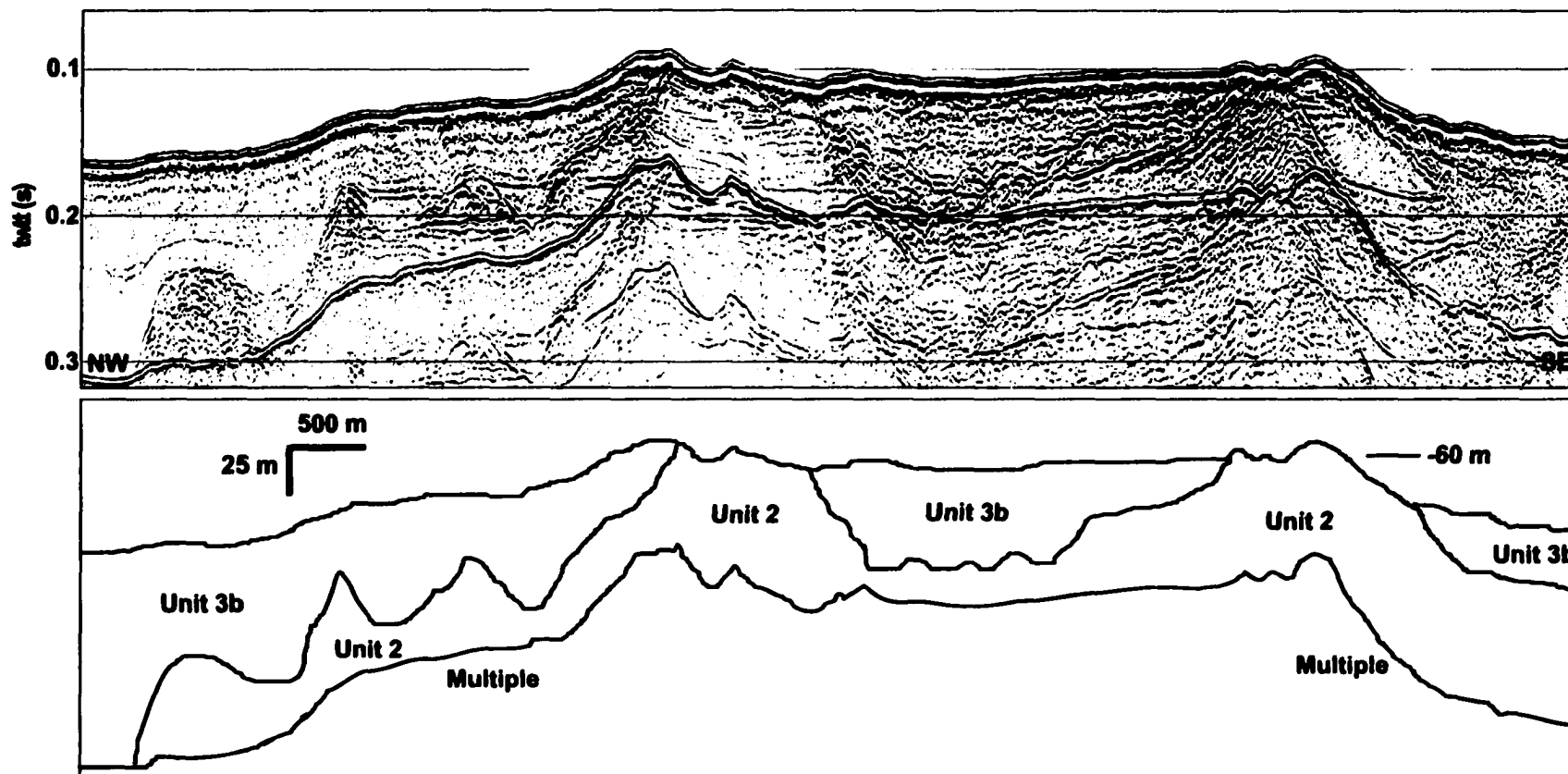


Figure 22. Airgun profile through a flat topped bank south of Victoria, showing some of the main seismic units. Reflectors in unit 2 sediments appear to be truncated in the shallow subsurface at a depth of around -60 m.

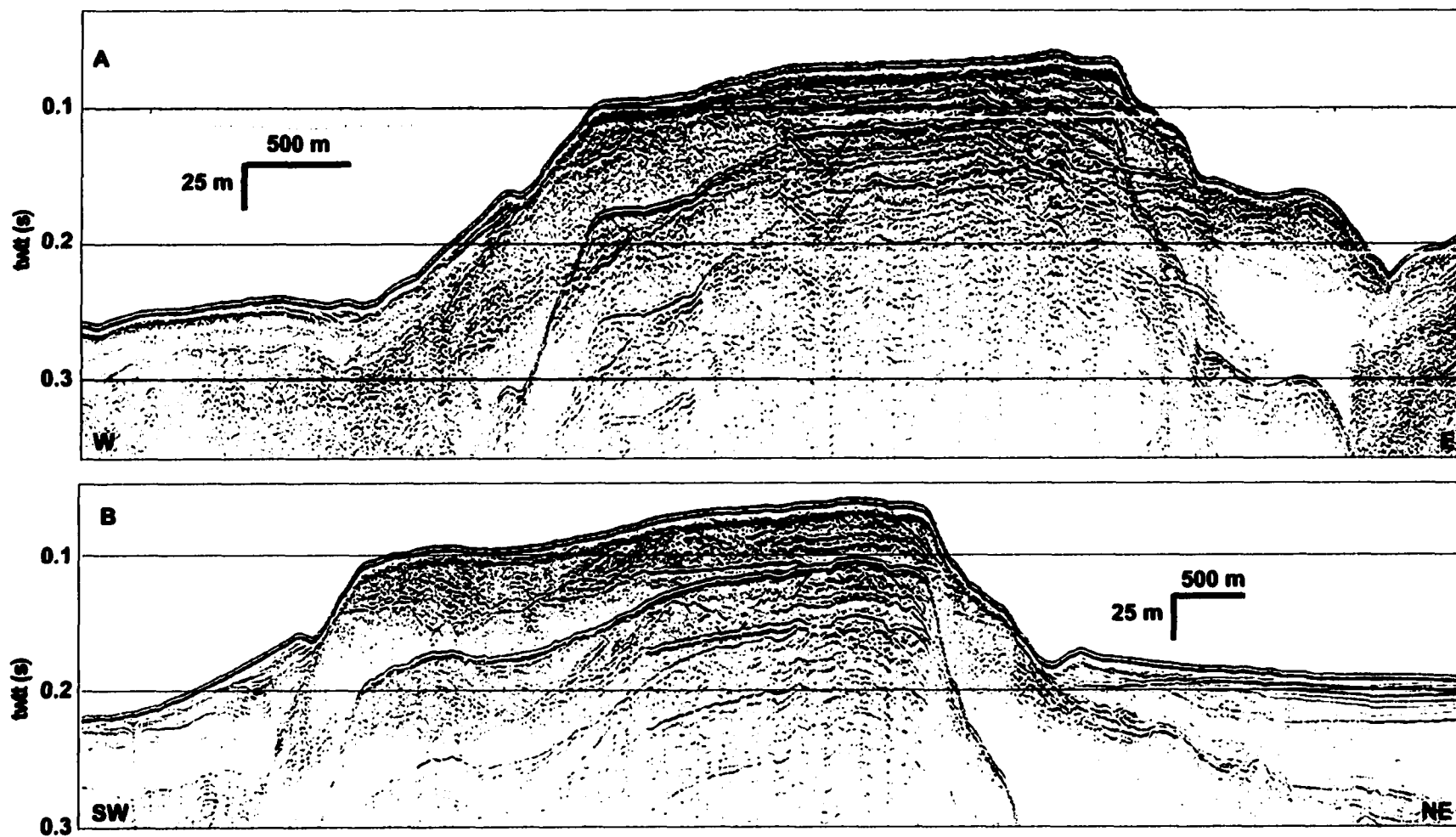


Figure 23. Airgun profiles through Eastern Bank. (A) is oriented west-east and (B) southwest-northeast. Interpretations are on following page.

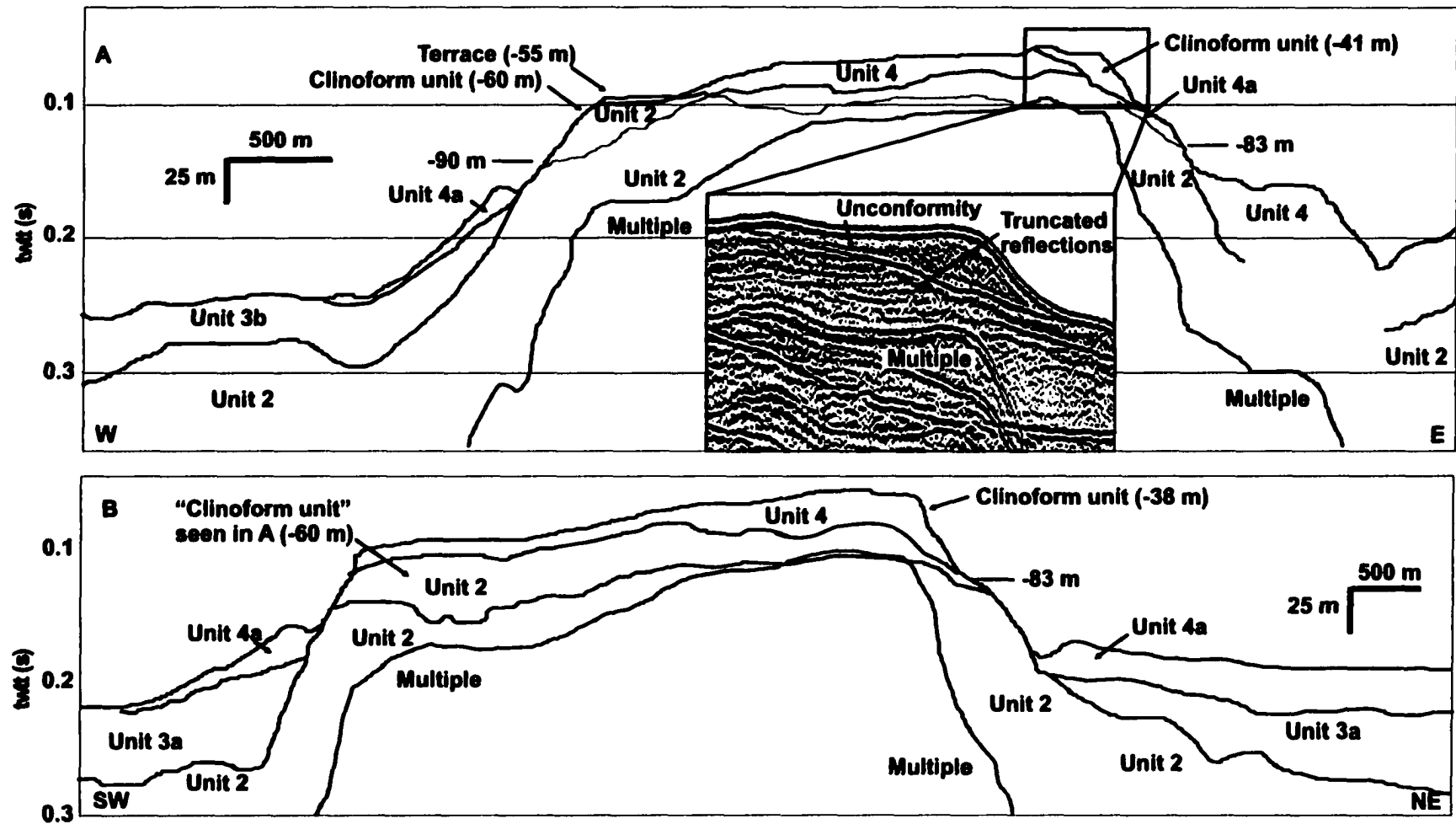


Figure 23. Continued from previous page. Clinoform units occur at a depths of 60 m and 41 m in (A). In (B), the clinoform unit at 60 m appears as a unit composed of semi-coherent reflectors. A small clinoform unit at 38 m occurs on the northern flank. The inset image in (A) shows deeper reflections truncated by an erosional unconformity beneath the clinoform unit at 41 m.

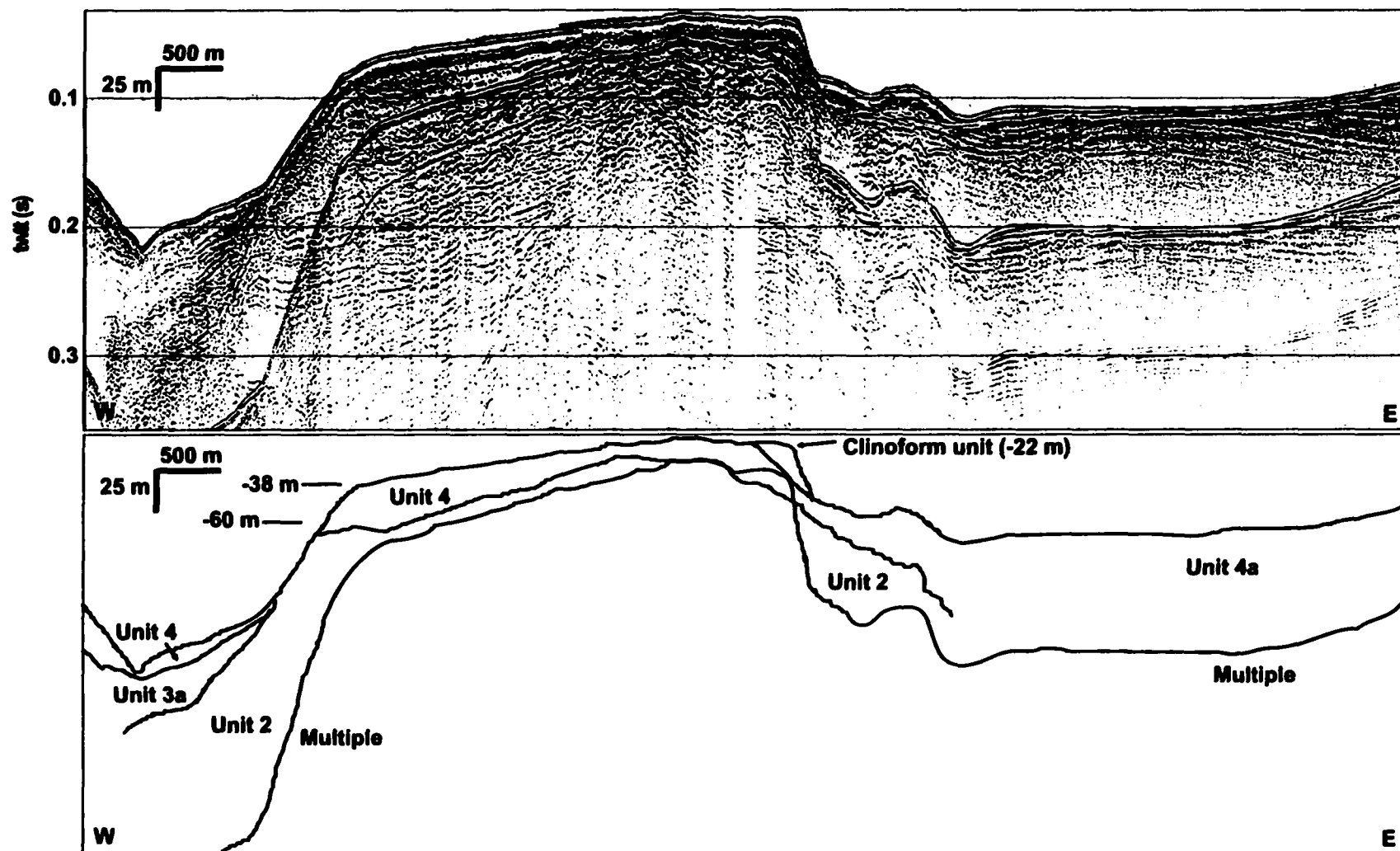


Figure 24. Airgun profile through Partridge Bank showing some of the main seismic units and a clinform unit at 22 m.

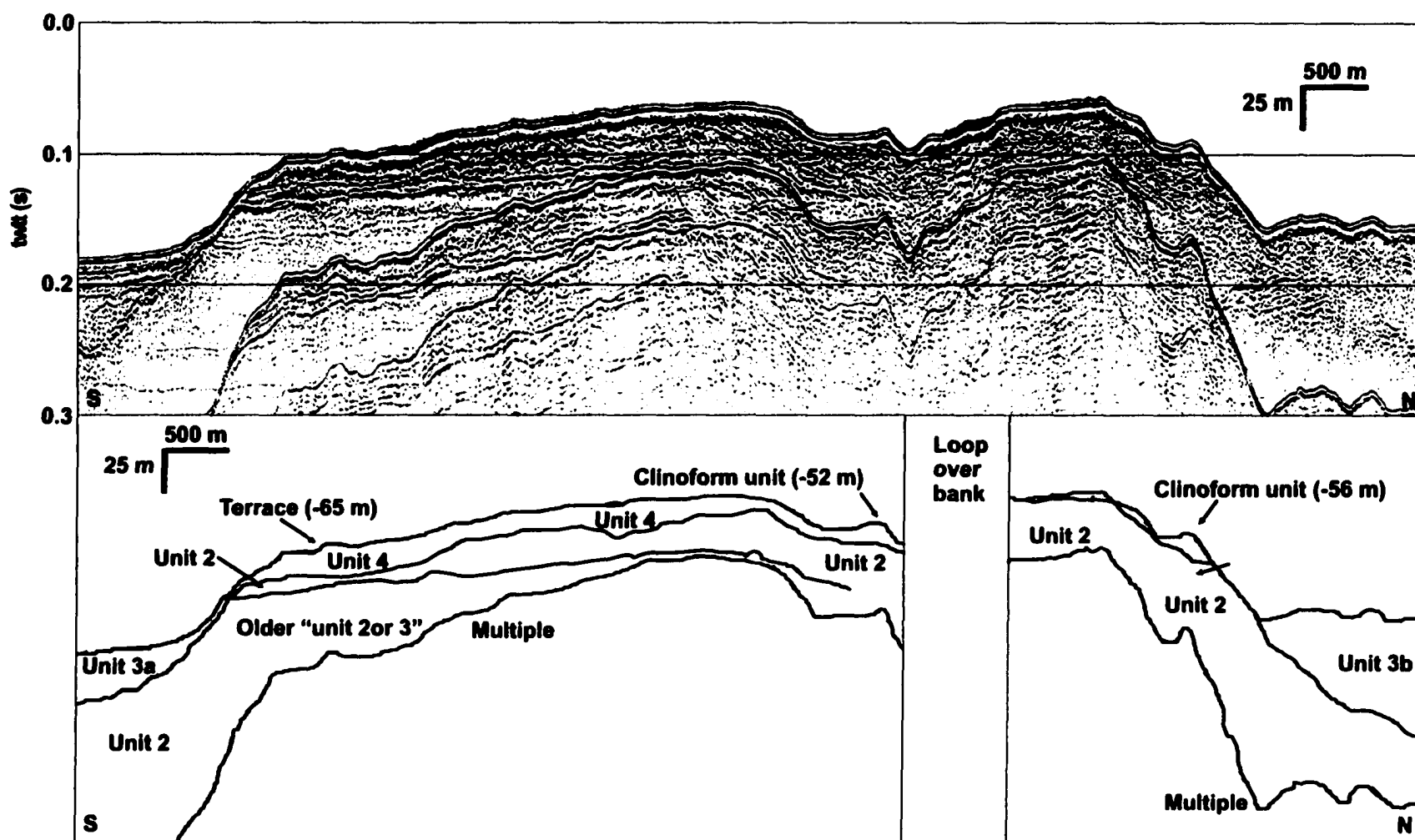


Figure 25. Airgun profile through the unnamed bank in the middle of the Strait, showing some of the main seismic units. A terrace occurs on the southern flank at a depth of 65 m, and a clinoform unit on the northern flank occurs at a depth between 52 and 56 m.



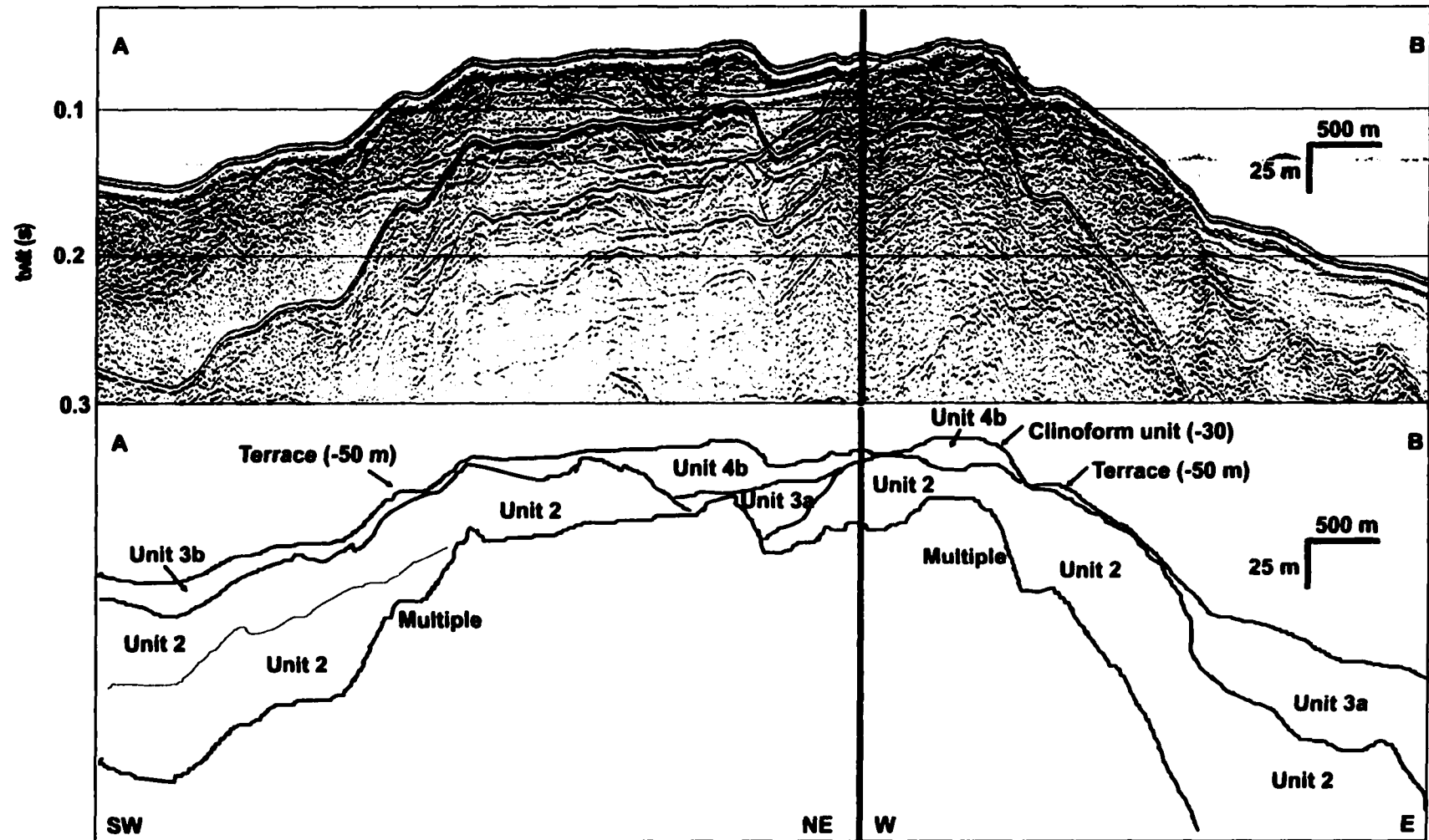


Figure 26. Airgun profile through Middle Bank, oriented southwest-northeast (A) and west-east (B). Showing a small clinoform unit at a depth of 30 m and terraces formed along its flank at 50 m. Reflectors in the sediments beneath the terraces appear to be truncated, as do the sediments in the shallow subsurface on the top of the Bank at 32 m.

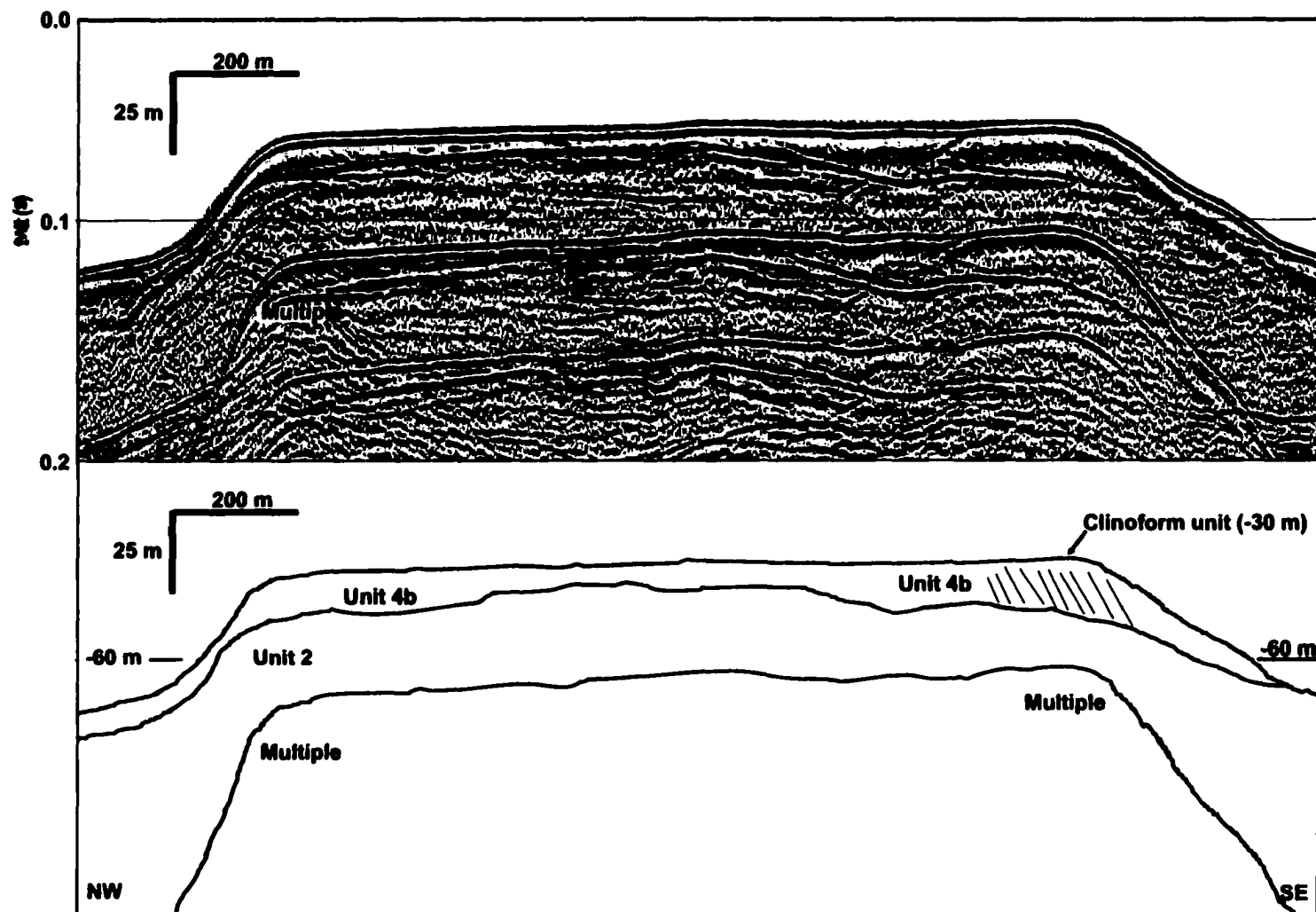


Figure 27. Airgun profile through Dallas Bank. The bank has a fairly flat top and reflectors in the shallow subsurface appear truncated, suggesting erosion. A clinoform unit on the southeastern flank occurs at 30 m.

The lowermost layer displays closely spaced discontinuous to semi-continuous reflections at its base and progressively more coherent reflections towards its top, giving it an acoustically well-stratified appearance. This layer may be overlain by a second layer, characterized by weak internal reflections, or sometimes a few widely spaced reflections, giving it an unstratified more transparent appearance in images. In the southeastern quadrant of the survey area, the second layer is overlain by a third, which is similar to the first layer, showing closely-spaced, coherent reflections (acoustically well-stratified). In airgun profiles, unit 3a appears similar to the Huntex profiles, but fewer internal reflections are resolved by the lower frequency airgun source (Fig. 18-20). Unit 3a is typically about 20 m thick, but locally varies between 0 and 50 m.

In the area west of the Victoria-Green Point Sill, and in the area between Victoria and Middle Bank, unit 3a shows a gradual lateral transition into unit 3b (Fig. 21). Unit 3b is distinct from unit 3a in that it displays relatively incoherent internal reflections in both single-channel and boomer records (Fig. 18 & 21), giving it an acoustically unstratified appearance. The incoherent reflections are not as strong as in unit 2 giving it a somewhat lighter tone than unit 2, but darker than unit 4. In addition, unit 3b is typically thinner than unit 3a, varying between 0 and 20-m thick. In some single-channel profiles, unit 3b is separated from unit 2 by a zone of hyperbolic reflections instead of a well-defined coherent reflection (Fig. 18).

#### **Unit 4**

Unit 4 represents the uppermost seismic unit, and overlies the other units in a variety of unconformable relationships, including non-conformable drape, offlap, and

downlap (Fig. 17, 19, 28-31), and bedforms are common (Fig. 30). Unit 4 is further subdivided into two subunits, unit 4a and unit 4b. Unit 4a is acoustically well stratified, but compared with unit 3a, reflections are not as strong and are more widely spaced, and the overall tone is usually lighter in seismic imagery (Fig. 19 & 28). Unit 4a occurs in nearshore areas, and on the flanks of some banks. In these locations, it occurs as wedge-shaped packages of inclined ( $<2^{\circ}$ ) reflections that downlap onto unit 3a (Fig. 19 & 28). Typically, unit 4a is 0 to 20 m thick, but locally reaches 100-m thick near Whidbey Island.

Unit 4b is acoustically unstratified and often appears darker in tone than unit 4a (Fig. 20), and is thinner, typically 0 to 10 m thick, and often has large scale ( $>1$  m) bedforms on its surface. The internal structure of individual bedforms can be seen in some seismic profiles (Fig. 30).

### **Unconformities**

Offshore of Victoria, in areas shallower than 65 m, the bounding reflection at the top of unit 3a often truncates the internal reflections within the unit, suggesting an unconformity (Fig. 31). In waters deeper than 65 m, the contact between unit 3 and overlying unit 4 appears conformable. In another location along Victoria's offshore, seismic-reflection data show a stepped or terraced sub-seafloor reflection at the surface of unit 3 (Fig. 29). Terrace tops occur at depths of 41, 43, 46, 51 and 60 m, and like the unconformity in Figure 31, they are buried beneath unit 4.

Unconformities and terraces are seen on many of the banks in the strait, as well. For instance, Figure 22 shows an airgun profile from an area of relatively shallow water

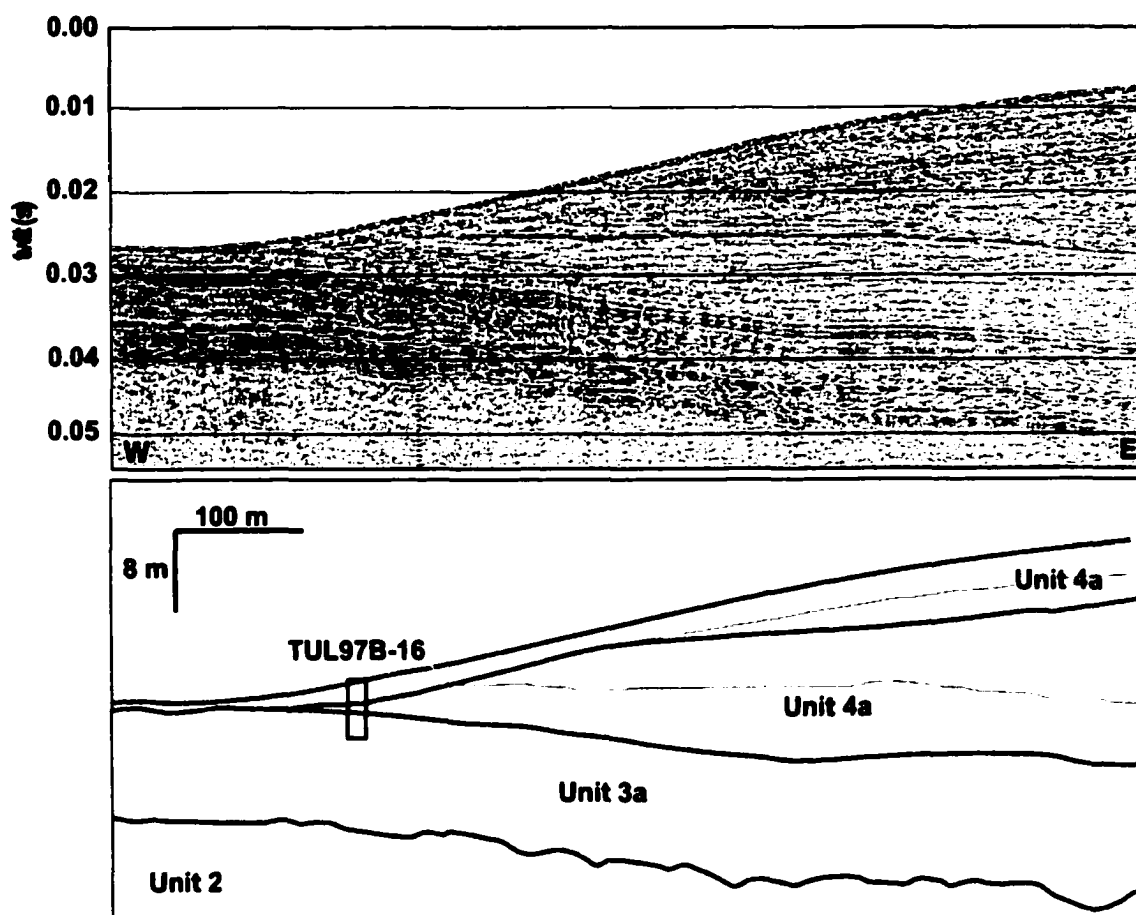


Figure 28. Hunttec boomer profile showing a thick section of unit 4a sediments. There appear to be several unconformities within unit 4a. Unit 4a overlies unit 3a which, in turn, overlies unit 2. Unit 3a sediments are stratified throughout their thickness, and the acoustically unstratified middle layer that occurs in the southeast is absent (e.g. Fig. 20). The position and approximate depth of penetration of piston core TULB97-16 is shown. Water depth at the deepest point is 104 m.

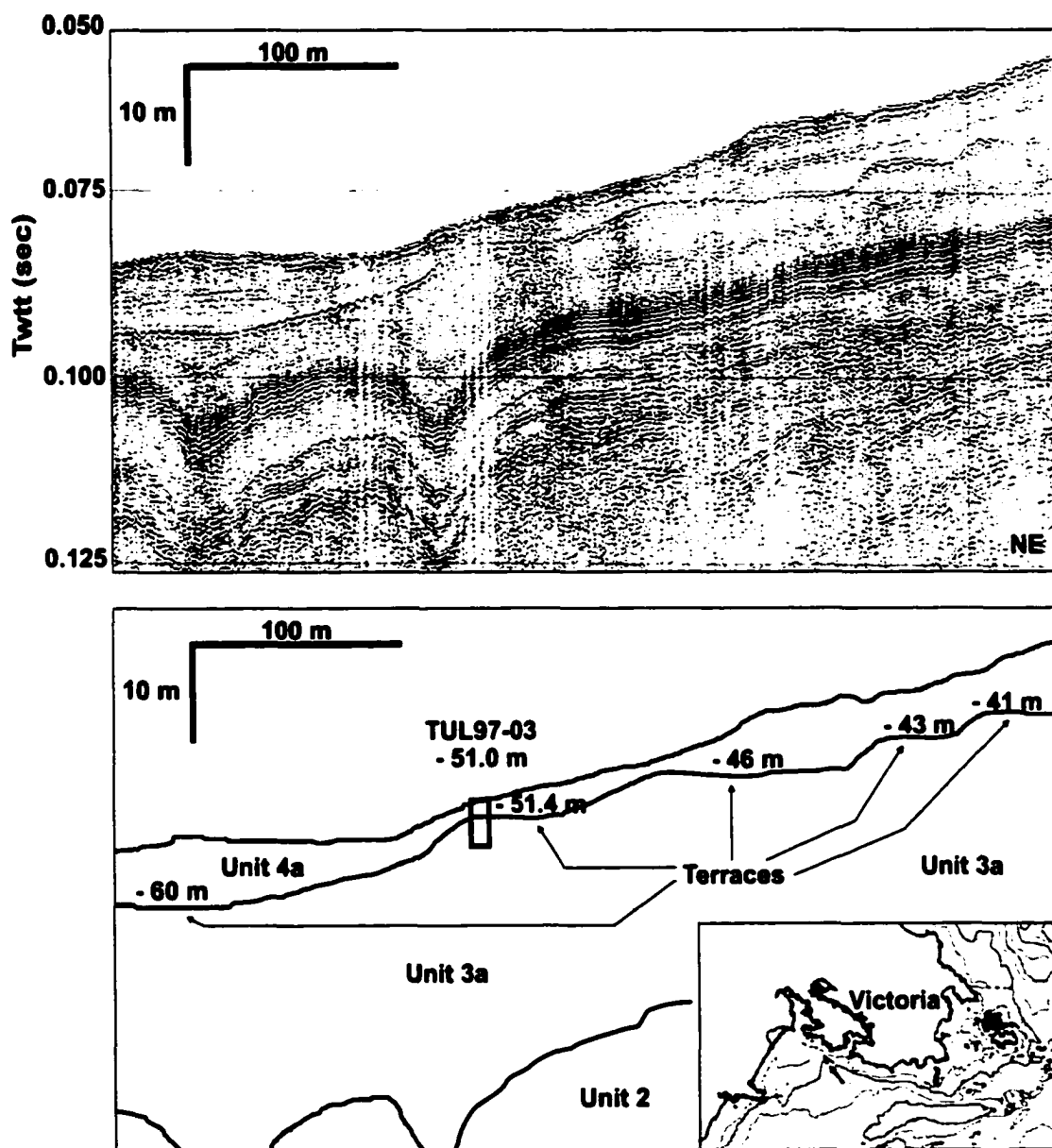


Figure 29. Seistec profile off Victoria showing a series of erosional terraces in unit 3a sediments.

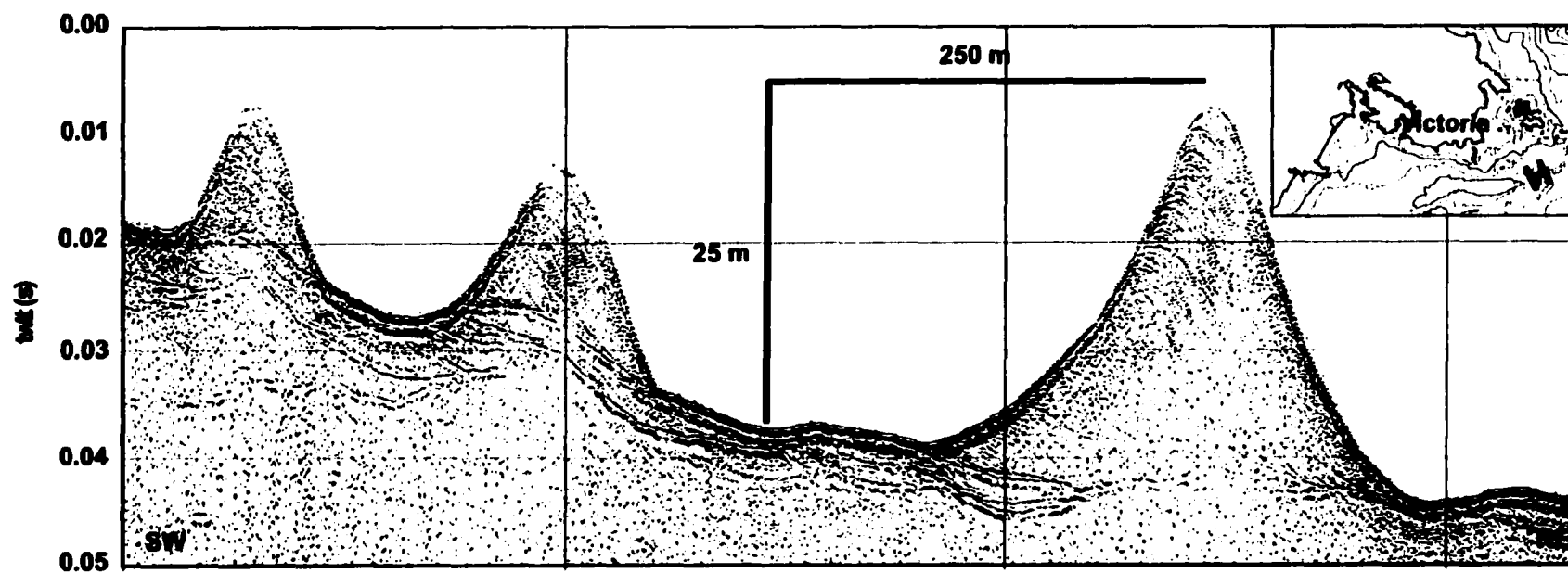


Figure 30. Huntec boomer profile through a sand wave field off Victoria. Clinoform reflectors are interpreted as cross-stratified beds and indicate migration is toward the northeast. Water depth at the deepest point is 97 m.

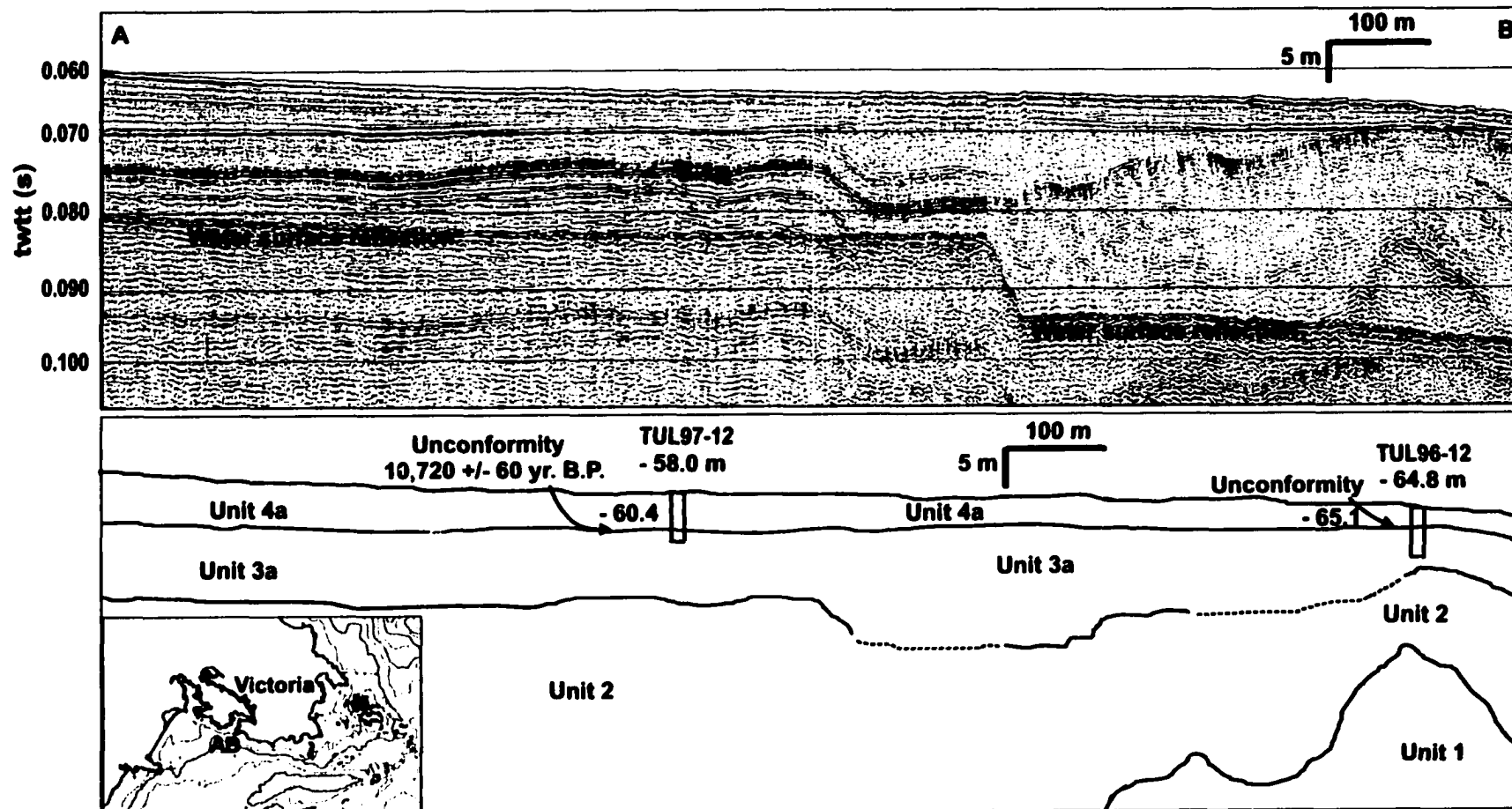


Figure 31. Huntect profile off Victoria, showing an erosional unconformity in unit 3a sediments. A shell at 60.4 m below the sea surface, just above the unconformity in core 97-12, yielded a date of 10720  $\pm$  60  $^{14}\text{C}$  yr. B.P. The same stratigraphic sequence is seen in core 96-12.



east of Constance Bank, where the seafloor rises to form an embankment with a relatively flat top at a depth of around 60 m. Reflections within unit 2 appear to have been truncated, suggesting erosion. Another terrace is seen on the western flank of an unnamed bank in the middle of the strait at a depth of 65 m (Fig. 25). Middle Bank was crossed by two airgun profiles oriented west-east and southwest-northeast (Fig. 26). There are terraces on the eastern and southern flanks at 50 m, and a flat area occurs on the bank's surface at a depth of 32 m.

There are fewer examples of terraces or unconformities in seismic data from along the Olympic Peninsula and offshore of Whidbey Island. This fact is probably because unit 3 is buried by the thick accumulations of unit 4, and because there is less seismic data from close to shore in these areas. However, in a seismic profile near Ediz Hook, clinoforms appear truncated by a seafloor terrace at a depth of 65 m, suggesting an erosional unconformity (Fig. 13). Unconformities occur also in unit 4 sediments in deeper water. For example, the wedge shaped deposits on the western flank of McArthur Bank and west of Whidbey Island (Fig. 19 and 28) show packages of parallel, inclined reflections that have slightly different orientations than in adjacent packages.

### **Climoform units**

Wedge shaped deposits composed of steeply dipping reflections ( $\sim 8^\circ$  to  $9^\circ$ ) form clinoform units on several of the banks and nearshore areas of the strait. These features share several common characteristics: (1) clinoforms dip toward deeper water; (2), they are deposited over seismic units 2 and 3, and appear to be associated with unit 4; and (3),

a prominent reflection dipping seaward at  $\sim 4^\circ$  defines the base of clinoform units and appears to truncate reflections in underlying units, suggesting erosional unconformities.

There are two airgun profiles through Eastern Bank (Fig. 23). One is oriented west to east and shows a clinoform unit with its top at a depth of 60 m on the bank's western flank (Fig. 23). The basal reflection (unconformity) slopes seaward from 53 to 90 m depth. Another clinoform unit in this profile occurs on the bank's eastern flank at a depth of 41 m and has a basal reflection sloping from 38 to 83 m. The second seismic profile through Eastern Bank is oriented southwest to northeast (Fig. 23). From this orientation, the clinoform unit that is seen in the east-west profile at a depth of 60 m is represented by a flat-topped unit composed of semi-coherent reflections, and a relatively undulous basal reflection. A smaller clinoform unit has its top at a depth of 38 m on the northern flank.

Other examples of clinoforms occur on the eastern flank of the un-named bank at a depth of 52 m, with a basal reflection sloping from 53 to 64 m (Fig. 25); on Middle Bank at a depth of 30 m (Fig. 26); on Dallas Bank at a depth of 30 m with a basal reflection sloping from 30 to 60 m (Fig. 27); and On Partridge Bank at a depth of 22 m, with a basal reflection sloping from 38 to 60 m (Fig. 24). There is a clinoform unit offshore of Green Point at a depth of 60 m, with a basal reflection sloping from 60 to 83 m (Fig. 32). In the vicinity of Ediz Hook, a seismic profile through the lobe-shaped platform reveals clinoforms seaward dipping graded to a depth of 48 m (Fig. 13).

A seismic profile in the approaches to Admiralty Inlet reveals two large clinoform units (Fig. 33). This terrain style ends in the gap between Dallas Bank and Partridge Bank where two lobes of sediment appear to splay across the ocean floor for a distance of

around 2000 m, on either side of a small bathymetric high. An airgun profile through one of these lobes shows it is 2400 m wide, 65 m thick, and its top occurs at 70 m water depth (in the location of the seismic profile; Fig. 34). The internal structure consists of clinoforms down-lapping at angles of 5 to 9° on both sides. The clinoforms appear to be truncated by the basal reflection in a capping layer of unit 4 at a depth of 80 m.

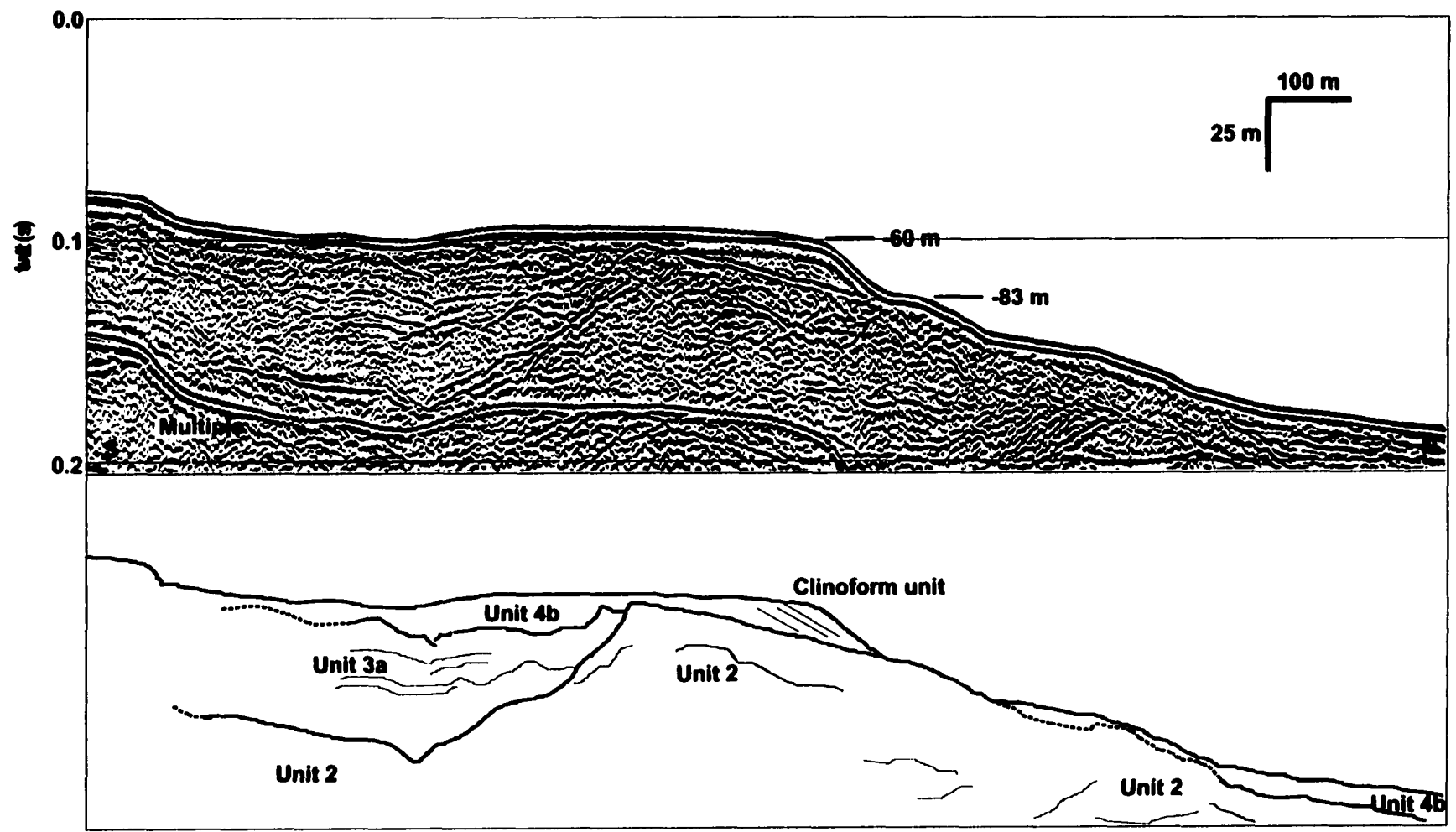


Figure 32. Single channel seismic section showing a clinoform unit offshore of Green Point at a depth of 60 m.

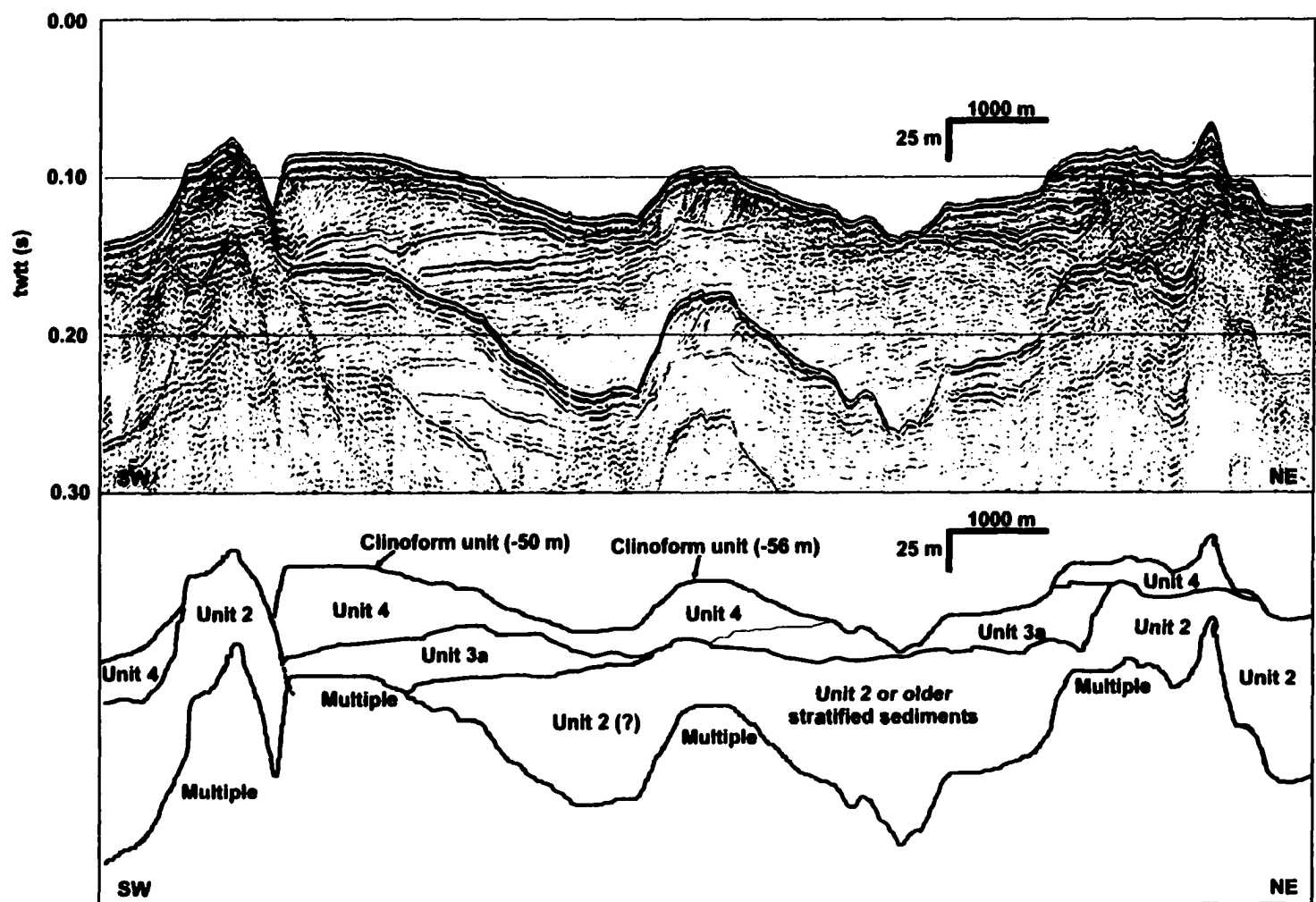


Figure 33. An airgun profile through two ridge features in Admiralty Inlet, at the entrance to Puget Sound, reveals two large clinoform units overlying units 3a and 2, or older stratified deposits.

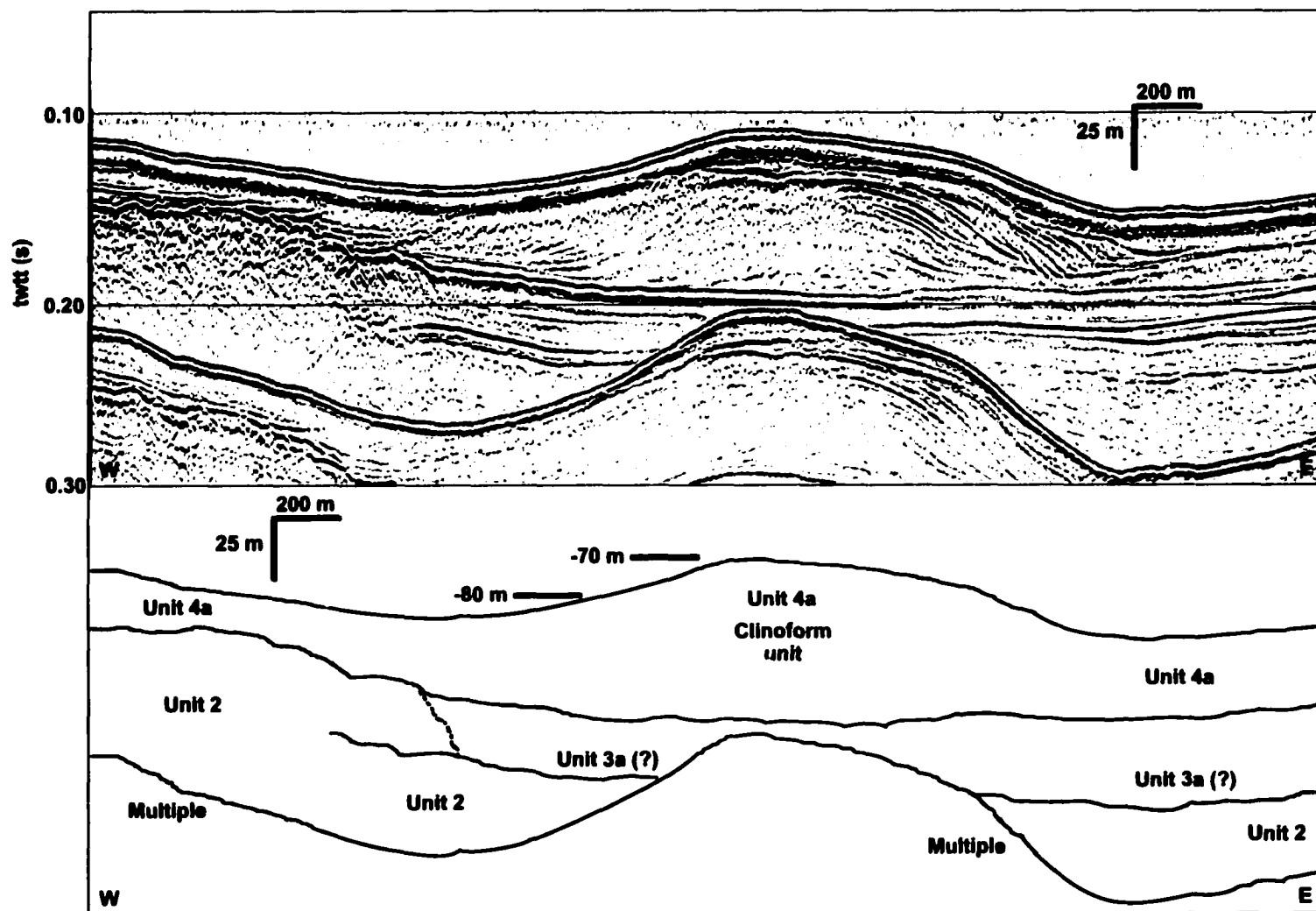


Figure 34. Airgun profile through a sediment lobe near the entrance to Admiralty Inlet. It differs from the examples in Figure 33 in that clinoforms dip down both sides of the lobe.

## **CHAPTER V**

### **LITHOSTRATIGRAPHY, SEDIMENTOLOGY, AND DISTRIBUTION OF SURFICIAL GEOLOGIC UNITS**

#### **Correlation of Cores to Seismic-reflection Profiles**

Since care was taken to position core sites directly over features selected from seismic-reflection profiles, it is assumed that cores have sampled the targeted surficial seismic units. It is also assumed that the pronounced regional reflections that separate the main seismic units correspond to the major changes in core lithology and sediment physical properties. However, there is less certainty in correlation between lithologic layers in cores and the internal reflections within a particular seismic unit. This uncertainty results because several factors control the nature of seismic-reflections. The amplitude and spatial frequency of reflections in seismic profiles are controlled by the amplitude and frequency bandwidth of the seismic source, the velocity-density contrast at bedding interfaces, and the spacing of contrasting surfaces. If contrasting surfaces are very close (i.e. thin beds) compared to the source wavelength, then reflections from each interface will interfere to produce a composite reflection, whose amplitude depends on whether the interference is constructive or destructive. An amplitude excursion may, therefore, represent a reflection from a single bedding surface, or from several closely spaced beds. For this reason, there is not necessarily a one-to-one correlation between the parallel reflections that occur in unit 3a and the lithologic changes in the cores. It is

believed, nevertheless, that the major lithologic changes are represented in seismic profiles as echo-character changes.

### **Lithology, Physical Properties, and Age**

#### **Units 1 and 2**

Because the high-amplitude surface reflection of unit 1 suggests very high density and/or high velocity (hard) material, no attempts were made to sample it. Similarly, unit 2 appears to have a highly reflective surface, and attempts to core it resulted in recovery of only one core from the top of Hein Bank (core TUL97B-10). This core contained 59 cm of pebbly-sand with abundant shell fragments that is interpreted to be a capping lag on the surface of unit 2, and not considered representative of the unit throughout its thickness.

#### **Unit 3**

Unit 3 was sampled in many cores (Table 1). The general composition is silty-clay with variable amounts of sand, gravel, and shell fragments (Fig. 35). Core TUL96B-12 (Fig. 36) sampled the top of the lower, acoustically stratified layer in unit 3a, which consists of light-gray silty-clay, interbedded with dark silt layers (1-5 cm thick) and lenses of fine sand (up to 1 cm thick). In addition, pebbles are scattered throughout the core, but are concentrated in diamicton layers a few centimeters thick. Some of the silty and sandy beds are laminated, fining upward sequences, suggestive of turbidites. Cores that sampled the acoustically unstratified middle layer of unit 3a (Fig. 37 and 38), consist of mostly massive silty-clay, and only rare pebbles and a few silt laminae < 1 cm thick.



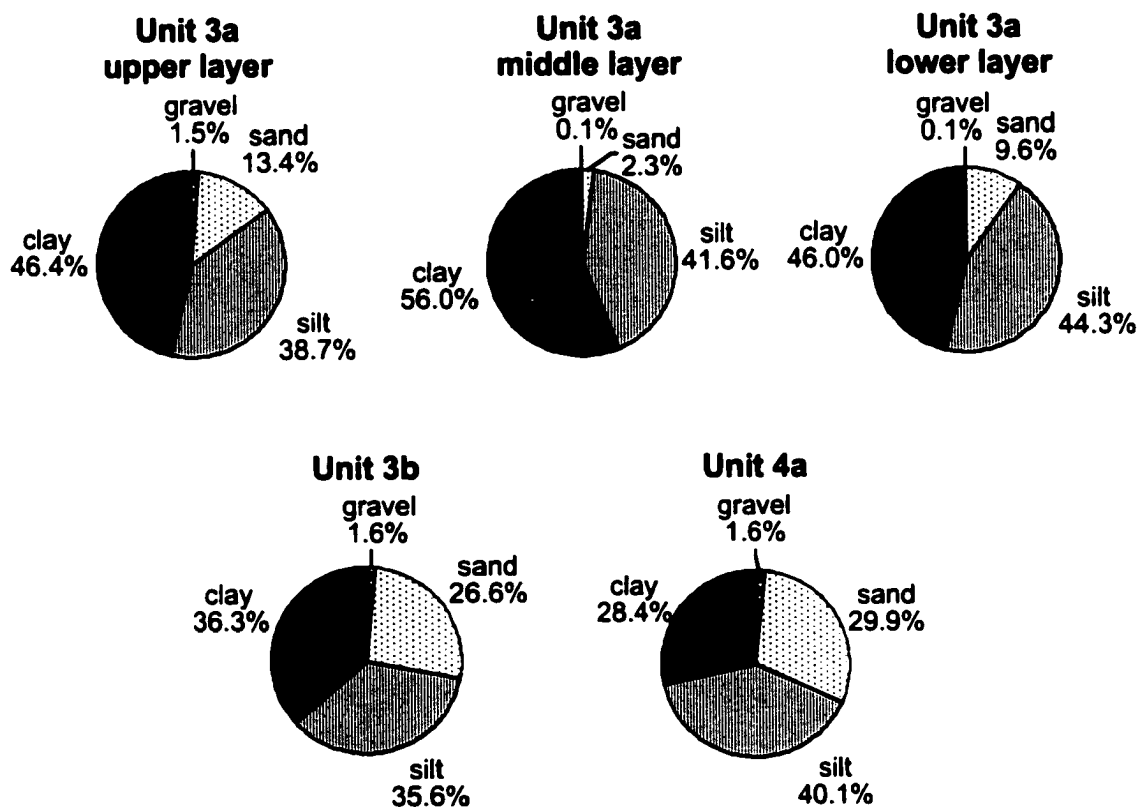


Figure 35. Average grain size (weight %) in the indicated seismic-acoustic units based on grain size measurements given in table 2.

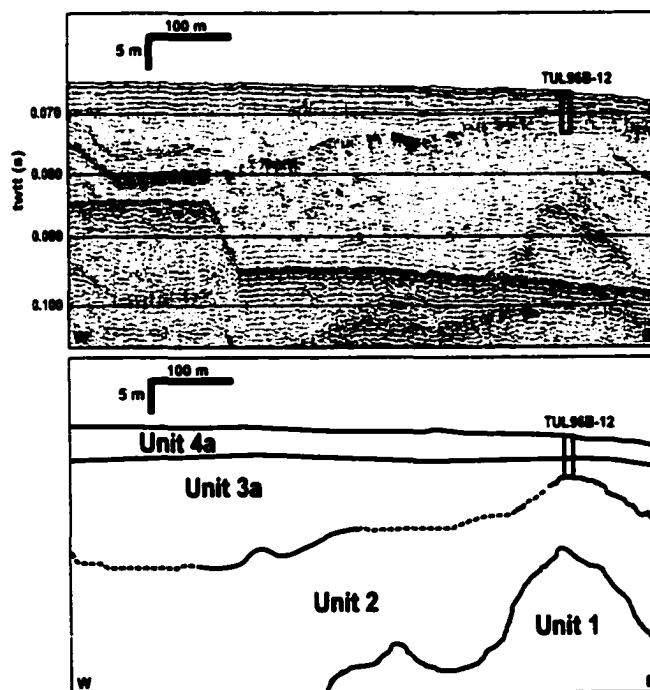
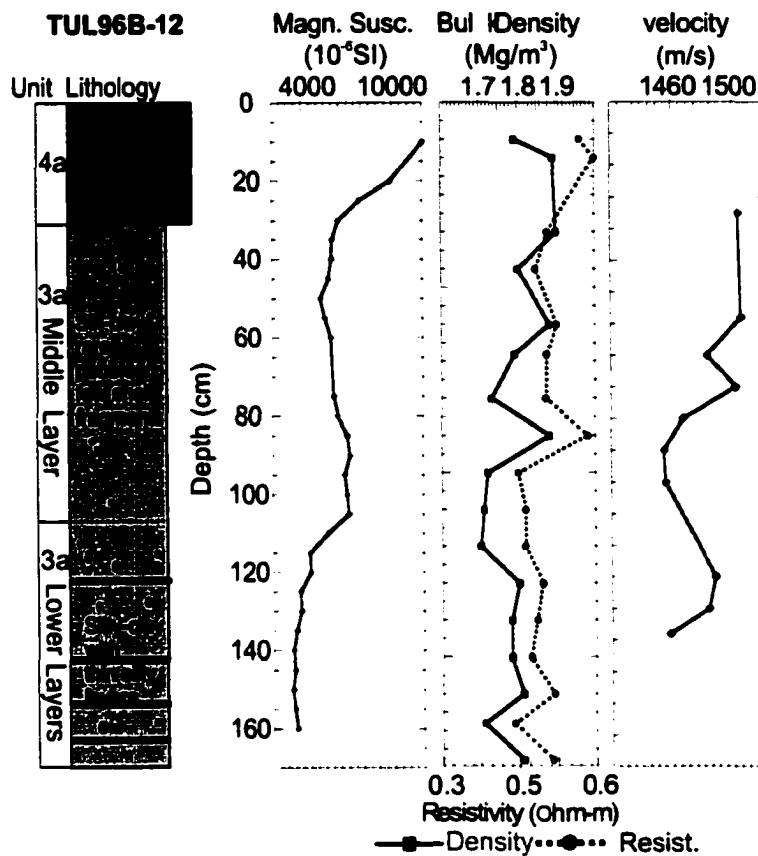


Figure 36. Lithologic description and physical properties measured in core TUL96B-12 that sampled both the middle acoustically unstratified layer of unit 3a, and the lower stratified layer. The core also sampled a 30 cm thick layer of unit 4a at the top.

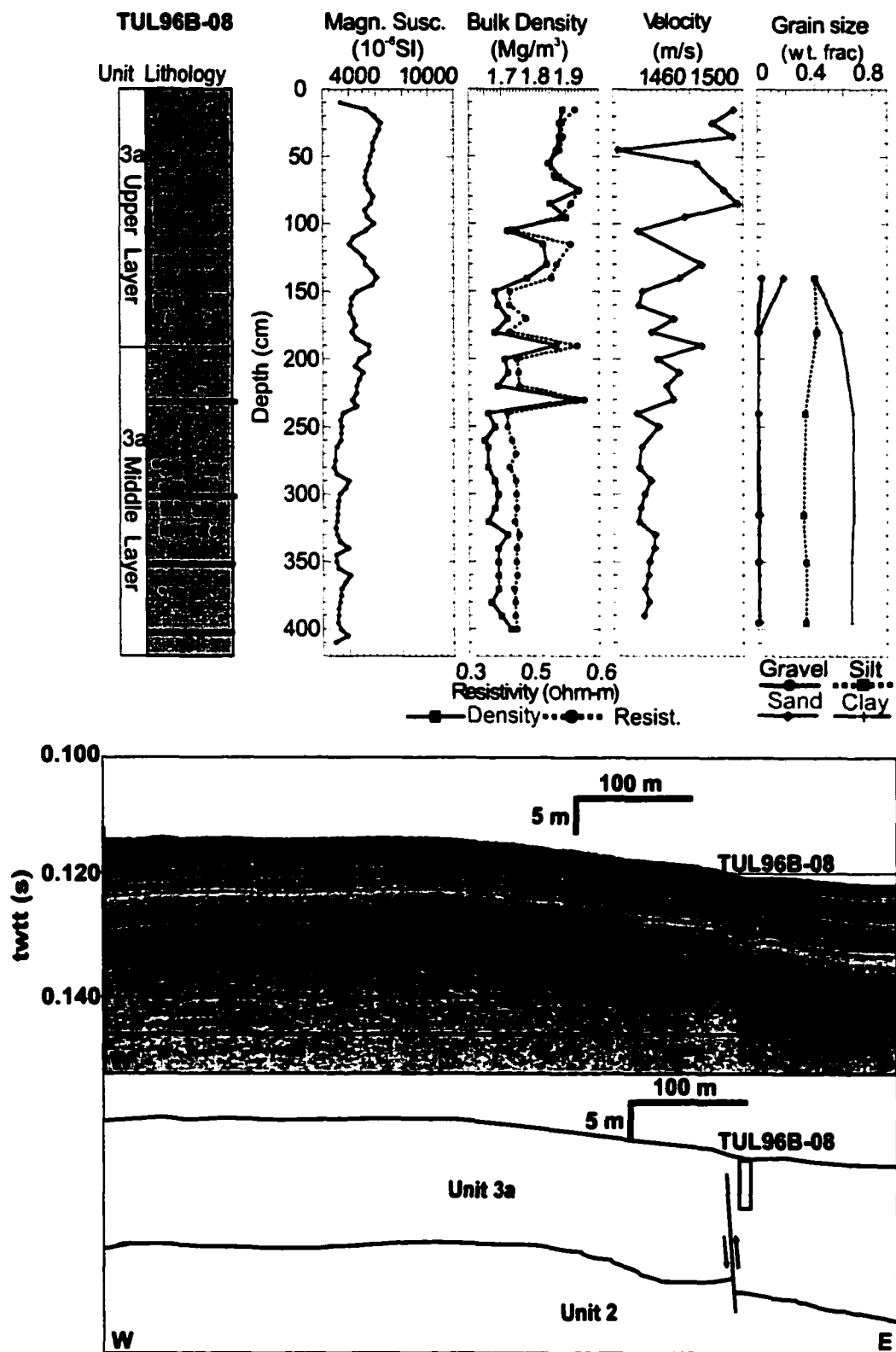


Figure 37. Lithologic description and physical properties measured in core TUL96B-08 that sampled both the upper acoustically stratified layer and the middle unstratified layer of unit 3a.

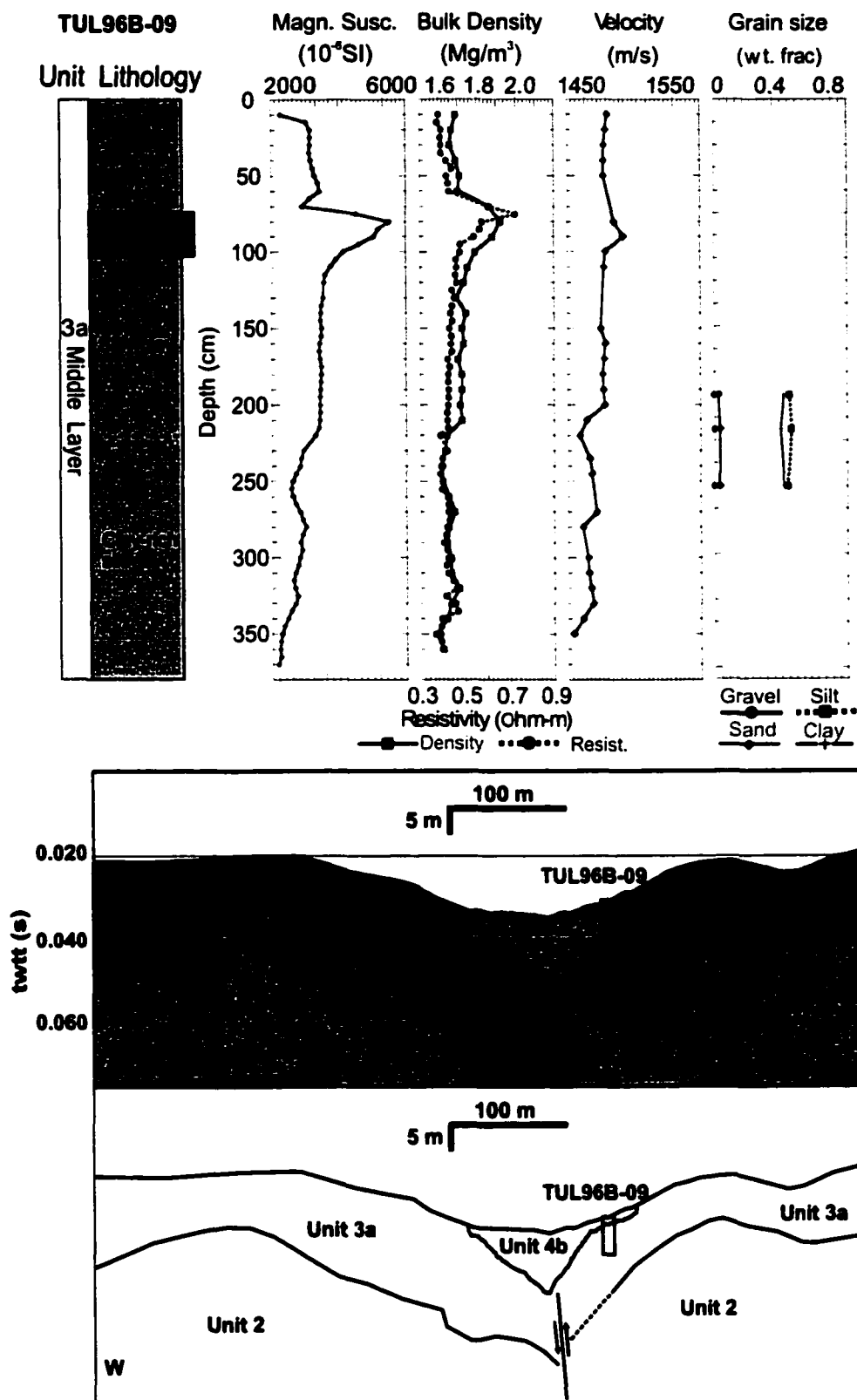


Figure 38. Lithologic description and physical properties measured in core TUL96B-09, showing an example of the acoustically unstratified middle layer of unit 3a.

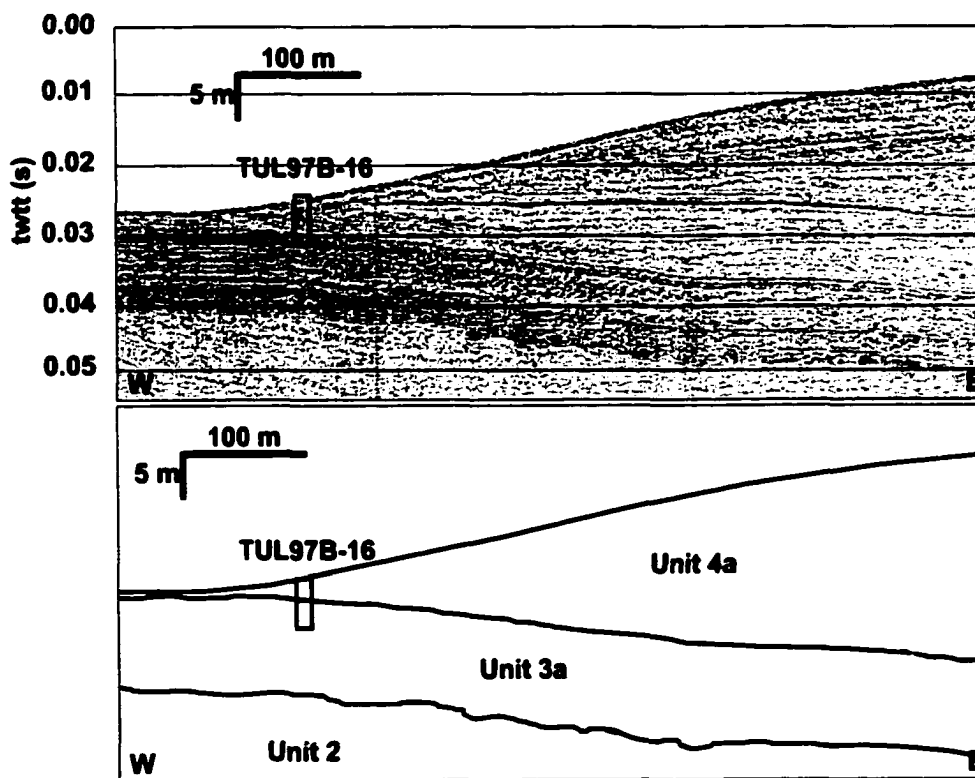
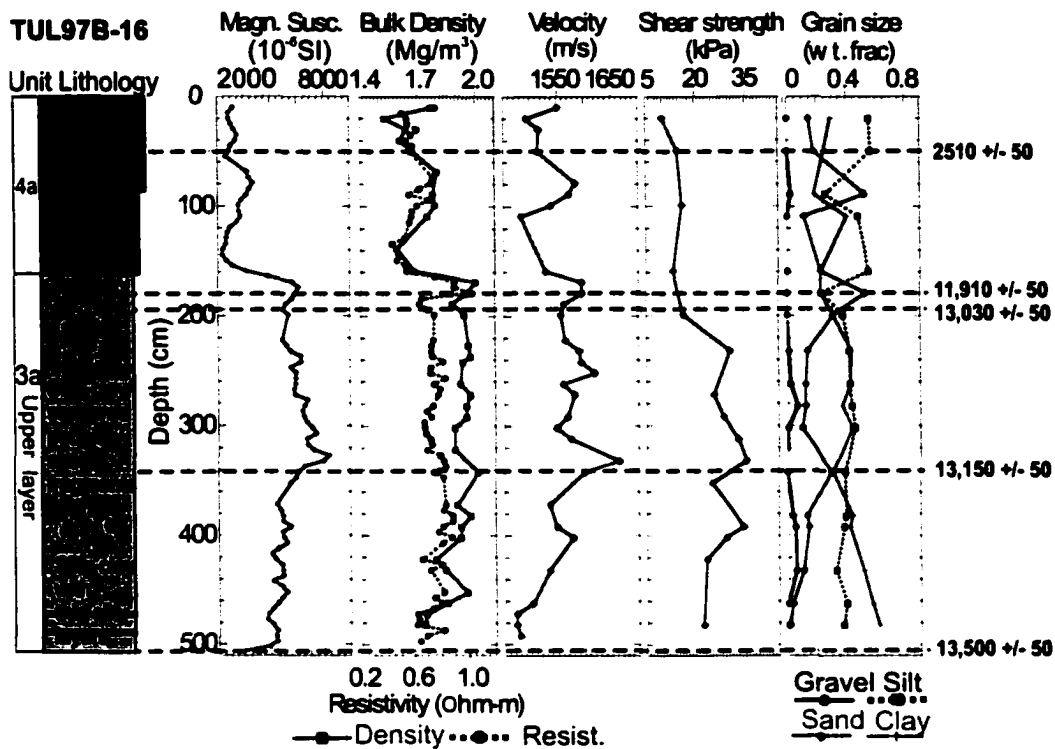


Figure 39. Lithologic description and physical properties measured in core TUL97B-16, considered representative of unit 4a and the upper layer of unit 3a.

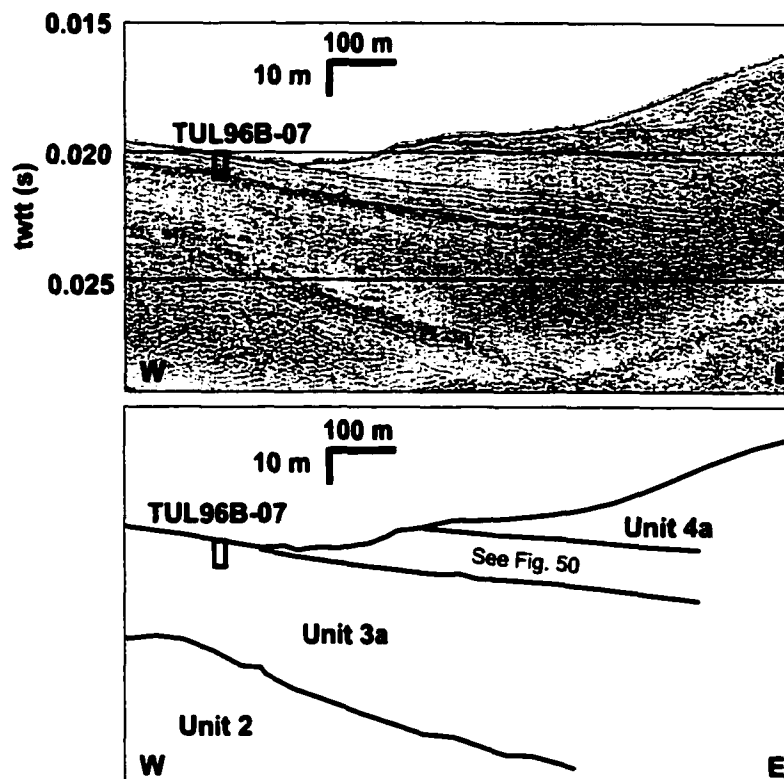
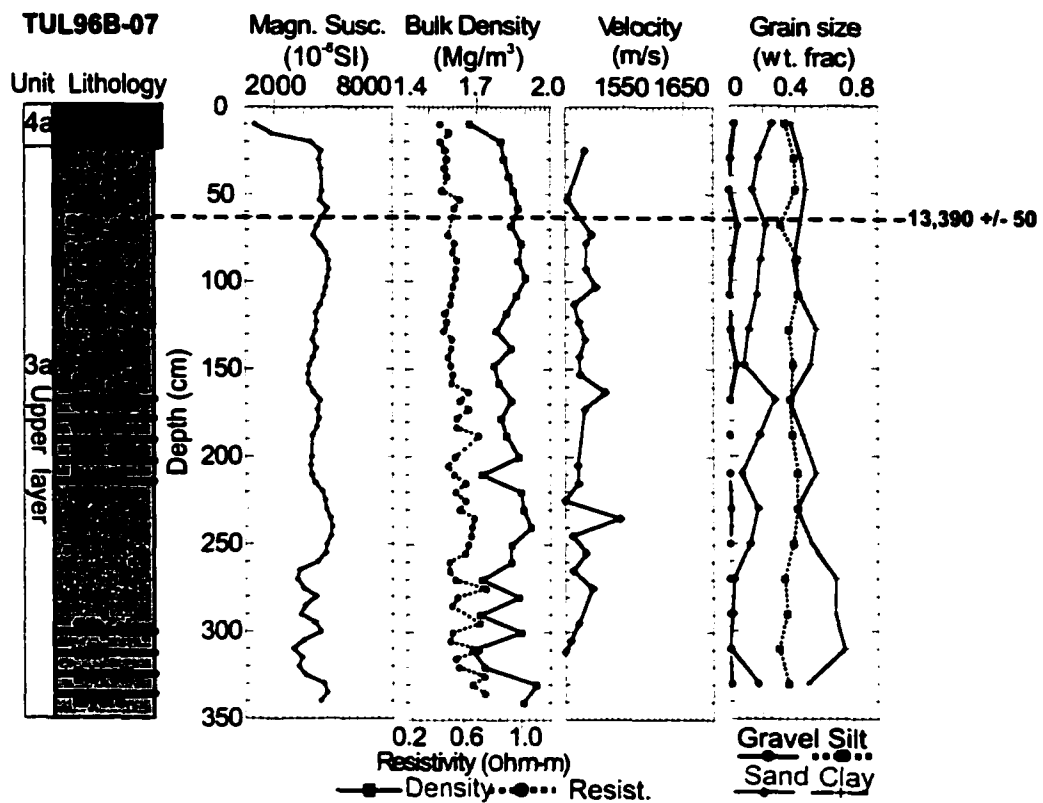


Figure 40. Lithologic description and physical properties measured in core TUL96B-07, which sampled the upper acoustically stratified layer of unit 3b.

Where present, the upper acoustically stratified layer of unit 3a consists of dark-gray silty lenses (1-3 cm thick) interbedded with light-gray silty-clay layers that are 10's of cm thick (Fig. 39 and 40). Pebbles are more common than in the middle layer (about 1 pebble per 10 cm), though less common than in the lower layer.

Core TUL96B-02 (Fig. 41) is from a transition region between the acoustically stratified unit 3a, and the unstratified unit 3b. The top of this core samples unit 3b, which contains a greater concentration of sand and pebbles than typically found in unit 3a. Toward the bottom of the core, the silty-clay component increases and sediments resemble those of unit 3a. Shell fragments were observed only in the top 20 cm of the core.

Sediment bulk densities in unit 3 fall between 1.65 and 2.00 Mg/m<sup>3</sup>, P-wave velocities range from 1450 to 1650 m/s, and shear strength was typically between 15.0 and 35.0 kPa. The upper layer of unit 3a has, typically, a greater range and overall larger values for measurements of velocity, magnetic susceptibility, and bulk density compared with the middle layer. The lower layer in unit 3a has an acoustic character similar to the upper layer and has a similar range of values for physical properties, although slightly greater on average, possibly due to its greater depth of burial. Unit 3b has higher values of bulk density and velocity (average of 1.89 Mg/m<sup>3</sup> and 1566 m/s) compared with unit 3a (Table 2).

Radiocarbon dates from shell material in unit 3 fall between 13,690 ± 50 <sup>14</sup>C yr B.P. and 11,910 ± 50 <sup>14</sup>C yr B.P. (Table 1). There is one exception to this range of dates from core TUL97B-04, where a date of 3360 ± 40 <sup>14</sup>C yr B.P. was obtained; however, it

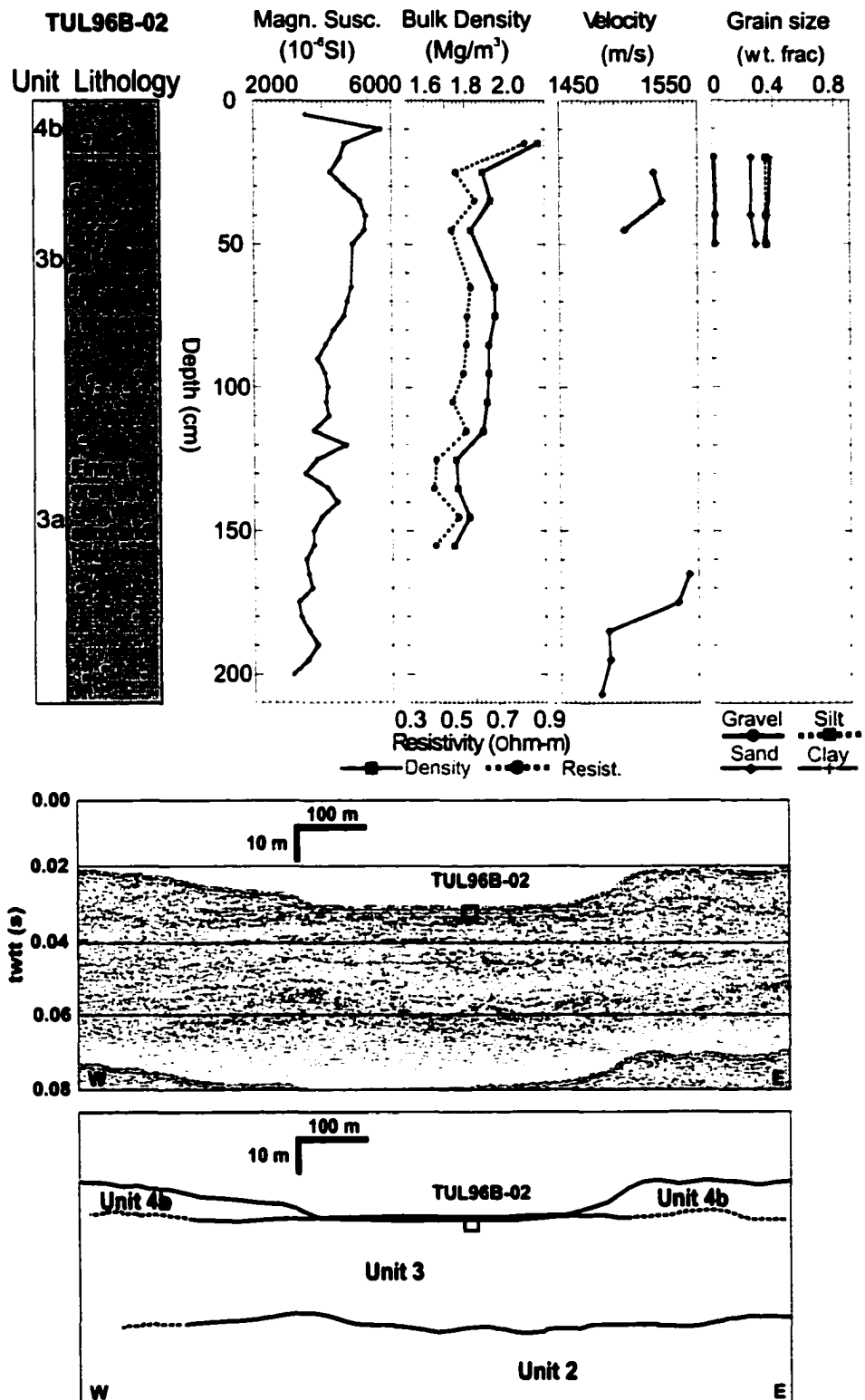


Figure 41. Lithologic description and physical properties measured in TUL96B-02 that sampled sediments from a transitional region between the acoustically stratified sediments of unit 3a and less well stratified sediments of unit 3b. At the top of the core is a thin layer of unit 4b that is not visibly resolved by the Hunttec system.



comes from just a few centimeters below the transition into unit 4, and so is probably from younger material reworked into unit 3.

#### **Unit 4**

Unit 4 is found in the top few centimeters of most cores, where it consists of predominantly sandy-silt, although, gravel, sand, silt or shell fragments may be the dominant constituent, on occasion. Lithologies of unit 4 are readily distinguished from unit 3 on the basis of color and grain-size. In addition, there is a marked difference in most of the physical properties between the two units; in particular unit 4 has lower bulk density, magnetic susceptibility, and shear strength compared with unit 3 (Table 2). The oldest date obtained from unit 4 was  $10,930 \pm 50$   $^{14}\text{C}$  yr B.P. and the youngest date was  $190 \pm 50$   $^{14}\text{C}$  yr-B.P (Table 1).

The sediments of acoustically stratified unit 4a are well represented in core TUL96B-04 (Fig. 42) and the top of core TUL97B-12 (Fig. 43). Unit 4a consists of mainly olive-green-colored, sandy mud with abundant shell fragments (mostly bivalves). There are also irregularly spaced, fining upward sequences (a few cm thick) with sharp basal contacts that are interpreted as turbidities. Wet bulk densities in unit 4 range from 1.40 to 1.80  $\text{Mg/m}^3$ , acoustic velocities are typically between 1450 and 1600 m/s, and shear strengths are less than 25.0 kPa.

Unit 4b was sampled in several cores. Typically, it is coarser grained than unit 4a, and is composed mainly of sand and variable concentrations of gravel and shell fragments. The predominance of sand resulted in shorter cores, and caused pore water to drain rendering most measurements of sediment physical properties unreliable.

Table 2. Average values for physical properties in selected cores considered representative of the main seismic-stratigraphic units

Unit		Bulk density (Mg/m <sup>3</sup> )	Velocity (m/s)	Mag. susceptibility (10 <sup>-4</sup> SI)	Shear Strength (kPa)	Grain size (weight %)				Core
						gravel	sand	silt	clay	
Unit 1		NS	NS	NS	NS	NS	NS	NS	NS	NS
Unit 2		NS	NS	NS	NS	NS	NS	NS	NS	NS
Unit 3	3a Upper facies	1.90	1552	5356	27.4	2.0	17.0	38.6	42.4	97B-16
		1.83	1479	4793	-	1.0	13.8	37.1	48.2	96B-07
		1.81	1494	5054	-	1.5	9.3	40.4	48.8	96B-08
		1.79	1480	5518	-	-	-	-	-	96B-12
	Middle facies	1.68	1451	3280	-	0.1	1.0	32.8	66.1	96B-08
		1.67	1461	2506	-	0.0	3.6	50.5	46.0	96B-09
	Lower facies	2.00	1606	6497	27.9	0.1	9.6	44.3	46.0	97B-12
		1.89	1566	4221	-	1.6	26.6	35.6	36.3	96B-02
	3b	-	-	-	-	-	-	-	-	-
	4a	1.69	1551	1300	13.5	0.5	23.8	48.5	27.2	97B-16
Unit 4		1.54	1436	1600	-	3.7	37.9	32.1	26.2	96B-04
		1.81	1576	2603	10.7	0.6	28.1	39.5	31.8	97B-12
	4b	-	-	-	-	-	-	-	-	-

NS = not sampled

- = not measured

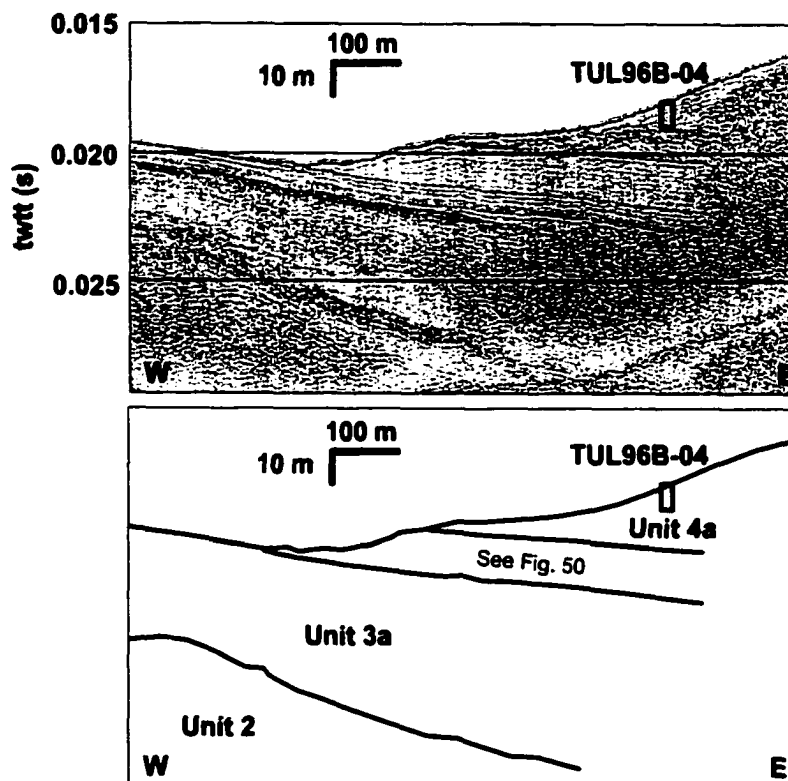
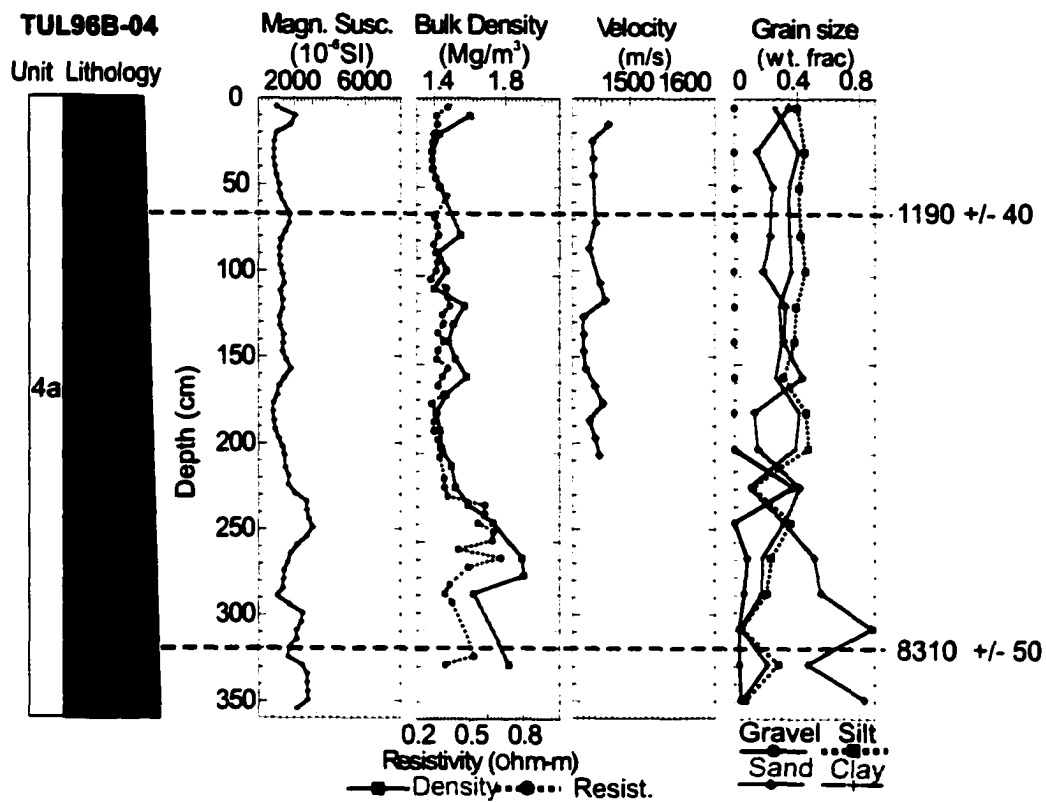


Figure 42. Lithologic description and physical properties measured in core TUL96B-04 that sampled the acoustically stratified sediments of unit 4b.

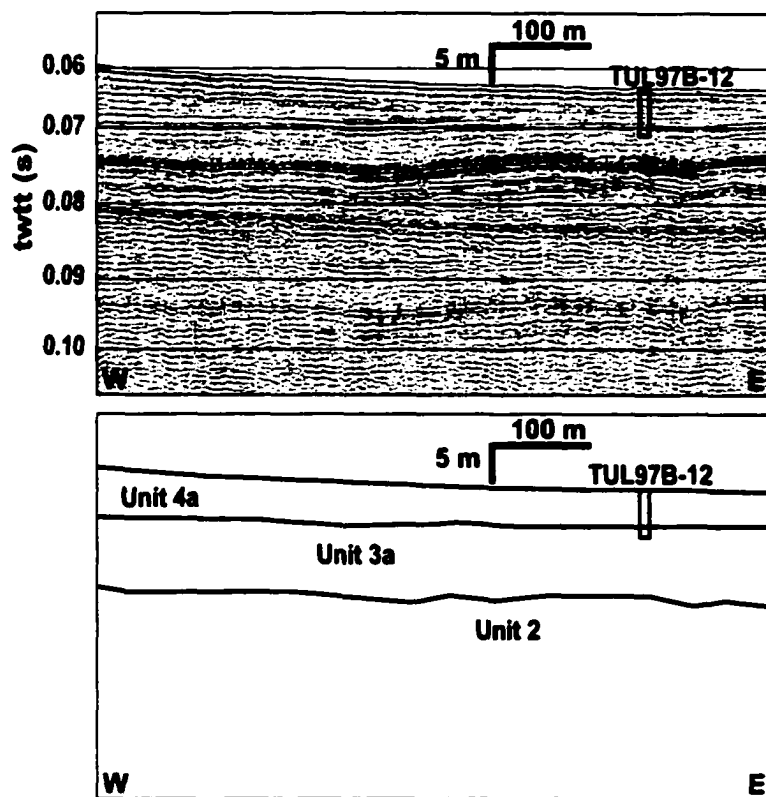
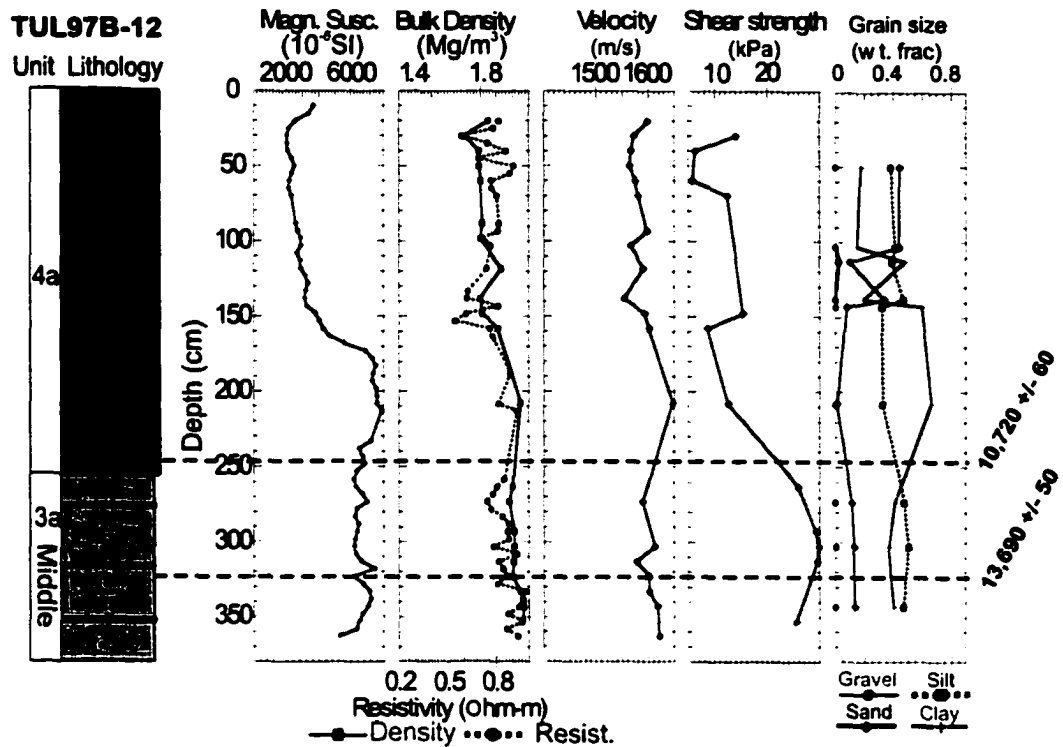


Figure 43. Lithologic description and physical properties measured in core TUL97B-12 that sampled the acoustically stratified sediments of unit 4a. The middle layer of unit 3a was sampled at the bottom of the core.

### **Distribution of Near-surface Geologic Units**

Figure 44 shows the distribution of the various seismic-geologic units where they crop out on the seafloor, as mapped from Huntect data. Wherever feasible, unit boundaries on Figure 44 were interpolated along depth contours between the control points picked from Huntect profiles. This technique produces a better map than simply connecting control points by straight lines because most of the units mapped are sediments, and water depth is a primary control on sediment characteristics.

Unit 1 crops out at the seafloor in several small areas off Vancouver Island and San Juan Island. Unit 2 crops out on the upper slopes and tops of some of the large banks in the Strait, and comes close to the surface in some coastal areas, where it can be traced to outcrops on land (e.g. Domack, 1983). Unit 3 dominates in the deeper portions of the strait, and in the area west of Eastern Bank. In areas covered by unit 3, subunit 3a is more common in the central region, and subunit 3b more common in the far west. Unit 4 is common close to the coasts, and in most of the area eastward of Hein Bank. Unit 4a dominates the seafloor geology along the entire southern and eastern margins of the strait, except near the entrance to Puget Sound, where unit 4b occurs (and some unit 3b). Unit 4a covers other large areas south of Victoria and west of McArthur Bank, and covers smaller areas around Hein and Middle Banks. Unit 4b is common locally, but mostly in areas of smaller extent than unit 4a. It occurs near the entrance to Puget Sound, and in the area between Middle and Constance Banks, and offshore of Ediz Hook and Dungeness Spit. Bedform fields associated with unit 4b are scattered throughout the strait, the largest of which occur in the western half of the study area.

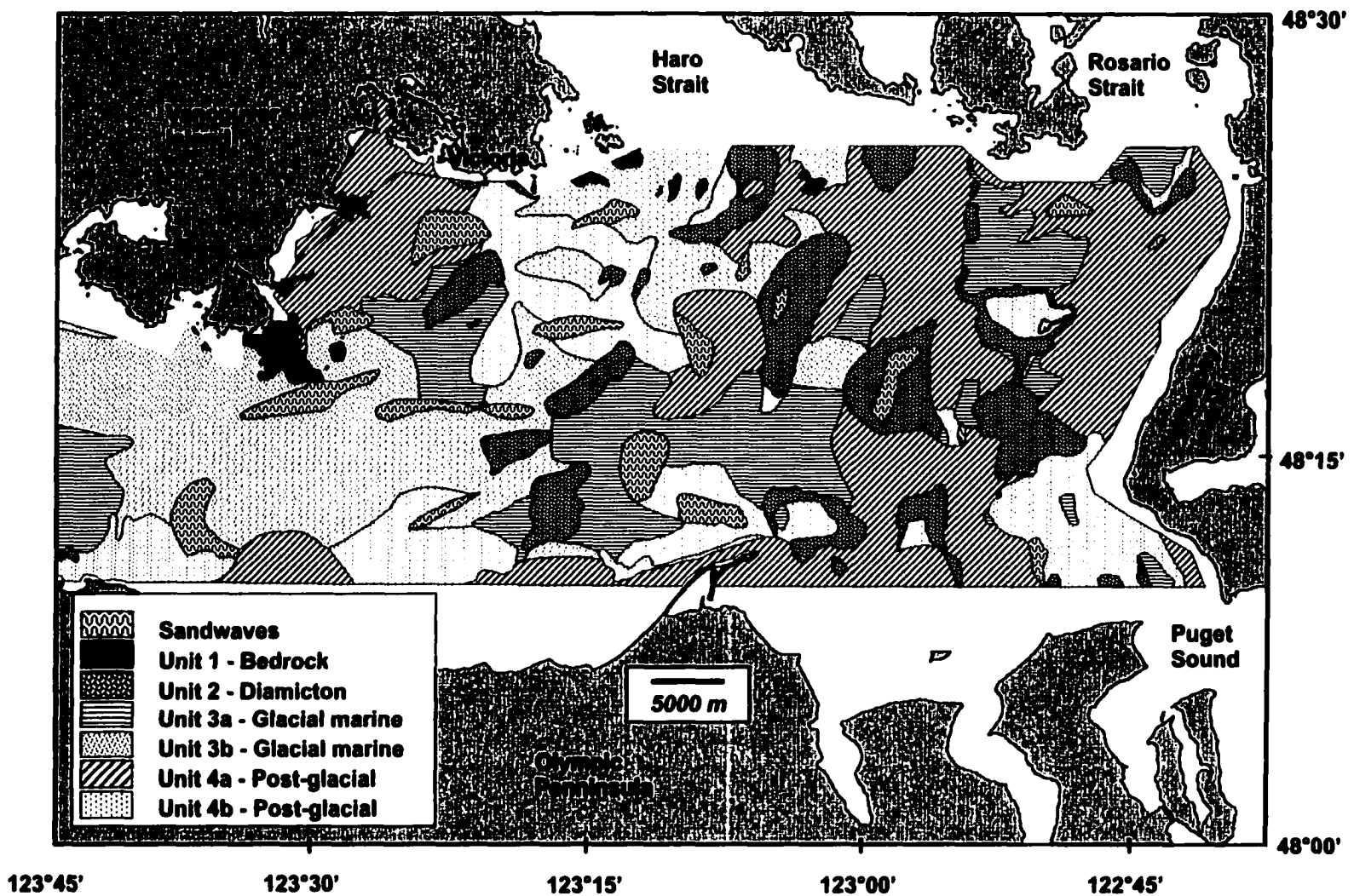


Figure 44. Distribution of the main seismic-lithologic units identified in eastern Juan de Fuca Strait. Compare distribution of seismic-geologic units with the physiography of the area (Fig. 1)

Available multibeam data cover only a small portion of the study region, and were excluded from Figure 44 since a surficial map based solely on seismic-reflection data will appear somewhat different than a map that includes multibeam data. One reason for this is the more complete coverage and superior vertical and horizontal resolution provided by multibeam data versus a grid of 2D-seismic profiles. Small features, or the continuity of features, could be missed between the lines of a seismic grid. Another reason is, the Hunttec system resolves layers thicker than 10-30 cm. Therefore, a very thin surficial layer would be indistinguishable from a thicker underlying layer, which would be mapped as the surficial unit. The multibeam systems, on the other hand, do not penetrate through more than a few centimeters, and so the thin surficial layer might be the unit mapped. For example, the surficial lags (unit 4b) that occur in some areas, rather than the underlying finer sediments of unit 3 (Fig. 40 and 41) For these reasons, the seafloor geology map (Fig. 44) should be considered a generalized map showing the major near-surface geologic units and features, rather than a strictly surficial geologic map. Although in many instances the near-surface and surficial units are the same. Separate surficial geology maps of the areas with multibeam coverage are presented below.

Figure 45 shows an interpretation of the multibeam data collected offshore of Victoria. As with Figure 44, Hunttec data were the primary basis for unit identification, but instead of interpolating unit boundaries along depth contours, they were drawn around areas of similar geomorphologic characteristics. There are three primary differences between the map based solely on Hunttec data (Fig. 44) and the map created with the addition of multibeam data (Fig. 45): (1) On the multibeam map, unit 2 is

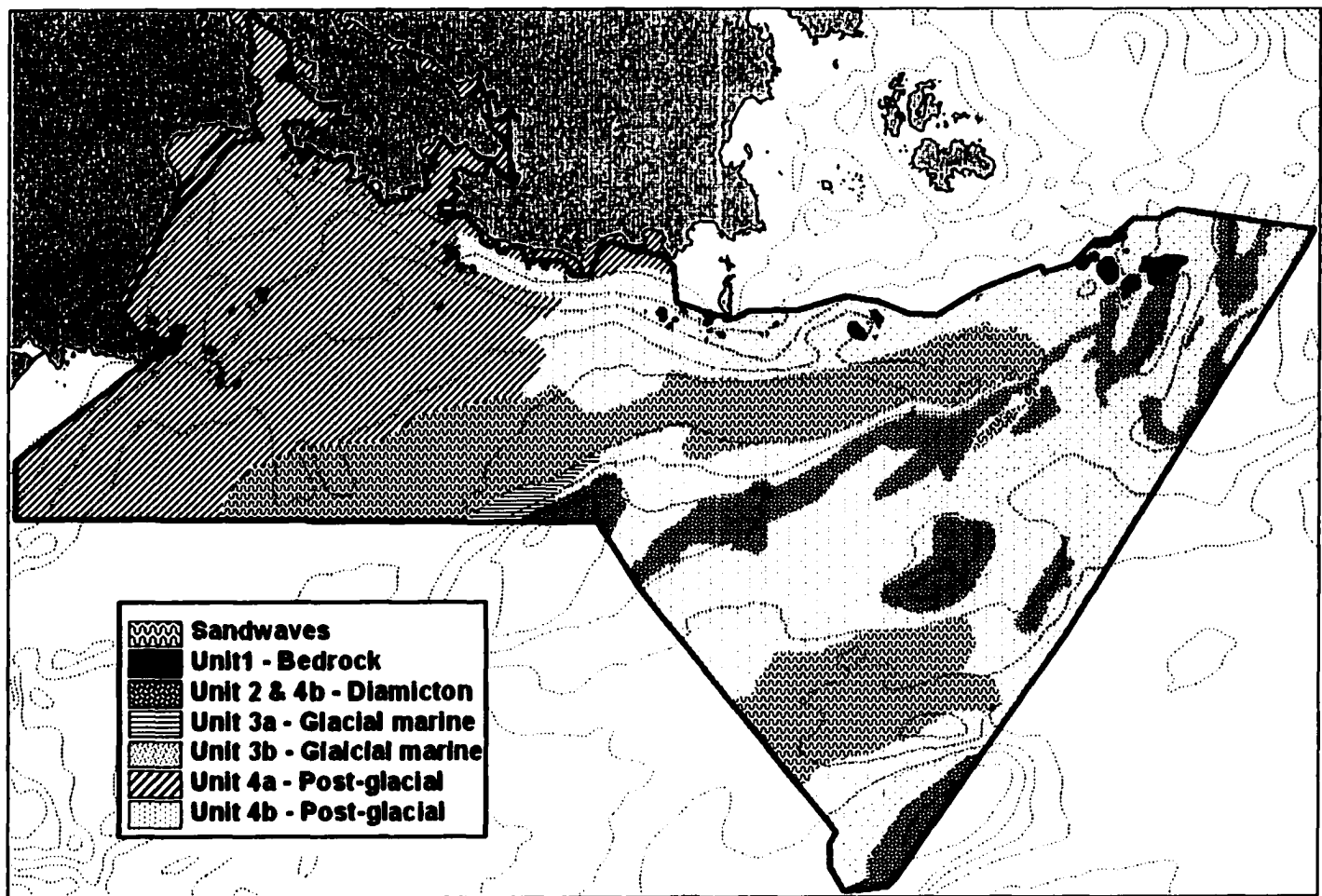
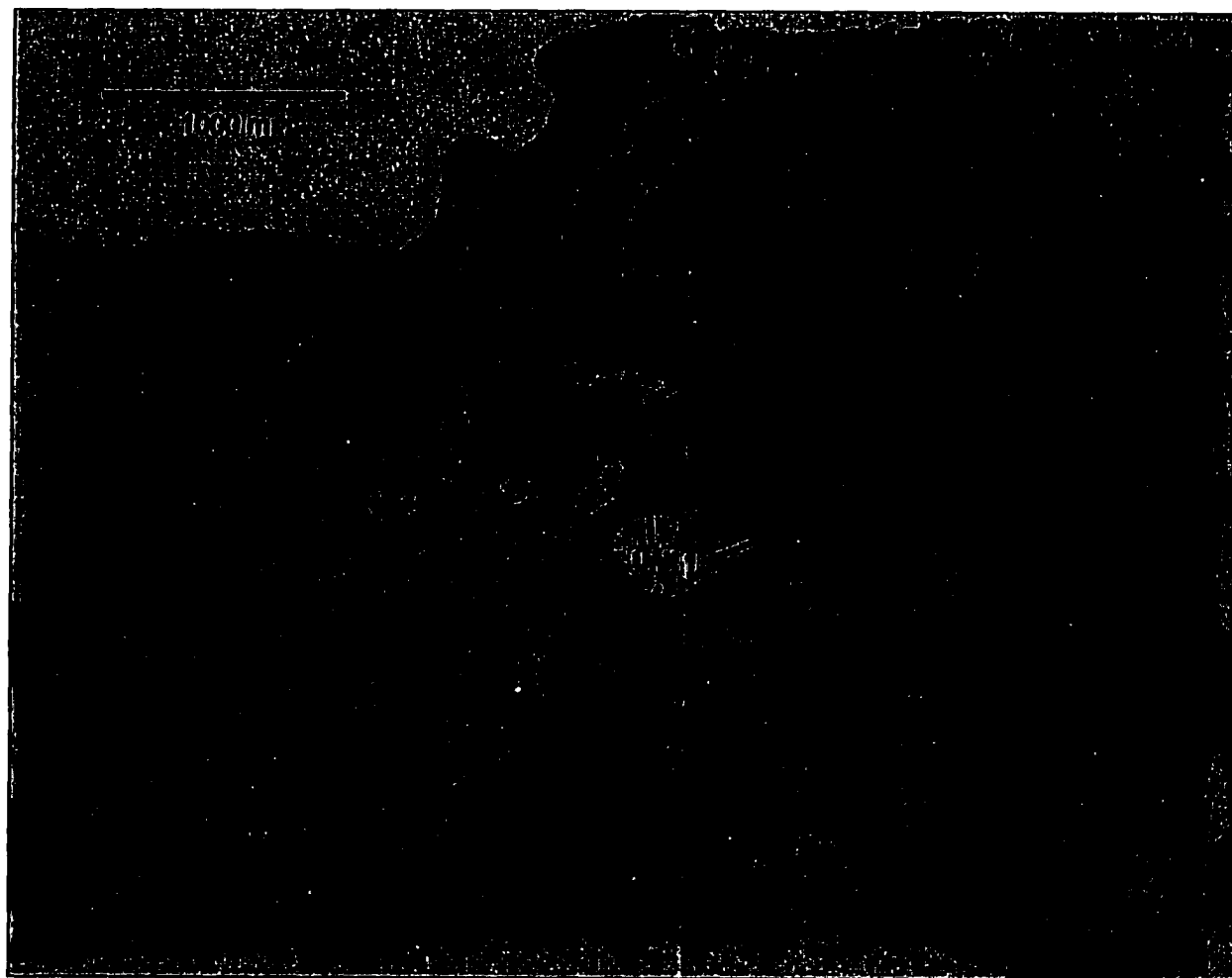


Figure 45. Distribution of the main seismo-lithologic units in the area of multibeam sonar coverage off Victoria.



shown to crop out in linear features on bank tops; (2) sand wave fields are shown to be more extensive; and (3), more small areas of bedrock outcrop were mapped. Figure 46 shows some interpretations of the surficial geology based on the multibeam data collected at Race Rocks. The main difference between this map and the same area on Figure 44 are the larger extent of unit 1, and the presence of the small depressions and crevices in the outcrop. Besides the larger scale of the multibeam maps (Fig. 45 and 46), the differences that exist between them and Figure 44 arise mainly from features being missed between seismic survey lines, and detection of smaller features such as the sand waves and crevices resolved by the superior resolution and spatial coverage of the multibeam systems.



**Figure 46.** EM3000 Multibeam bathymetry from the Race Rocks area (location is shown on Figure 2). The area of highly irregular, fractured, and undulating topography corresponds to acoustic unit 1. Unit 4b and/or unit 3b in-fills cracks and crevices within unit 1. Unit 3b crops out at the sea floor surrounding unit 1. To the northeast, bedforms (unit 4b) are visible.

## **CHAPTER VI**

### **DISCUSSION**

#### **Interpretation of Seismic-geologic Units**

Interpretations of the surficial and near-surface seismic-geologic units within eastern Juan de Fuca Strait are derived from the geomorphologic, seismic-acoustic, and lithologic characteristics described in chapters 2, 3, and 4. The setting is one of rapid retreat of a marine ice margin at the end of the last glaciation, followed by rapid sealevel change that continued into the Holocene (see Introduction).

#### **Unit 1**

At the base of the stratigraphic succession is unit 1, found in small outcrops on the seafloor near Victoria and San Juan Island. Although unit 1 was not sampled, it is found at Race Rocks (Fig. 46), Trial Island, and Discovery Island (Fig. 1), where outcrops rise above the sea surface to form rocky islets that are composed of fractured pillow basalts. The small crevices seen in the multibeam data are the likely cause of the hyperbolic reflections that characterize the surface reflection of unit 1 in seismic imagery (Fig. 18 and 19). The close proximity of other unit 1 outcrops suggests they are probably of the same material.

#### **Unit 2**

Unit 2 was not sampled, but is interpreted as ice-contact sediment such as till or diamicton deposited beneath or in the immediate vicinity of the ice margin. Although no

dates were obtained, unit 2 is thought to consist mainly of deposits of the last phase of glaciation in the strait. These interpretations are based on: (1) a seismic-reflection character similar to sediments from other areas of the British Columbia shelf, where they are interpreted as ice-contact in origin (Luternauer *et al.*, 1989; Barrie and Bornhold, 1989; Barrie *et al.*, 1991), and elsewhere in the world (Sylvitski, 1992; Davies *et al.*, 1997); (2), the marine section can be correlated with exposures on land where ice-contact sediments occur in the same stratigraphic position as in seismic profile (Hicock *et al.*, 1980; Domack, 1983); and (3), it crops out or comes close to the surface within shallow banks, where the thickest accumulations occur (Fig. 22-27), and where morphologic features suggestive of moraines are found (Fig. 15, 45 ).

The stratigraphy of unit 2 is much more complex in the banks than in the inter-bank basins. The numerous reflections seen in seismic data suggest a stratigraphy that is probably the product of the ice-advance and retreat phases of not just the last glaciation, but earlier glaciations as well, and is further complicated by post-glacial reworking.

### **Unit 3**

Unit 3 is interpreted to be glacial-marine sediment based on its stratigraphic position above the ice-contact sediments of unit 2, and on its seismic and sedimentologic characteristics. Overall, the sediments that comprise unit 3 are gray-colored, organic- and microfossil-poor silty-clay with variable amounts of sand and pebbles, and turbidites are common. Such sediments are typical of glacial-marine sediments observed on the British Columbia shelf (Anderson, 1968; Linden and Schurrer, 1988; Luternauer *et al.*, 1989; Davies *et al.*, 1997; Bornhold *et al.*, 1998), and in coastal exposures around the

strait (Hicock *et al.*, 1980; Domack, 1983). In addition, radiocarbon dating of shell material in these sediments yielded dates between  $13,690 \pm 50$   $^{14}\text{C}$  yr B.P. and  $11,910 \pm 50$   $^{14}\text{C}$  yr B.P. (Table 1), indicating unit 3 was deposited during the period of final ice retreat, and is, therefore, correlated with the Everson deglacial sediments (Capilano sediments in Canada) that occur throughout the region (Easterbrook, 1992; Dethier *et al.*, 1995).

The two subunits of unit 3 (3a and 3b) are a result of two different depositional environments, determined primarily by proximity to the retreating ice margin, and by water energy (waves and tides). The lowermost layer of unit 3a (e.g. Fig 20) is interpreted as a marine ice-marginal facies because it directly overlies unit 2 (ice-contact sediments). Although, the bottom of the lowest layer was not sampled, its upper parts (in core TUL97B-12) consist of bedded mud with ice-rafted pebbles, thin layers (few cm) of pebble-rich diamicton, sandy debris-flow deposits, and very few shell fragments. Such sediments are typical of the dynamic and variable depositional processes near ice-margins (Lonne, 1995; Powell and Molnia, 1989; Sylvitski, 1992). Reflections become more continuous toward the top of this layer, which probably results from the greater number of turbidites (albeit thinner and finer-grained than in the lower part of the layer). There are fewer diamicton layers also. These characteristics and the overall finer grain-size are typical of sediments deposited somewhat farther from the ice margin (Powell and Molnia, 1989; Sylvitski, 1992).

The acoustically transparent middle layer of unit 3a is conformable with the lowermost layer and is characterized by a finer grain-size; mostly massive silty-clay, fewer turbidites, and fewer ice-rafted pebbles. This facies is typical of an ice-distal

environment, where sedimentation is dominated by settling from meltwater plumes rather than debris flows and ice-rafting (Powell and Molnia, 1989; Sylwitski, 1992).

The uppermost acoustically stratified layer in unit 3a only occurs in the southeastern quadrant of the study area. This layer has similar seismic character to the lower layer, and a similar range of values for sediment physical properties. Values of bulk density and velocity in the upper layer of unit 3a are only slightly less than in the lower layer (Fig. 37-39), which is probably due to less consolidation as a result of their shallower burial depth. The sediment and physical properties similarities between the upper and lower layers of unit 3a probably reflect the more abundant ice-rafted debris in these layers compared with the middle layer of unit 3a. The origin of the upper layer in unit 3a is uncertain, but it could represent a return to a more ice-proximal depositional environment, perhaps due to a local re-advance of the ice margin. Domack (1983) suggested ice-rafting may become an important sediment source in the distal region, simply because the influx from overflow plumes becomes less important. Alternatively, the third facies may represent some local phenomenon by which ice-rafting became more common again, possibly because of rapid calving as a result of faster ice margin recession.

West of the Victoria-Green Point Sill, and in the area between Victoria and Middle Bank, and in some troughs between banks, unit 3a is absent and its stratigraphic position is occupied by unit 3b instead. Some seismic profiles show a gradual lateral transition from unit 3a into unit 3b (Fig. 21 and 41). Unit 3b is acoustically unstratified, and darker in tone compared with unit 3a, and core samples show it to be coarser-grained: containing a larger proportion of pebbles and sand, and more shell fragments. The

coarser grain-size probably accounts for the higher values of bulk density and acoustic velocity compared with unit 3a (Fig. 41). Like unit 3a, unit 3b is also interpreted to be of glacial-marine origin, and believed to be coeval with unit 3a, but deposited in areas where stronger currents winnowed out much of the finest material.

#### **Unit 4**

The fact that unit 4 overlies unit 3, and its sediments are relatively organic-rich, leads to its interpretation as a post-glacial unit. An early post-glacial age for unit 4 is supported by radiocarbon dates, most of which fall between 8000 and 11,000  $^{14}\text{C}$  yr B.P. (Table 1). The strait lacks a major modern source for these sediments, so most deposits of unit 4 probably formed shortly after ice retreated, when sealevel change and more abundant melt-water streams resulted in a greater sediment supply.

Unit 4 is divided into two subunits, 4a and 4b. Unit 4a is found around many of the banks and along the borders of the strait, where it occurs in acoustically stratified deposits with reflections dipping gradually seaward (Fig. 28). The sediments are composed of sandy-mud with variable concentrations of pebbles and shell fragments. Fine sandy and silty turbidites are common. Deposits of unit 4a around the banks may have originated from reworking of the bank tops and coastal bluffs and subsequent transportation into the inter-bank basins during the early post-glacial sealevel low stand. Unit 4b is acoustically unstratified, probably because it lacks the contrasting surfaces provided by the bedded debris flow deposits that characterize unit 4a. Unit 4b is usually found farther offshore, but adjacent to areas covered by unit 4a, and occurs in thinner deposits, and is often associated with sand wave fields. Most deposits of unit 4b occur in

regions of strong currents, such as the entrance to Puget Sound, between Victoria and Constance Bank, and shallow areas like the top of the bank that hosts Smith Island. Unit 4b in these locations is probably a coarser-grained, reworked or winnowed deposit, coeval with unit 4a. Deposits of unit 4b off the Olympic Peninsula are probably the distal continuation of the “delta-like” clastic wedges of unit 4a found closer to shore.

Although many deposits of unit 4 are considered to be early Holocene in age, several radiocarbon dates indicate some of these sediments are more recent (Table 1), and there is evidence for active processes. For example, the abundant bedform fields associated with unit 4b are evidence that sediment is probably being transported at present (Mosher and Thomson, 2000). The largest observed bedforms occur in a dune field just east of Victoria. Individual dunes at this location are among the largest in the world, reaching a maximum 25 m in height with 500 m wavelengths in 90 m of water (Mosher and Thomson, 2000) (Fig. 30).

In addition to the abundant bedforms in unit 4b, there are sediment drifts around the base of some banks (they are considered part of unit 4a). These drifts have a depression running parallel to the foot of the bank, which is likely to be an erosional moat (Fig. 23). These moats are free of “ponded” sediment, suggesting they are being maintained at present.

The spits along the Olympic Peninsula (Ediz Hook, Dungeness Spit, and several smaller ones) are also recent features maintained by sediment supplied by small nearby rivers and coastal erosion. The strait presently lacks large fluvial input, so erosion of pre-existing deposits provides the predominant modern source of sediment. Important pre-existing deposits may include the thick deposits of glacial-marine sediment that occur in



the shallower marine banks, and extensive cliff exposures of glacial sediments around the Strait.

### **Ice Retreat History**

There are only two limiting dates for the onset of deglaciation in western Juan de Fuca Strait: A date of  $14,460 \pm 200$   $^{14}\text{C}$  yr B.P. comes from peat overlying till on the western tip of the Olympic Peninsula (Huessner, 1973), and a date of  $14,400 \pm 400$   $^{14}\text{C}$  yr B.P. comes from a shell in glacial-marine sediments in the western strait (Anderson, 1968). Some time after  $14,400 \pm 400$   $^{14}\text{C}$  yr B.P., the ice margin retreated into the eastern strait (the study area), where the layered, and overall fining-upward sequence of glacial sediments (units 2 and 3a) implies progression from an ice-proximal to ice-distal depositional environment. In addition, abundant ice-rafted debris indicates iceberg calving was an important process that probably contributed to rapid grounded retreat in contact with the encroaching ocean. Eventually the retreating ice margin reached the zone of relatively shallow water over the Victoria-Green Point Sill (Fig. 47), where ice retreat stalled, allowing ice-proximal sediments to accumulate in the thick deposits of unit 2 found there. From the available dates, it cannot be said exactly when ice arrived at the Victoria-Green Point Sill, but it was sometime after  $14,400$   $^{14}\text{C}$  yr B.P., and a date of  $13,690 \pm 50$   $^{14}\text{C}$  yr B.P. (core TUL97B-12) from the base of a glacial-marine section offshore of Victoria, indicates ice had retreated from the sill before then. Radiocarbon dates obtained from glacial-marine sediments in the central strait, east of the Victoria-Green Point Sill, have a narrow range and do not come from the base of the glacial-

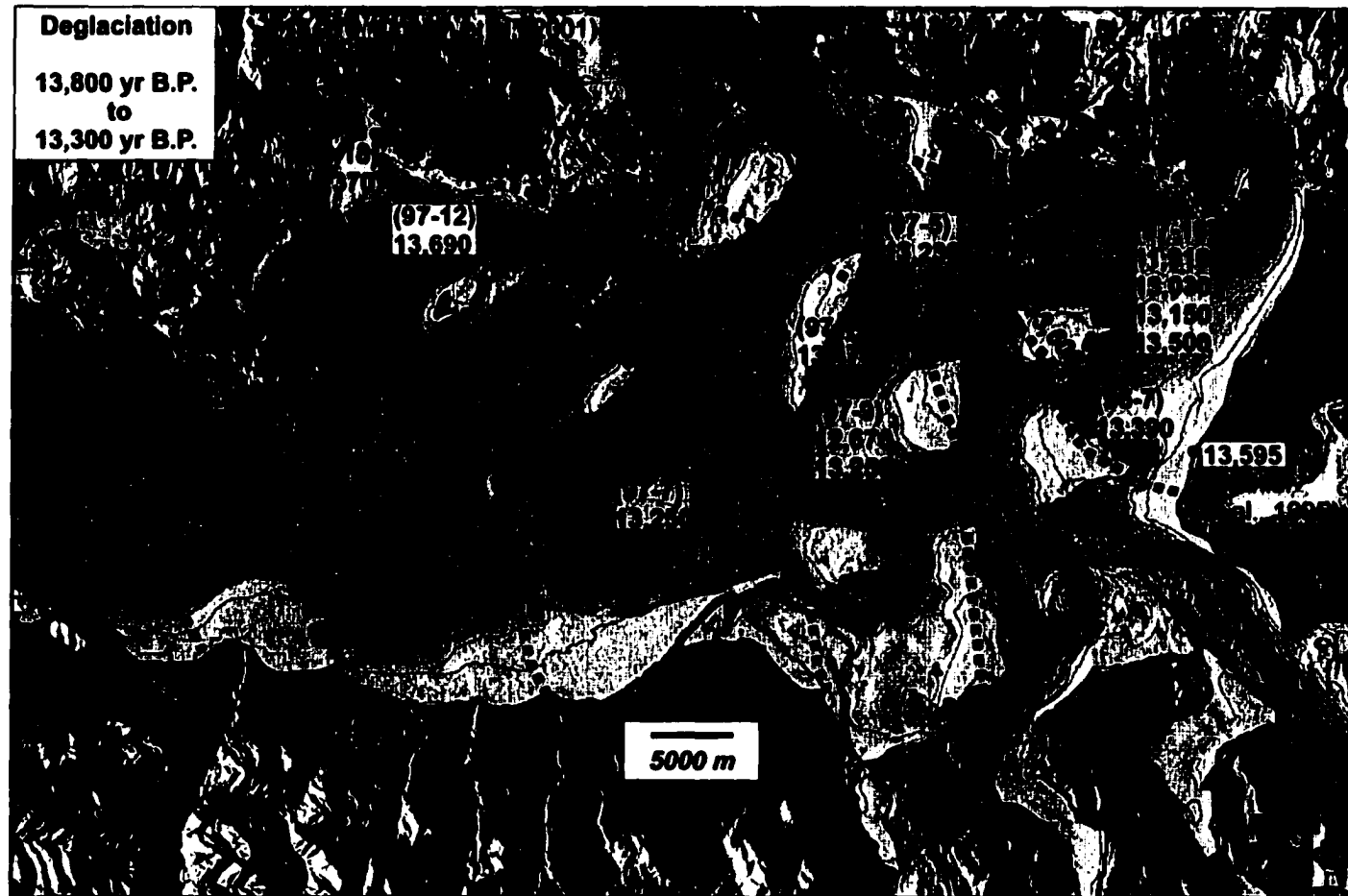


Figure 47. Distribution of C-14 dates in TUL96B and TUL97B cores from glacial-marine sediments. Only two dates (high-lighted) are from the base of the glacial-marine section, and can be considered as local limiting ages for the position of the ice margin. Dashed lines schematically represent possible positions of the ice margin during deglaciation. Ice retreated in contact with the encroaching ocean, which was +90 m above present sea-level in the north, and +50 m in the south (see Figure 53).

marine section; therefore, they cannot provide precise limiting ages for the position of the ice margin in this region. The narrow range of dates does attest to rapid recession, although retreat may have stalled briefly on the banks.

The stratigraphy of the banks is complex (e.g. Fig. 18 and 31), and is probably the product of the ice-advance and retreat phases of not just the last glaciation, but earlier glaciations as well, and is further complicated by post-glacial reworking. Mosher and Hamilton (1998) show similar results in the Strait of Georgia to the north. Airgun profiles through the unnamed bank, Middle Bank, and Eastern Bank, show a deeper, major, roughly horizontal reflection that spans the entire bank. This reflection is interpreted as the boundary between sediments of the last glaciation and the deposits of an earlier phase. Several of these banks, particularly those in the east, have their steepest slopes on the eastern side, which is typical of the ice-proximal side of morainal banks, and in the glacial sediments seismic-reflections dip predominantly westward. This morphology and internal structure suggest ice retreat was essentially eastward in the study area, although the wider regional trend was northward.

The position of another probable major pause in ice retreat is marked by an extensive morainal complex that includes McArthur Bank, Smith Island, and Partridge Bank (Fig. 47). A short moraine segment that extends south from Partridge Bank suggests the moraine complex may have stretched across Admiralty Inlet to Dallas Bank. A date from glacial-marine sediments east of McArthur Bank indicates ice had retreated off the bank before  $13,500 \pm 50$   $^{14}\text{C}$  yr B.P. (core TUL97B-16), and probably before  $13,595 \pm 145$   $^{14}\text{C}$  yr B.P. based on a date from glacial-marine sediments on Whidbey Island (Dethier *et al.*, 1995). Meanwhile, the Puget Lobe had been retreating northward,

passing Seattle by  $13,700 \pm 50$   $^{14}\text{C}$  yr B.P. (QL-4067; Porter and Swanson, 1998). Sometime between  $13,700 \pm 50$  and  $13,595 \pm 145$   $^{14}\text{C}$  yr B.P. ice retreated out of Admiralty Inlet.

The seafloor in Admiralty Inlet has a ridge and trough topography giving it a channelized appearance. Channel dimensions are similar to channels farther south in Puget Sound, where they are thought to be a result of subglacial fluvial scour (Booth and Hallet, 1993). Subglacial channels were probably carved into the substrate beneath the Juan de Fuca Lobe as well, but have since been buried, and are not readily traced from one adjacent seismic profile to the next. Admiralty Inlet, on the other hand, has been kept relatively clear of post-glacial sedimentation, probably by the strong tidal currents that flow in and out of Puget Sound (Thomson, 1981). In the outer approaches to Admiralty Inlet, a seismic profile over two elongate ridge-like features reveals they are composed of clinoform reflections (Fig. 33). Their clinoform structure and large size suggests they are prograded deposits left by a high volume flow. Nearby, between Dallas Bank and Partridge Bank, where two lobes of sediment splay onto the ocean floor, a seismic profile through one of the lobes shows clinoforms down-lapping on both sides (Fig. 34). This “delta-like” feature is interpreted as a submarine fan, where clinoforms represent foreset beds. The cap of later post-glacial sediments indicates post-depositional reworking, and that they are unlikely to be modern features. The available data suggests two plausible interpretations for these features. One proposed origin is, deposition from sediment laden water of a possible flood event, or multiple events, that may have accompanied drainage of ice-marginal lakes in Puget Sound as Admiralty Inlet was deglaciated. Alternatively, they may have been deposited from strong tidal currents,

laden with the easily eroded components of abundant glacial sediments left by retreating glaciers.

Following deglaciation of Admiralty Inlet and inundation of Puget Sound (Easterbrook, 1992), ice retreated rapidly northward, perhaps stalling briefly when the San Juan Islands were reached. Lawson Bank, in Rosario Strait, is interpreted as a terminal moraine deposited at this time, and Salmon Bank appears to be a large deposit of proximal outwash. Early dates from shells in glacial-marine sediments in Saanich Inlet ( $13,270 \pm 70$   $^{14}\text{C}$  yr B.P.; Cowan, 2001) on San Juan Island ( $13,240 \pm 70$   $^{14}\text{C}$  yr B.P.; BETA-70791; Dethier *et al.*, 1995), and east of Whidbey Island near Mount Vernon on the mainland ( $13,370 \pm 70$   $^{14}\text{C}$  yr B.P.; USGS-782; Dethier *et al.*, 1995), indicate the land areas surrounding the eastern strait were free of ice by around 13,300  $^{14}\text{C}$  yr B.P. By 13,000  $^{14}\text{C}$  yr B.P., glaciers had receded to the international boundary, about 50 km north of the study area (Armstrong, 1981). The youngest date from glacial-marine sediments in the study area is  $11,910 \pm 50$   $^{14}\text{C}$  yr B.P. (core TUL97B-16), which is consistent with the range of dates in the Everson (Capliano) glacial-marine sediments throughout the region (Easterbrook, 1992).

### **Rate of Ice Retreat**

The rate of ice retreat in eastern Juan de Fuca Strait can be calculated from suitable limiting dates for the position of the ice margin. The date of  $13,690 \pm 50$   $^{14}\text{C}$  yr B.P. (core TUL97B-12) comes from near the base of the glacial-marine section, as does the date of  $13,595 \pm 145$   $^{14}\text{C}$  yr B.P. from Whidbey Island (Dethier *et al.*, 1995). Considering the error associated with these dates, it took between 0 and 290 years for ice

to retreat from the location of core TUL97B -12 to the site on Whidbey Island; a west to east distance of 45 km. Given the ice-contact to ice-distal sequence of glacial marine sediments, near instantaneous retreat is clearly unrealistic. The maximum time of 290 years yields a retreat rate of 150 m/yr. The difference between the mean ages is 95 years, giving a retreat rate of 475 m/yr. The faster rate is considered the most likely, as it is comparable to the retreat rate of 340 m/yr calculated for the Puget Lobe (Porter and Swanson, 1998), which calved into pro-glacial lakes along portions of its margin, and for calving glaciers in Alaska, which retreated at 500 m/yr following the Little Ice Age (Brown *et al.*, 1982). With an estimate of the average ice retreat rate available (475 m/yr) it is possible to back calculate and estimate when the retreating Juan de Fuca Lobe entered the eastern half of the strait. Given a distance of 25 km from the site of core TUL97B-12 to the western margin of the study area, ice had retreated into eastern Juan de Fuca Strait by ~13,750 yr B.P. ( $^{14}\text{C}$  equivalent).

### **Sealevel History**

#### **Erosional Unconformities**

Glacial-marine sediments in eastern Juan de Fuca Strait were deposited as ice retreated and relative sealevel was at its highest, but subsequent crustal uplift caused a rapid regression, which was bound to rework existing glacial-marine sediments and influence early post-glacial sedimentation. Along the Victoria water front the terraces at -15, -35, -50, and -65 m (Fig. 7) suggest wave-cut terraces, perhaps representing former subtidal zones. It is unlikely that coring here would be successful in yielding reliable dates for the age of the terraces, however, since there appears to be only a thin layer of

post-glacial sediments, if any, and the chaotic seismic signature suggests they are coarse grained. Fortunately, the post-glacial wedge emanating from Esquimalt Harbour provides a thick layer of finer grained post-glacial sediment. In seismic profiles from this area, the reflection at the base of the post-glacial unit appears to truncate reflections within the underlying glacial-marine sediment, suggesting an erosional unconformity. Several cores penetrated this unconformity at three different sites in the area of Esquimalt Harbour (Fig. 7, 29, 31, and 48), where it is interpreted as an erosional surface carved into existing glacial-marine sediments by wave action during a lower-than-present sealevel stand.

At one site, off Victoria, the unconformity is traced as deep as 65 m below the sea surface, the same depth as the deepest terrace in Figure 7. In waters deeper than around 65 m, the contact between the glacial-marine and post-glacial sediments appears conformable. Cores 96-12 and 97-12 sampled the unconformity near its greatest depth (Fig. 31). Each core contains a layer of glacial-marine mud overlain by a post-glacial layer of coarse sandy-mud, pebbles, and shell fragments. The sharp contact between the glacial-marine sediments and post-glacial sediments is probably the unconformity seen in seismic data (Fig. 31). A Radiocarbon date from just above the unconformity indicates it is of early post-glacial age ( $10,720 \pm 60$   $^{14}\text{C}$  yr B.P.; core TUL97B-12), and in no location is the unconformity observed to be overlain by more glacial sediments. This unconformity is interpreted as an erosional surface carved into existing glacial-marine sediments by wave action during a lower sealevel stand.

The second site is closer to shore and several cores reached the unconformity at different depths offshore. The cores come from depressions between the series of six

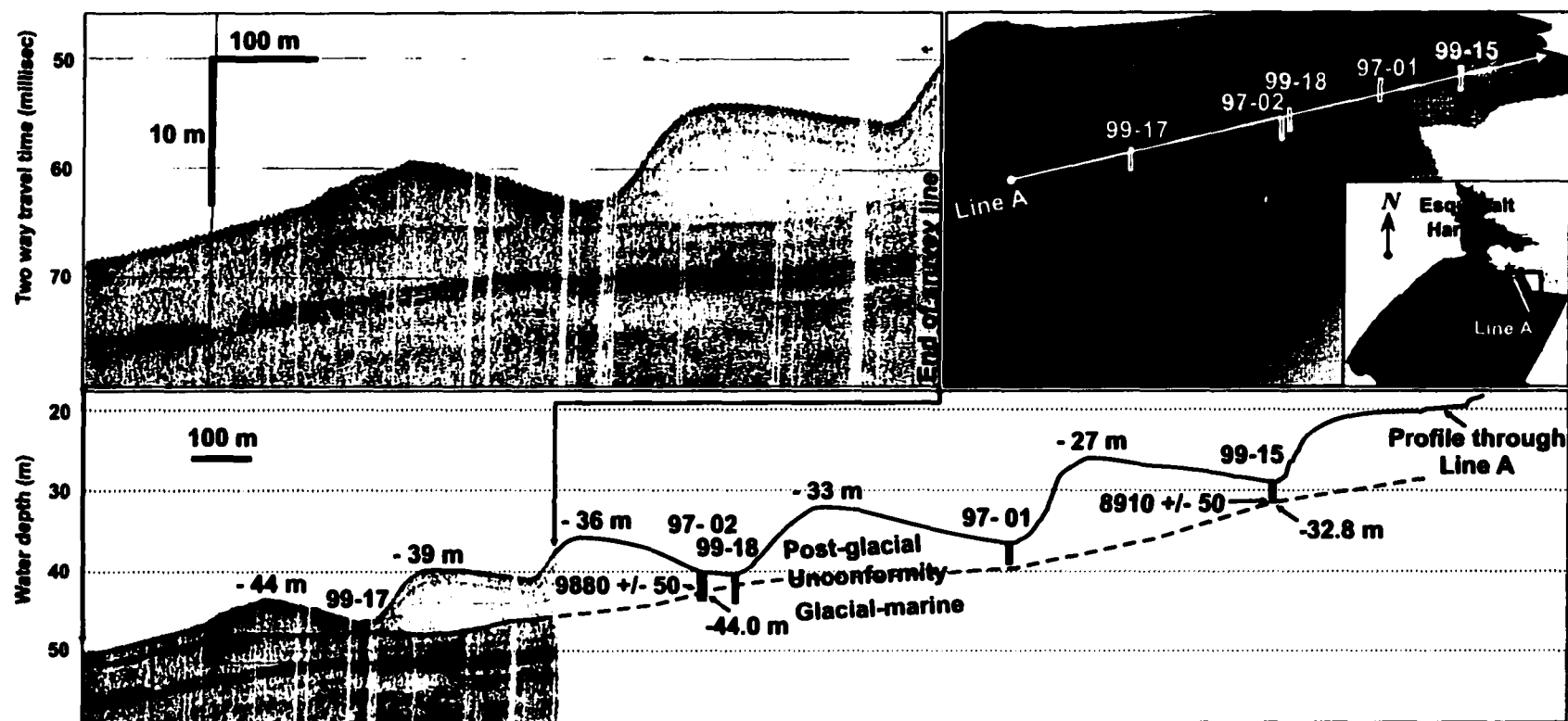


Figure 48. Seistec profile (upper left), 3D view (upper right), and bathymetric profile (bottom; Line A) through ridge features near Esquimalt Harbour. Black bars indicate locations of TUL97 and TUL99 cores and their approximate depth of penetration. Several cores penetrate an unconformity between the post-glacial and glacial-marine sediments (see text).



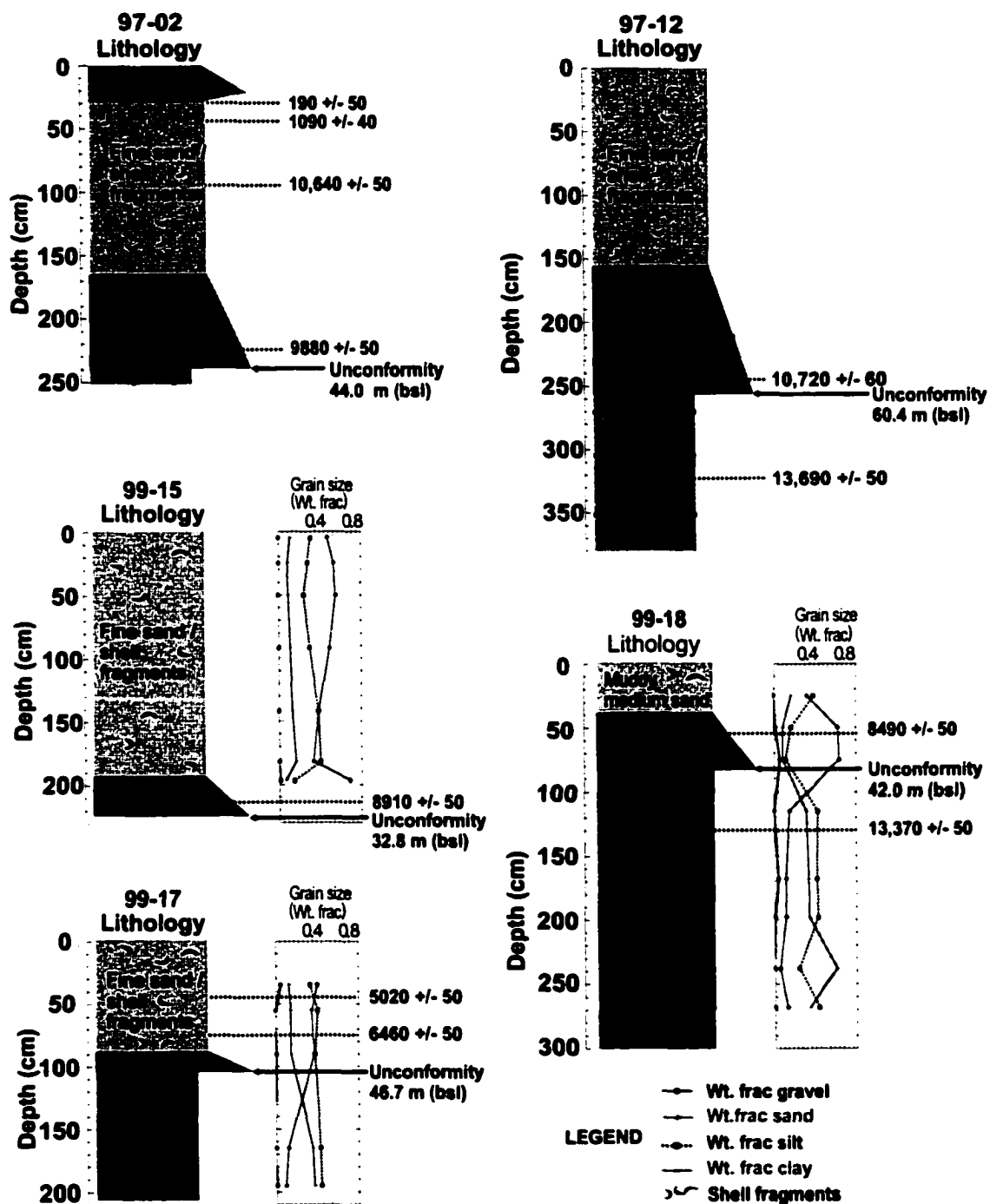


Figure 49. Five cores penetrate an unconformity off Victoria; each contains a layer of glacial-marine mud (unit 3a) overlain by a post-glacial layer of coarse sandy-mud, pebbles, and shell fragments that fines upward to fine sandy mud with shell fragments (unit 4). The sharp contact between the glacial-marine sediments and post-glacial sediments is considered to be the unconformity identified in seismic section (Fig. 31). Radiocarbon dates from just above the unconformity indicate it is of early Holocene age.

ridges near Esquimalt (Fig. 11 and 48). The origin of these ridges is uncertain. They could represent deformation in the post-glacial sediments (rotational slumping) that did not continue into the underlying glacial-marine sediments. The post-glacial layer is considerably thinner in these depressions than it otherwise would be, allowing the unconformity to be sampled at a higher level closer to shore. The cores contain a similar sequence of glacial-marine and post-glacial sediments separated by a sharp contact as seen in cores TUL96B-12 and TUL97B-12 (Fig. 49). If the unconformity in figure 48 was the result of erosion during lower sealevel, then the post-glacial unit is probably time-transgressive, deposited at progressively higher levels (closer to the present shoreline) as sealevel rose. This hypothesis is supported by radiocarbon dates, which indicate the unconformity is older in deeper water and younger in shallow water. The dates are  $9880 \pm 50$   $^{14}\text{C}$  yr B.P. at 44 m below the sea surface in core TUL97B-02, and  $8910 \pm 50$   $^{14}\text{C}$  yr B.P. at 33 m in core 99-15. A date of  $8490 \pm 50$   $^{14}\text{C}$  yr B.P. in core TUL99-18, which comes from almost the same location as core TUL97B-02, creates a discrepancy in the trend of increasing age of the unconformity offshore, but this date comes from a higher level above the unconformity than in other cores.

At the third site, a series of four terraces appear to be cut into glacial-marine sediments at depths of 51, 53, 56, and 60 m below the sea surface (Fig. 29). No dates were obtained, but core TUL97B-03 shows the terraces have been buried by the same sequence of post-glacial sediments that bury the unconformity, suggesting they are of similar age, and thus formed during transgression.

The unconformity and terraces discussed thus far suggest sealevel may once have been around 60 to 65 m deeper during early post-glacial times than at present. If so, then all the major banks in the strait would have been exposed. These banks have relatively flat areas on their tops and flanks, and seismic profiles from these areas often show a reflection at the seafloor, or in the shallow subsurface, that truncates reflections within the glacial sediments at a depth of  $60 \pm 20$  m. Examples occur near Constance Bank (Fig. 22), on the un-named bank (Fig. 25), and on Middle Bank (Fig. 26). Terraces are found also along the waterfront east of Dungeness Spit, where they occur at depths close to terraces off Victoria (Fig. 13)

On several of the banks, seismic profiles reveal wedge shaped units containing seaward dipping clinoforms. At the base of each clinoform unit, there is a seaward dipping reflection that cuts through the bank diamicton, suggesting an erosional surface. Examples occur on the western flank of Eastern Bank sloping from a depth of 60 m to 90 m, and on the eastern flank sloping from about 38 m to 83 m (Fig. 23); on the western flank of Partridge Bank sloping from 38 m to 60 m (Fig. 24); and on the eastern flank of the unnamed bank sloping from 52 m to 60 m (Fig. 25). A similar feature occurs beneath the clinoform unit off Green Point, sloping from a depth of 60 m to 83 m (Fig. 35). These unconformities were probably eroded when falling sealevel brought bank surfaces into the wave zone. Once the bank tops became subareal, terrestrial processes would have acted on the exposed tops, and wave erosion would have continued along the shorelines. As sealevel began to rise again, subareal portions were transgressed and wave action would have resumed, flattening and redistributing sediments on the banks, until

their tops fell below the erosional wave base. Some bank tops (e.g. Partridge Bank) may still be above the erosional wave-base, however.

Although the unconformities discussed above occur as deep as 80 to 90 m, sealevel may have some meters above this level since erosion would have begun at the erosional wave-base; the minimum depth where waves had sufficient energy to mobilize the available sediment. Komar and Miller (1975) show that the threshold of grain movement under waves is a function of water depth, wave period, wave height, and wave length. In the eastern strait, waves are typically less than 2 m high, with periods of around 6 s, and wave lengths of 55 m (Thomson, 1981). These waves have the ability to mobilize coarse sand (2 mm) at depths of up to 25 m assuming they are non-cohesive; cohesive sediments are more resistant. Hence, the unconformities are not a precise indicator of the past sealevel in which they formed, particularly in the more open areas of the strait, where waves are larger and the wave base deeper. Subtracting 25 m from the maximum depth of these unconformities yields a sealevel of around 65 to 75 m lower than present. This depth is close to the depths of the unconformities observed in more sheltered areas, such as the approaches to Esquimalt Harbor, where the unconformity probably records the paleo-sealevel more precisely (Fig. 29 and 31).

### **Clinofom Units**

Wedge shaped clinofom units occur on the western flank of Eastern Banks at a depth of 60 m and on the eastern flank at 43 m (Fig. 23); on Partridge Bank at a depth of 22 m (Fig. 24); the eastern side of the unnamed bank in the middle of the strait at 52 to 56 m (Fig. 25); on Middle Bank at 30 m (Fig. 26); and, on Dallas Bank at 30 m depth (Fig.

27). There is a clinoform unit offshore of Green Point at a depth of 60 m (Fig. 32). The clinoform units are prograded depositional features that are probably associated with the transgressive period. As sealevel rose, bank tops would have been reworked by waves and sediments would have prograded over former areas of erosion, creating the clinoform units. As sealevel continued to rise, sediment transport would have decreased as wave and current energy fell below the entrainment threshold of the available sediment. Preferential erosion of the finer material is indicated by a coarse lag on the surface of Hein Bank (core TUL97B-10, which sampled 59 cm of pebbly sand with abundant shell fragments); similar lags probably formed on the other Banks also, but were not sampled. These lags would have formed armoring caps that protected underlying sediments from continued erosion, and probably reduced the time interval during which these clinoform wedges were active.

Not all clinoform units are interpreted as post-glacial deposits. The large clinoform unit on the western flank of Eastern Bank at 60 m depth, for example, is more likely a glacial deposit, such as a proximal outwash (Fig. 23). The distinction between this clinoform unit and most others (e.g. the one at a depth of 41 m on the eastern flank) is the larger size and the much more irregular basal reflector that separates the clinoforms from the underlying, older glacial deposits.

Climoform units do not occur on all the banks. For example, Middle Bank was crossed by two airgun profiles with similar orientation to the lines that crossed Eastern Bank, but there are no clinoform units apparent on the seismic profiles. Their absence may result from gaps in seismic survey coverage, or profiles orientated in such a way that

they are not recognized, or, perhaps, conditions were not conducive to their formation in all areas.

### **Drowned Spits**

Submerged features with similar morphology to the modern spits, Ediz Hook and Dungeness Spit, are found along the Olympic Peninsula (Fig. 13). At Ediz Hook, these features occur at depths of 6, 8, and 25 m, and at Dungeness Spit another occurs at 15 m (Fig. 13). The close proximity and similar morphology of these features compared with the modern spits, and their similarity to drowned barrier spits and barrier beaches from other locations (Rampino and Saunders, 1981; Oldale, 1985; Jensen and Stecher, 1992; Wellner *et al.*, 1993; Roy *et al.*, 1994; Forbes *et al.*, 1995), leads to their interpretation as drowned barrier spits. The drowned spits off the Olympic Peninsula are probably analogous to the modern ones and thus formed within a few meters of sealevel. There are presently no dates, but they probably formed during sealevel transgression. To be regressive features they would have had to survive not only a period of subareal exposure, but the following transgression as well.

The preservation of barrier-spits and barrier-islands during changing sealevel is determined by the nature and quantity of sediment available, wave and current energy, rate of sealevel change, and coastal physiography (Roy *et al.*, 1994). During conditions of dropping or stable sealevel, they will widen in the seaward direction through progradation. Under conditions of rising sealevel and sufficiently abundant sediment, barrier build-up can keep pace with sealevel rise, and maintain a prograded character (Swift, 1975). On the other hand, higher rates of sealevel rise, or insufficient sediment

supply, cause instability, and one of the following may happen: (1) the spit is destroyed and sediment deposited elsewhere; (2), the system may become transgressive and migrate landward via shoreface erosion, wash over, and net deposition on the landward side (Roy *et al.*, 1994); or (3), if the rate of sealevel rise is very rapid, the spit can be overstepped and drowned in place (Rampino and Saunders, 1981; Oldale, 1985; Forbes *et al.*, 1995). The latter scenario appears to describe the fate of paleo-spits along the Olympic peninsula.

### **Partially Isolated Low Stand Basin**

Other evidence for sealevel low stands includes isolated basins; local, formerly marine basins that are cut off from the ocean when sealevel falls below the deepest point on the perimeter of the basin (e.g. Josenhans *et al.*, 1997). Sedimentation in the basin may then become lacustrine, lagoonal, or otherwise reflect the change in depositional environment. Investigation of possible isolated basins starts with considering Saanich Inlet, a small fjord just to the north of Victoria (just north of the study area). The sill across its entrance is at a depth of 75 m, but the stratigraphy indicates it has always been a marine basin since ice retreated (Mosher and Moran, 2001). The search for isolation basins elsewhere in the strait was, therefore, restricted to basins with a perimeter depth of -75 m or shallower. One such basin is located just west of Whidbey Island (Fig. 50). The deepest location on the perimeter of this basin is about 75 m on the north side, and the sill at its southern side is at 55 m. Interpretation of seismic-reflection data over these locations indicates the seafloor consists of glacial sediments and has not undergone extensive modification since ice retreated. A low stand of 75 m would have cut this basin

off completely, but other low stand features this deep have not been observed. Nevertheless, sediments within the basin contain a sequence that differs from the typical stratigraphy of the strait. Glacial-marine sediments in this basin are not directly overlain by the usual post-glacial olive colored sandy mud, but instead, are overlain by light-green, silty-clay containing shell fragments, followed by a thin laminated silt bed, then a layer of gray silty-clay with shell fragments, and finally, then the normal post-glacial sediments (Fig. 50). The abundant bivalve shell fragments in the green silty-clay layer indicates a marine origin, so it is unlikely that this basin was ever completely isolated. Nevertheless, the green silty-clay, is unique to this basin, and the fine grain-size indicates deposition in quiescent waters. These observations might be explained by partial isolation of the basin, which would have occurred if sealevel fell below the level of the sill along the southern margin at a depth of 55 m. The northern entrance to the basin would have been restricted considerably at this depth also, creating a marine embayment.

If partial isolation resulted in the green silty-clay when sealevel fell below 55 m, then it is plausible that deposition of this sediment stopped when sealevel rose above -55 m again during the subsequent transgression. If this scenario is true, then the date from the top of the green mud indicates relative sealevel was around 55 m below present at  $10,630 \pm 50$   $^{14}\text{C}$  yr B.P. Unfortunately, there are no dates from the base of the green silty-clay, and so no direct age for when it began accumulating. However, an indirect age was determined based on the assumption of a constant sedimentation rate (1.4 cm/yr) and from the thickness of the unit estimated from the Huntet profile (6.75 m), giving an average of 11,176 yr B.P. ( $^{14}\text{C}$  equivalent) for the base of the green mud.





The Huntec profile from this basin shows that both the green and gray silty-clays have been partly eroded (Fig. 50). It seems that at some time during transgression circulation within the basin increased and the finest sediments were eroded, perhaps after the surrounding banks were completely re-submerged.

### **Drowned Fluvial Features**

Drowned river channels and submerged deltas are good evidence of low sealevel stands, but are often buried or eroded during transgression, leaving no expression on the seafloor. Seismic-reflection profiles may reveal in-filled channels and delta forsets, however. For example, an airgun profile off Victoria reveals a concave-up reflection cutting through glacial-marine sediments (Fig. 51). Some buried channels in glaciated terrain may be of sub-glacial origin, therefore, only channels filled in with post-glacial sediments can be considered possible post-glacial river channels. The site was not cored, but the relative transparency of the channel fill suggests it is post-glacial. The base of the U-shaped reflection occurs at -47 m, which may represent the base of a post-glacial river channel in the location of the seismic profile. The channel may be graded to an even lower level farther offshore, but the depth of -47 m is close to the depth of one of the terraces off Victoria.

Submerged deltas are also good evidence of sealevel low stands. The clinoforms indicated on the seismic profile from the Ediz Hook area (Fig. 13) are interpreted as submerged delta forsets that prograded to a depth of -48 m, probably during early post-glacial times. Subsequent reworking during transgression deposited a smaller wedge of over the clinoform unit.

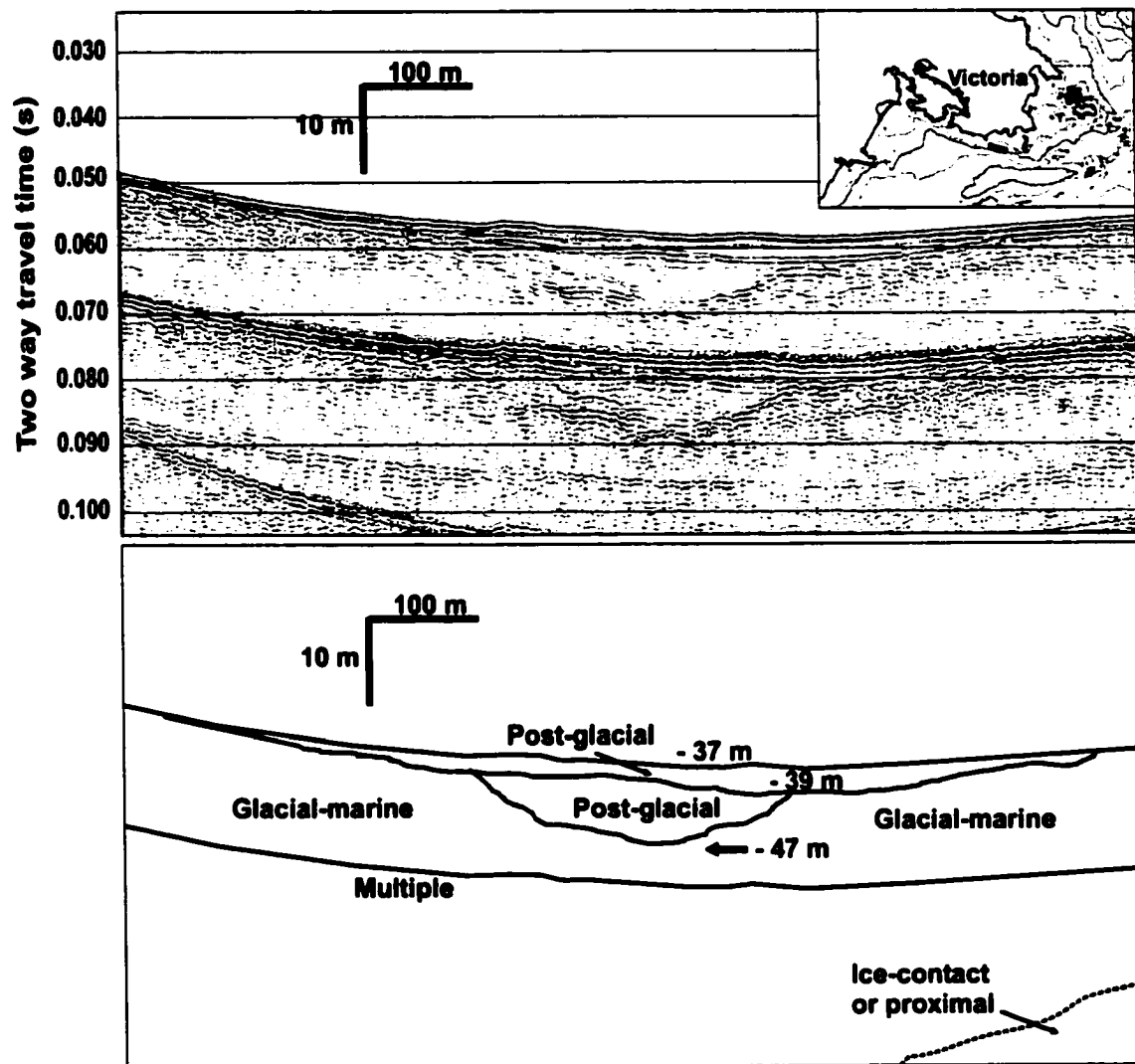


Figure 51. Hunttec profile showing a possible submerged river channel offshore of Victoria

## **Sealevel Curve and Rates of Sealevel Change**

Prior to about 13,750 yr B.P. (calculated date;  $^{14}\text{C}$  equivalent), the eastern strait was filled with ice. By  $13,270 \pm 60$   $^{14}\text{C}$  yr B.P. (ODP1034C; Huntley *et al.*, 2001) the strait was completely deglaciated, but the crust was still isostatically depressed, resulting in a period of maximum marine submergence of 90 m above the present level (Huntley *et al.*, 2001). Subsequent rapid isostatic rebound caused relative sealevel to fall, reaching a level the same as today at around  $11,700 \pm 170$   $^{14}\text{C}$  yr B.P. (I-3675; Clague *et al.*, 1982). Isostatic rebound continued, however, and eustatic sealevel was still low (~80 m below present), resulting in terrestrial emergence and relative sealevels significantly lower than present. Defining the timing and magnitude of this sealevel lowering is critical in establishing an accurate sealevel history for this region and allows the total amount and rates of vertical crustal motion to be quantified. These are critical parameters in models of crustal dynamics that attempt to separate the neotectonic contribution to sealevel change from the eustatic and isostatic components. The age data obtained from the aforementioned submerged features (wave eroded unconformities and terraces, drowned spits, a partially isolated basin, and drowned fluvial features) in eastern Juan de Fuca Strait have allowed construction of an updated relative sealevel curve for the region (Fig. 52). This evidence is summarized below.

Dates from the aforementioned distinctive green silty-clay unit in a small basin near Whidbey Island indicate partial isolation of the basin at about 11,176 yr B.P. (calculated date;  $^{14}\text{C}$  equivalent) as sealevel dropped below the 55 m isobath during regression. Typical post-glacial sedimentation resumed during transgression at  $10,630 \pm 50$   $^{14}\text{C}$  yr B.P., probably when sealevel rose above the 55 m isobath again. At some time

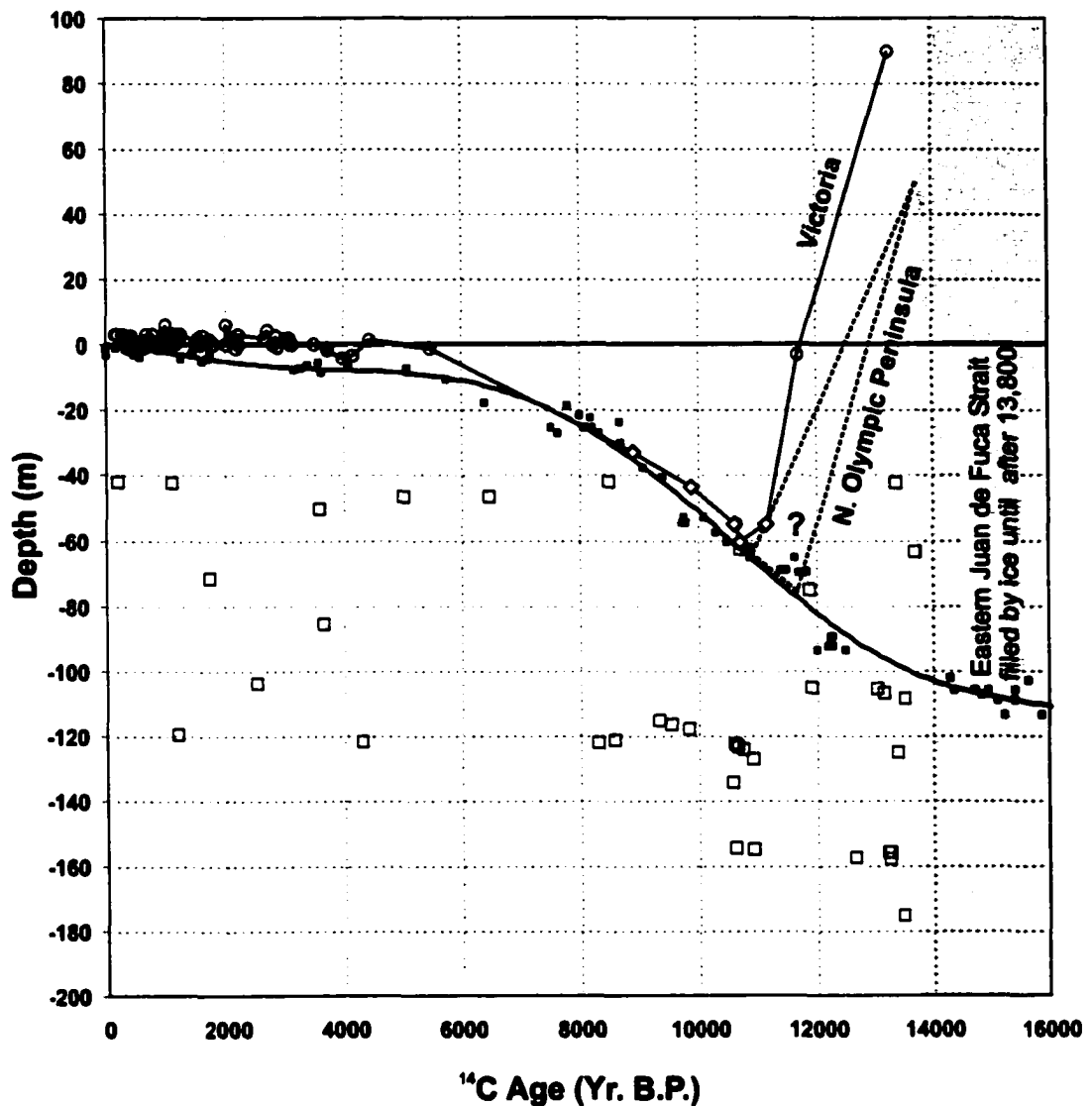


Figure 52. Relative sea-level curve for eastern Juan de Fuca Strait (heavy line), possible sea-level curves for the Olympic Peninsula (dashed heavy line; see discussion), and global eustatic sea-level curve (light line). Previously published data (o) are from Mathews, et al. (1970), Clague, et al. (1982), Linden and Schurrer (1988), and Hutchinson (1992). The global sea-level data (o) are from Barbados corals (Fairbanks, 1989). New dates from this study (□) are all from marine sediments. Five of these dates (o) are from evidence interpreted to closely constrain the depth of sealevel at these times (see text for discussion). The maximum observed lowstand of -60.4 m occurred at 10,720  $\pm$  60 yr B.P.

between these dates sealevel reached the low stand minimum. There are several unconformities on the banks that can be traced to depths of up to 90 m, but these likely formed at the erosional wave base, which may have been up to 25 m below the sea surface in the more open areas of the strait and, therefore, probably record a sealevel of around 65 m below the present. However, since the high stand along the Olympic peninsula was 50 m (it was less deeply buried by ice than Victoria was), and since its was deglaciated at roughly the same time as Victoria, the peninsula may have experienced its low stand somewhat earlier when eustatic sealevel was deeper, resulting in a deeper low stand than at Victoria. This assumes rebound occurred at the same rate.

The approaches to Esquimalt Harbour were probably sheltered from waves of the open strait, and the unconformity there is probably a more precise indication of the sealevel in which it formed. At this locality, core TUL97B-12 penetrated the unconformity at a depth of 60.4 m below the sea surface. Sediments just above the unconformity date to  $10,720 \pm 60$   $^{14}\text{C}$  yr B.P. This site may, therefore, record the minimum relative sealevel attained during regression. Some support for a low stand of around this magnitude comes from a post-glacial rebound model, which accounts for mantle viscosity and ice sheet thickness and extent (James *et al.*, 2000). Mantle viscosity was adjusted to produce a sealevel curve that fit the land-based data for southeastern Vancouver Island. This experiment predicted a 50 m low stand at 10,000 yr B.P. ( $^{14}\text{C}$  equivalent).

Additional dates from sediments just above the unconformity in the Esquimalt offshore area are:  $9880 \pm 50$   $^{14}\text{C}$  yr B.P. at 44.0 m below the sea surface in core TUL97B-02;  $8910 \pm 50$   $^{14}\text{C}$  yr B.P. at 32.8 m in core TUL99-15; and Linden and Schurrer (1998)

dated the unconformity at a depth of 55 m to between  $9670 \pm 140$   $^{14}\text{C}$  (RIDDL-265) and  $10,650 \pm 230$   $^{14}\text{C}$  yr B.P. (RIDDL-258). The later of these two dates agrees closely with the date of  $10,630 \pm 50$   $^{14}\text{C}$  yr B.P. from the isolated basin off Whidbey Island. Remaining control points on the sealevel curve (Fig. 52) are from Clague *et al.* (1982) and Hutchinson (1992). The global eustatic curve comes from Caribbean coral reef sites studied by Fairbanks (1989).

The relative sea-level curve (Fig. 52) shows a rapid regression after ice retreated, followed by a more gradual transgression toward the present. The form of this curve results from the net effect of opposing global eustatic sealevel rise and local isostatic rebound. The sealevel curve can be used to calculate rates of relative sealevel change and total crustal motion. Initially, isostatic rebound dominated, resulting in a rapid fall in relative sealevel at an average rate of 59.0 mm/yr (150.4 m in 2550 years). The global eustatic rise during this time was 37.3 m; therefore, the average rate of crustal uplift was 73.6 mm/yr (187.7 m in 2550 years). By around  $10,720 \pm 60$   $^{14}\text{C}$  yr B.P., isostatic rebound was complete and the eustatic component dominated, resulting in a more gradual rise in sealevel until the present. The average rate of relative sealevel rise during transgression was 5.6 mm/yr (60.4 m in 10720 years). The eustatic rise during this time was 61.4 m, giving an average rate of crustal uplift of less than 1 mm/yr (1 m in 10720 years). Figure 53 depicts stages of post-glacial sealevel in eastern Juan de Fuca Strait.

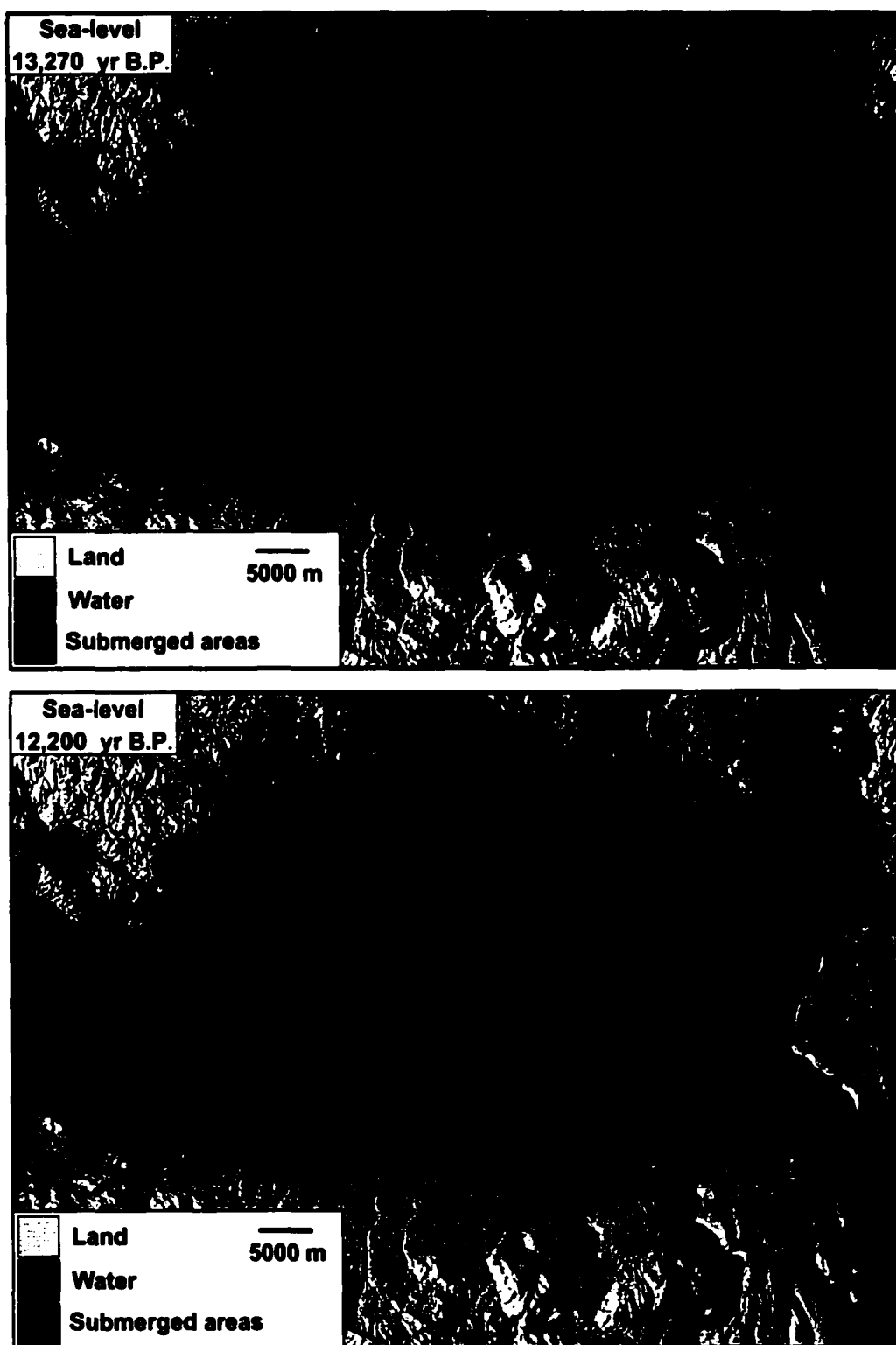


Figure 53. Schematic diagram showing areas flooded and emerged at the indicated stages during sealevel change that followed deglaciation (Fig. 47). High-stand limits are after Huntley et al. (2001); +90 m, and Dethier et al. (1995); +50 and +70 m. Low-stand limits are from this study.



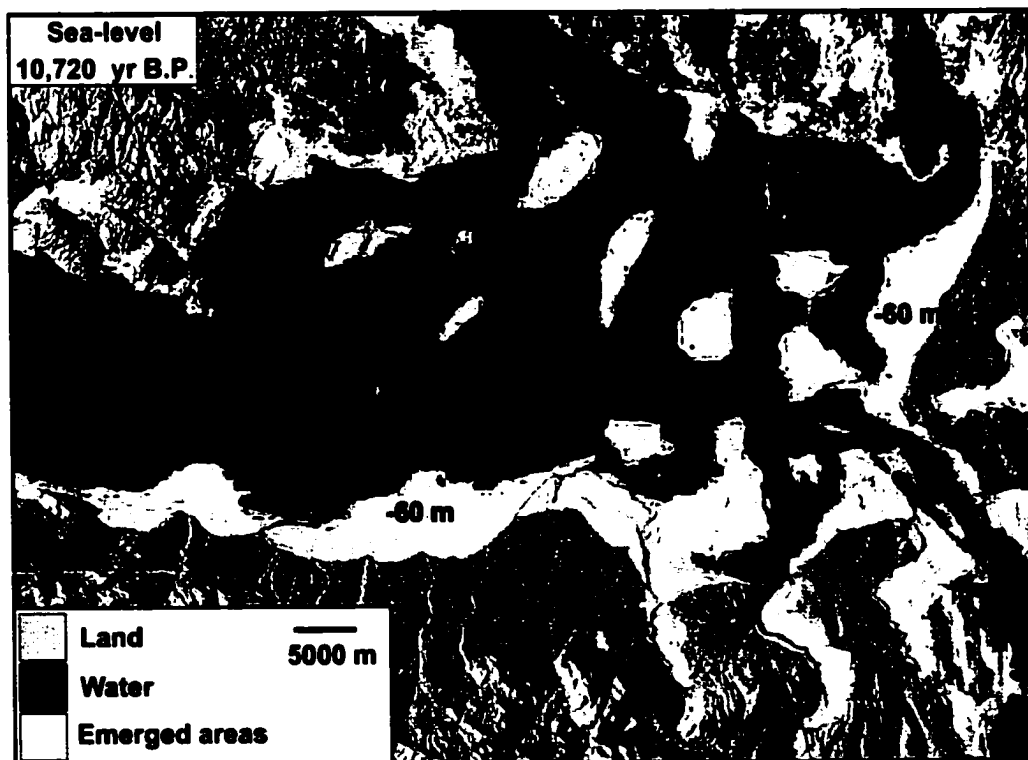
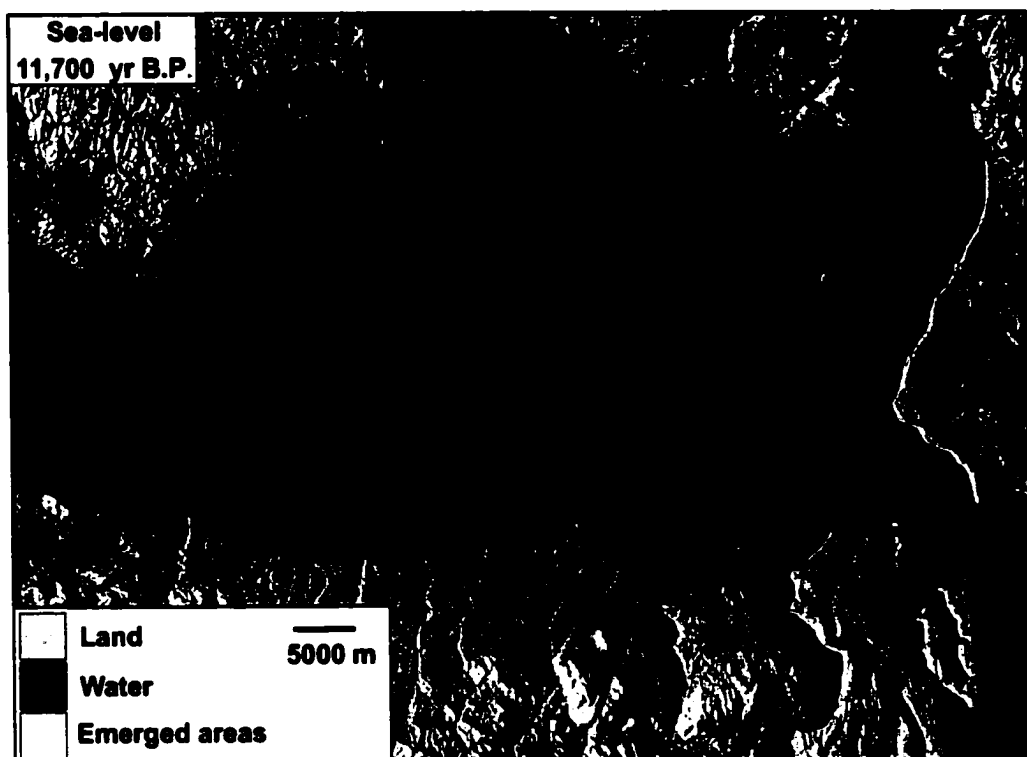


Figure 53. Continued.

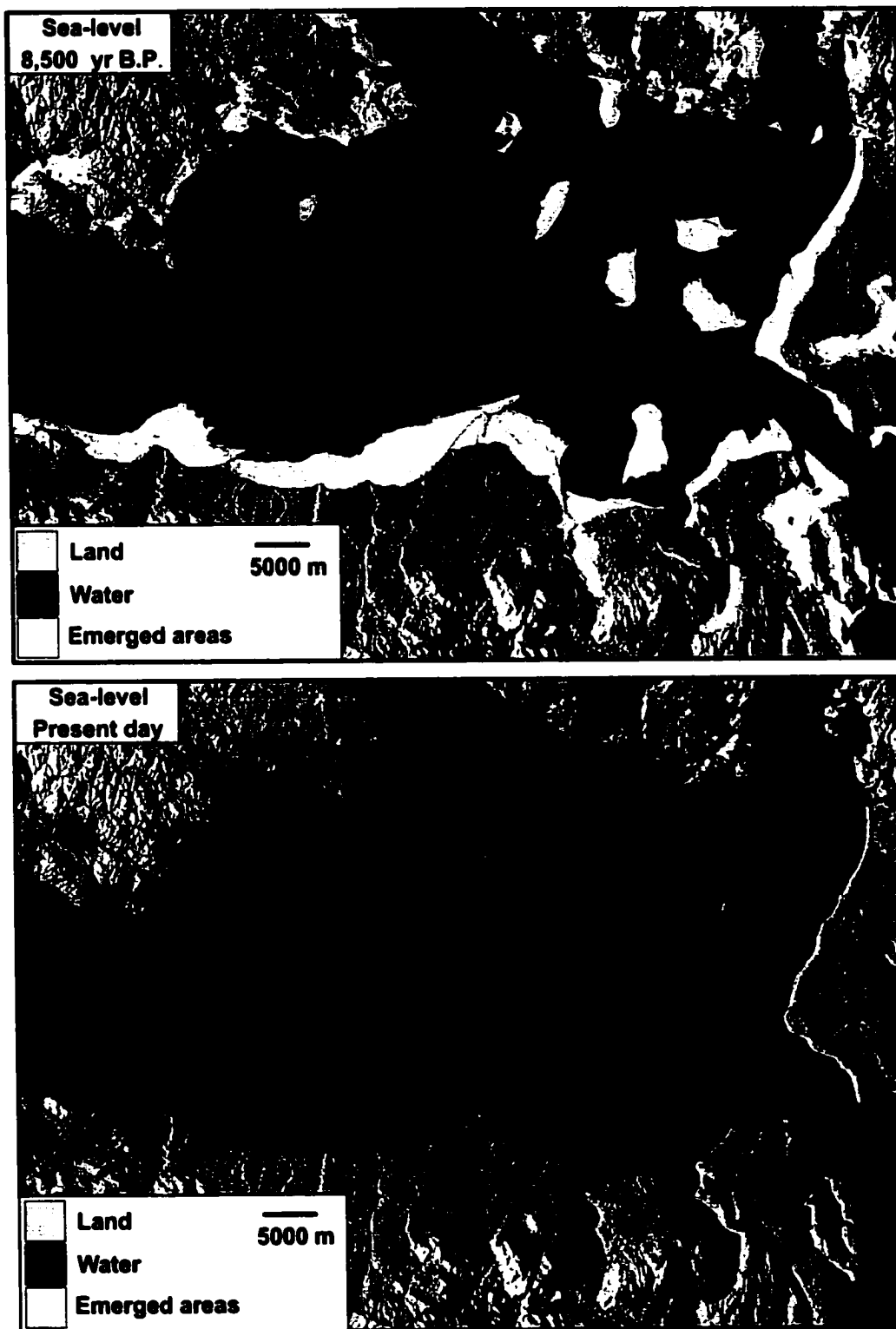


Figure 53. Continued.

## **CHAPTER VII**

### **CONCLUSIONS**

A combination of short sediment cores and high-resolution seismic-reflection data were used to identify and map four main surficial seismic-geologic units in eastern Juan de Fuca Strait (Fig. 44). In stratigraphic succession, from bottom to top (oldest to youngest), these units include bedrock (unit 1), ice-contact sediments (unit 2), glacial-marine sediments (unit 3), and post-glacial sediments (unit 4). Bedrock (unit 1) crops out only in nearshore environments off Vancouver Island and San Juan Island, and Ice-proximal sediments (unit 2) crop out on the numerous morainal banks. In other areas, these units are buried to variable depths by glacial-marine (unit 3) and post-glacial (unit 4) sediments.

A series of banks, including Middle and Hein Banks, and the offshore extension of Dungeness Spit, divides the strait into two major areas based on the dominant near-surface geologic units; post-glacial sediments (unit 4) are most common to the east and glacial-marine sediments (unit 3) to the west. This distribution resulted from a combination of: (1) burial of the glacial-marine sediments by post-glacial sediments that were supplied in greater abundance in the east by erosion of coastal bluffs and shallow banks; and (2), the main tidal stream, which is in the west, resulted in faster bottom currents that mobilized sediment into bedform fields and left winnowed deposits and surficial lags (units 3b and 4b).

Although there is relatively little modern input of sediment into the strait, erosion and reworking of older deposits occurs today. For example, along the Olympic Peninsula and western Whidbey Island, small rivers and erosion of coastal bluffs supply sediment to extensive beaches and barrier-spits. Even in deeper areas, currents are probably strong enough to move finer material exposed at the ocean floor. The abundant bedform fields associated with unit 4b and the drifts around some banks are evidence that sediments are being actively transported.

The layered and overall fining-upward sequence of glacial-marine sediments (unit 3a) suggests progression from an ice-proximal to ice-distal depositional environment. Radiocarbon dates between  $13,690 \pm 50$   $^{14}\text{C}$  yr B.P. and  $11,910 \pm 50$   $^{14}\text{C}$  yr B.P. (Table 1) indicate the sequence was deposited during the last phase of glacier retreat from the strait. Unit 3 is, therefore, correlated with the Everson (Capilano) deglacial sediments that occur throughout the region (Easterbrook, 1992). Overlying post-glacial sediments (unit 4) date between  $10,930 \pm 50$   $^{14}\text{C}$  yr B.P. and  $190 \pm 50$   $^{14}\text{C}$  yr B.P. (Table 1), but most dates are older than 8000 yr B.P., probably reflecting a more abundant supply of sediment in early post-glacial times.

Deglaciation began in the western strait shortly after 15,000 yr B.P. (Heusser, 1973) and the retreating ice margin had entered the eastern strait (the study area) by ~13,750 yr B.P. In less than 200 years it had receded to Whidbey Island, by around 13,600 yr B.P.; retreating at an average rate of around 475 m/year (Fig. 47). The thick deposits of ice-contact sediment (unit 2) found in morainal banks, however, suggests ice retreat was probably episodic, with times of rapid calving retreat separated by periods when retreat slowed when ice reached the banks.

Figure 52 shows a new sealevel curve for eastern Juan de Fuca Strait. Immediately following deglaciation, the crust was still isostatically depressed and sealevel reached its maximum high stand of 90 m at  $13,270 \pm 60$   $^{14}\text{C}$  yr B.P. (Huntley *et al.* 2001). Subsequent rapid isostatic rebound caused relative sealevel to fall, passing through the 0 m isobath by around  $11,700 \pm 170$   $^{14}\text{C}$  yr B.P. (Clague *et al.*, 1982), and by  $10,720 \pm 60$   $^{14}\text{C}$  yr B.P. sealevel had reached the deepest observed low stand of around 60.4 m below present. The low stand along the Olympic Peninsula may have been slightly deeper since the crust there probably recovered from its thinner ice load sooner, when eustatic sealevel was deeper, but only if it rebounded at the same rate as at Victoria (or faster). Figure 53 depicts stages of post-glacial sealevel in eastern Juan de Fuca Strait.

During this regressive phase, relative sealevel fell 150.4 m at an average rate of 59.0 mm/yr; meanwhile the eustatic sealevel rise was 37.3 m, yielding an average rate of crustal uplift of 73.6 mm/yr. By  $10,720 \pm 60$   $^{14}\text{C}$  yr B.P. most isostatic rebound was complete and eustatic rise took over as the dominant control on sealevel, resulting in a more gradual transgression. During transgression, relative sealevel rose 60.4 m at 5.6 mm/yr, whereas the eustatic rise was 61.4 m, giving an average rate of crustal uplift of less than 1 mm/yr.

## **REFERENCES**

- Alley, N. F., and Chatwin, S. C. 1979. Late Pleistocene history and geomorphology, southwestern Vancouver Island, British Columbia. *Canadian Journal of Earth Science*. 16: 1645-1657.
- Anderson, F. E. 1968. Seaward terminus of the Vashon continental glacier in the Strait of Juan de Fuca. *Marine Geology*. 6: 419-438.
- Archie, G. E. 1942. The electrical resistivity log as an aid in determining some reservoir characteristics. *Transactions AIME*. 146: 54-62.
- Armstrong, J. E. 1981. Post-Vashon Wisconsin glaciation, Fraser Lowland, British Columbia. *Geological Survey of Canada, Bulletin 322*. pp 34.
- Armstrong, J. E., Crandell, D. R., Easterbrook, D. J., and Noble, J. B. 1965. Late Pleistocene stratigraphy and chronology in southwestern British Columbia and northwestern Washington. *Geological Society of America Bulletin*. 76: 321-330.
- Armstrong, J. E., and Clague, J. J. 1977. Two major Wisconsin lithostratigraphic units in southwest British Columbia. *Canadian Journal of Earth Science*. 14: 1471-1480.
- Barrie, J. V., Bornhold, B. D., Conway, K. W., and Luternauer, J. L. 1991. Surficial geology of the northwestern Canadian continental shelf. *Continental Shelf Research*. 11: 701-715.
- Bard, E., Hamelin, B., and Fairbanks, R. G. 1990. U-Th ages obtained by mass spectrometry in corals from Barbados; sea level during the past 130,000 years. *Nature*. 346: 456-458.
- Barrie, J. V., and Bornhold, B. D. 1989. Surficial geology of Hecate Strait, British Columbia continental shelf. *Canadian Journal of Earth Science*. 26: 1241-1254.

- Barrie, J. V., Bornhold, B. D., Conway, K. W., and Luternauer, J. L. 1991. Surficial geology of the northwestern Canadian continental shelf. *Continental Shelf Research*. 11: 701-715.
- Blum, P. 1997. PP Handbook: A guide to the shipboard measurement of physical properties of deep-sea cores by the Ocean Drilling Program. ODP Technical Note 197. pp. 117.
- Blunt, D. J., Easterbrook, D. J., and Rutter, N. W., 1987, Chronology of Pleistocene sediments in the Puget Lowland, Washington: Washington Division of Geology and Earth Resources Bulletin. 77: 321-353.
- Booth, B. D., and Hallet, B. 1993. Channel networks carved by subglacial water: Observations and reconstruction in the eastern Puget Lowland of Washington. *Geological Society of America Bulletin*. 105: 671-683.
- Bornhold, B. D., Firth, J. V., Adamson, L. M., Baldauf, J. G., Blais, A. P., Elvert, M., Fox, P. J., Hebda, R., Kemp, A. E. S., Moran, K., Morford, J. H., Mosher, D. C., Prairie, Y. T., Russell, A. D., Schultheiss, P., Whiticar, M. J., Jonasson, B., Cowan, E., Fillipelli, G., Gieskes, Joris, Ishibashi, Junichiro, James, Rachael H., Jensen, G. D., McQuoid, M. R., Robert, F., Georgia L. 1998. Proceedings of the Ocean Drilling Program, Part A: Initial Reports, 169S: 11-61.
- Boyce, E. R. 1974. Deep sea drilling project procedures for shear strength measurement of clayey sediment using a modified Wykeham Farracne Laboratory vane apparatus. DSDP vol. 36.
- Brown, C. S., Meier, M. F., and Post, A. 1982. Calving speed of Alaska tidewater glaciers, with application to Columbia Glacier. USGS Professional Paper 1258-C.
- Burrough, P. A. 1986. Principles of Geographical Information Systems for Land Resource Assessment, Monographs on Soil and Resources Survey No. 12, Oxford Science Publications - Clarendon Press, Oxford. pp. 153.
- Clague, J. J. 1977. Quadra Sand: a study of the late Pleistocene geology and geomorphic history of coastal southwest British Columbia. *Geological Survey of Canada Paper* 77-17: pp. 24.

- Clague, J. J., Armstrong, J. E., Mathews, W. H. 1980. Advance of the late Wisconsin Cordilleran Ice Sheet in Southern British Columbia since 22,000. *Quaternary Research*. 13: 322-326.
- Clague, J. J. 1981. Late Quaternary geology and geochronology of British Columbia. Part 2. Summary and discussion of radiocarbon-dated Quaternary history; Geological Survey of Canada, Paper 80-35. pp. 41
- Clague, J. J., Harper, J. R., Hebda, R. J., Howes, D. E. 1982. Late Quaternary sealevels and crustal movements, coastal British Columbia. *Canadian Journal of Science*. 19: 597-618.
- Clague, J. J., Saunderson, I. R., and Roberts, M. C. 1988. Ice-free conditions in southwestern British Columbia at 16 000 years BP. *Canadian Journal of Earth Science*. 25: 938-941.
- Cowan, E. A., 2001. Late Pleistocene glaciomarine record in Saanich Inlet, British Columbia, Canada. In Bornhold, B. D., and Kemp, A. E. S. (eds.), *Late Quaternary Sedimentation in Saanich Inlet, British Columbia, Canada—Ocean Drilling Program Leg 169S*. Marine Geology. 174: 43-57.
- Davies, T. A., Bell, T., Cooper, A. K., Josenhans, H., Ployak, L., Solheim, A., Stoker, M.S., and Stravers, J. A., 1997. Glaciated continental margins: an atlas of acoustic images. Chapman and Hall, London. pp. 315
- Dearing, J. A. 1994. Environmental Magnetic Susceptibility: using the Bartington MS2 System, Chi Publishing, Kenilworth. pp. 104.
- Dethier, D. P., Pessl, F. Jr., Keuler, R. F., Balzarini, M. A., Pevear, D. R. 1995. Late Wisconsinan glaciomarine deposition and isostatic rebound, northern Puget Lowland, Washington. *Geological Society of America Bulletin*. 107: 1288-1303.
- Domack, E. W. 1983. Facies of late Pleistocene glacial-marine sediments on Whidbey Island, Washington: An isostatic glacial-marine sequence. in Molnia, B. F., ed. *Glacial-marine Sedimentation*. New York, Plenum. pp. 335-570.



Easterbrook, D. J. 1992. Advance and retreat of Cordilleran ice sheets in Washington, U. S. A. *Geographie Physique et Quaternaire*. 46: 51-68.

Easterbrook, D. J., 1994, Chronology of pre-late Wisconsin Pleistocene sediments in the Puget Lowland, Washington, in Lasmanis, R., and Cheney, E. S., *eds.*, *Regional geology of Washington State: Washington Division of Geology and Earth Resources Bulletin*. 80: 191-206.

Fairbanks, R. G. 1989. A 17,000-year glacio-eustatic sealevel record: influence of glacial melting rates on the Younger Dryas event and deep-ocean circulation. *Nature*. 342: 637-642.

Forbes, D. L., Shaw, J., and Taylor, R. B. 1995. Differential preservation of coastal structures on paraglacial shelves: Holocene deposits of southeastern Canada. *Marine Geology*. 124: 187-201.

Herzer, R. H., and Bornhold, B. D. 1982. Glaciation and post-glacial history of the continental shelf off southwestern Vancouver Island, British Columbia. *Marine Geology*. 48: 285-319.

Heusser, C. J. 1973. Environmental sequence following the Fraser advance of the Juan de Fuca lobe, Washington. *Quaternary Research*. 3: 284-306.

Hicock, S. R., Dreimanis, A., and Broster, B. E. 1980. Submarine flow tills at Victoria, British Columbia. *Canadian Journal of Earth Sciences*. 18: 71-80.

Hicock, S. R., Hebda, R. J., and Armstrong, J. E. 1982. Lag of Fraser glacial maximum in the Pacific Northwest: Pollen and macrofossil evidence from western Fraser Lowland, British Columbia. *Canadian Journal of Earth Science*. 19: 2288-2896.

Hughes Clarke, J. E. 1998a. Detecting small seabed targets using high frequency multibeam sonar: *Sea Technology*. 39: 87-90.

- Hughes Clarke, J. E. 1998b. The effect of fine scale seabed morphology and texture on the fidelity of SWATH bathymetric sounding data: Proceedings Canadian Hydrographic Conference 1998, Victoria. pp. 168-181.
- Hughes Clarke, J. E., Gardner, J. V., Torresan, M. and Mayer, L. 1998c. The limits of spatial resolution achievable using a 30kHz multibeam sonar: model predictions and field results. IEEE Oceans 98, Proceedings (1998) 3: 1823-1827.
- Hughes Clarke, J. E., Mayer, L. A. and Wells, D. E., 1996, Shallow-water imaging multibeam sonars: A new tool for investigating seafloor processes in the coastal zone and on the continental shelf: Marine Geophysical Research. 18: 607-629.
- Huntley, D. H., Bobrowsky, P. T., and Clague, J. J. 2001. Surficial geology, stratigraphy and geomorphology of the Saanich Inlet area, southeastern Vancouver Island, British Columbia. In Bornhold, B. D., and Kemp, A. E. S. (Eds.). Late Quaternary Sedimentation in Saanich Inlet, British Columbia, Canada—Ocean Drilling Program Leg 169S, Marine Geology. 174: 27-41.
- Hutchins, R. W., McKeown, D. L., and King, L. H., 1976, A deep-tow high resolution seismic system for continental shelf mapping: Geoscience Canada. 3: 95-100.
- Hutchinson, I. 1992. Holocene sealevel change in the Pacific Northwest: A catalogue of radiocarbon dates and an atlas of regional sealevel curves. Institute of Quaternary Research, Simon Fraser University, discussion paper 1. pp. 99.
- IKB Technologies. 1997. Velocimeter Manual: IKD Velocimeter test unit V2.0. Written communication IKB Technologies, 1997. pp. 23.
- James, T. S., Clague, J. T., Wang, K, Hutchinson, I. 2000. Postglacial rebound at the northern Cascadia subduction zone. Quaternary Science Reviews. 19: 1527-1541.
- Jensen, J. B., and Stecher, O. 1992. Paraglacial barrier-lagoon development in the Late Pleistocene Baltic Ice Lake, southwestern Baltic. Marine Geology. 107: 81-101.
- Johnson, S. Y., Rhea, S. B., Dadisman, S. V., and Mosher, D. C., Blakely, R. J., Childs, J. R. 2001a. Active tectonics of the Devils Mountain Fault and related

structures, northern Puget Lowland and eastern Strait of Juan de Fuca region, Pacific Northwest. U. S. Geological Survey Professional Paper, Report: P1643. pp 45.

- Johnson, S. Y. and Mosher, D. C. 2001b. Regional geology of the eastern Juan de Fuca Strait, in: Mosher, D. C. and Johnson, S. Y. (Eds.), Rathwell, G. J., Kung, R. B., and Rhea, S. B. (Compilers), Neotectonics of the eastern Juan de Fuca Strait; a digital geological and geophysical atlas. Geological Survey of Canada Open File Report D3931.
- Johnson, S. Y., Rhea, S. B., Dadisman, S. V., and Mosher, D. C. 2001c. Depth to the base-of-Quaternary in the eastern Juan de Fuca Strait region, in: Mosher, D. C. and Johnson, S. Y. (Eds.), Rathwell, G. J., Kung, R. B., And Rhea, S. B. (Compilers), Neotectonics of the eastern Juan de Fuca Strait; a digital geological and geophysical atlas. Geological Survey of Canada Open File Report D3931.
- Josenhans, H., Fedje, D., Pienitz, R., and Southon, J. 1997. Early humans and rapidly changing Holocene sea levels in the Queen Charlotte Islands – Hecate Strait, British Columbia, Canada. *Science*. 277: 71-74.
- Komar, P. D., and Miller, M. C. 1975. The initiation of oscillatory ripple marks and the development of plane-bed at high shear stresses under waves. *Journal of Sedimentary Petrology*. 45: 697-703.
- Linden, R. H., and Schurrer, P. J. 1988. Sediment characteristics and sealevel history of Royal Roads Anchorage, Victoria, British Columbia. *Canadian Journal of Earth Science*. 25: 1800-1810.
- Lonne, I. 1995. Sedimentary facies and depositional architecture of ice-contact glaciomarine systems. *Sedimentary Geology*. 98: 13-43.
- Luternauer, J. L., Conway, K. W., Clauge, J. J., Blaise, B. 1989. Late Quaternary geology and geochronology of the central shelf of western Canada. *Marine Geology*. 89: 57-68.
- Mathews, W. H., Fyles, J. G., Nasmit, H. W. 1970. Post-glacial crustal movements in southwestern British Columbia and adjacent Washington state. *Canadian Journal of Earth Science*. 7: 690-702.

- Mayers, I. R., and Bennet, L. C. Jr. 1973. Geology of the Strait of Juan de Fuca. *Marine Geology*. 15: 89-117.
- Mosher, D. C., and Bornhold, B., 1995. Geophysical Survey of Victoria Harbour Approaches. Geological Survey of Canada Open File Report No. 3211. pp. 25
- Mosher, D. C., and Hamilton, T. S. 1998. Morphology, structure, and stratigraphy of the offshore Fraser Delta and adjacent Strait of Georgia. *Bulletin - Geological Survey of Canada*, Report: 525. pp. 147-160.
- Mosher, D. C., and Moran, K. 2001. Post-glacial evolution of Saanich Inlet, British Columbia: results of physical property and seismic-reflection stratigraphic analysis. In Bornhold, B. D., and Kemp, A. E. S. (Eds.), *Late Quaternary Sedimentation in Saanich Inlet, British Columbia, Canada—Ocean Drilling Program Leg 169S*. *Marine Geology*. 174: 59-77.
- Mosher, D. C., Hewitt, A. T., Hamilton, T. S. 1997. Neotectonic Activity in the Eastern Juan de Fuca Strait: Quantitative Seismic-reflection Mapping. AGU annual Meeting, December, 1997.
- Mosher, D. C., MacDonald, R., Hewitt, A. T., and Hill, W. T., 1998. Small airgun arrays for high resolution geophysical surveying. *Current Research, 1998A*, Geological Survey of Canada.
- Mosher, D. C. and Thomson, R. E., 2000. Massive submarine sand dunes in the eastern Juan de Fuca Strait, British Columbia. *Marine Sand wave Dynamics, International Workshop, March 23-24, 2000. University of Lille 1, France, Proceedings*, Trentesaux, A., and Garlan, T. (eds.). pp. 131-142.
- Mosher, D. C. and Johnson, S. Y. (eds.), 2001. Neotectonics of the eastern Juan de Fuca Strait; a digital geological and geophysical atlas. Geological Survey of Canada Open File Report D3931.
- Mullineaux, D. R., Waldron, H. H., and Rubin, M. 1965. Stratigraphy and chronology of late interglacial and early Vashon glacial time in the Seattle area, Washington. *United States Geological Survey, Bulletin* 1194-0.

- Oldale, R. N. A drowned Holocene barrier spit off Cape Ann, Massachusetts. *Geology*. 13: 375-377.
- Porter, S. C., and Swanson, T. W. 1998. Radiocarbon age constraints on rates of advance and retreat of the Puget Lobe of the Cordilleran Ice Sheet during the last glaciation. *Quaternary Research*. 50: 205-213.
- Powell, R. D. and Molnia, B. F. 1989. Glaciomarine sedimentary processes, facies and morphology of the south-southeast Alaska shelf and fjords. *in* Powell, R. D. and Elverhoi, A. *eds*. *Modern Glaciomarine Environments: Glacial and Marine Controls of modern lithofacies and biofacies*. *Marine Geology*. 85: 359-390.
- Rampino, M. R., and Saunders, J. E. 1981. Evolution of barrier islands of southern Long Island, New York. 1981. *Sedimentology*. 28: 37-47.
- Robinson, S. W., and Thompson, G. 1981. Radiocarbon corrections for marine shell dates with application to southern Pacific Northwest Coast prehistory. *Syesis*. 14: 45-57.
- Roy, P. S., Cowell, P. J., Ferland, M. A., and Thom, B. G. 1994. Wave dominated coasts. *in* Carter, R. W. G. and Woodroffe, C. D. *Coastal Evolution*. Cambridge. pp. 517.
- Simpkin, P. G., and Davis, A. 1993. For seismic profiling in very shallow water, a novel receiver. *Sea Technology*, September, 1993, 21-28.
- Stokes, G. G. 1891. *Mathematical and Physical Paper III*. Cambridge University Press.
- Stuiver, M., and Polach, H. A. 1997. Discussion: reporting of C-14 data. *Radiocarbon* 19: 355-363.
- Stuiver, M., Reimer, P. J., Bard, E., Beck, J. W., Burr, G. S., Hughen, K. A., Kromer, B., McCormac, G., van der Plicht, J., and Spurk, M. 1998. INTCAL98 Radiocarbon Age Calibration, 24,000-0 cal BP. *Radiocarbon*. 40: 1041-1084.

- Swift, D. J. 1975. Tidal sand ridges and shoal-retreat massifs. *Marine Geology*. 18: 105-114.
- Sylvitski, J. P. M. 1992. Glaciomarine environments in Canada: an overview. *Canadian Journal of Earth Science*. 30: 354-371.
- Thomson, R. E. 1981. Oceanography of the British Columbia Coast. Special publication of Fisheries and Aquatic Sciences 56. pp. 291
- Thorson, R. M. 1980. Ice-sheet glaciation of the Puget Lowland, Washington, during the Vashon Stade (Late Pleistocene). *Quaternary Research*. 13: 303-321.
- Thorson, R. M. 1989. Glacio-isostatic response of the Puget Sound area, Washington. *Geological Society of America Bulletin*. 101: 1163-1174.
- Thorson, R. M. 1996. Earthquake recurrence and glacial loading in western Washington. *Geological Society of America Bulletin*. 108: 1182-1191.
- United States Army Corps of Engineers. 1976. Ediz Hook beach erosion control. General Design Memorandum. 21: pp. 14.
- Wellner, R. W., Ashley, G. M., Sheridan, R. E. 1993. Seismic stratigraphic evidence for a submerged middle Wisconsin barrier; implications for sealevel history. *Geology*. 21: 109-112.
- Wyllie, M. R. J., Gregory, A. R., and Gardner, L. W. 1956. Elastic wave velocities in heterogeneous and porous media. *Geophysics*. 21: 41-70.

## **APPENDIX**

### **ADDITIONAL PHYSICAL PROPERTIES BACKGROUND**

#### **Grain-size**

Grain-size is often determined by a combination of methods, including settling tube, X-ray absorption, and sieving. For large grains (>few mm), which settle very quickly, different sieve mesh sizes are used to separate the sample into different size ranges. For smaller grains settling methods are preferable. These methods are based on the fact that the measured terminal velocity of a spherical particle settling through a viscous medium can be related to the size of the particle by Stokes' law (Stokes, 1891):

$$D^2 = 18(h/t)\eta / (\rho_s - \rho_l)g$$

Where, (D) is grain diameter, (h) is the distance the particle falls in a given time interval (t), and ( $\eta$ ) is viscosity of the medium through which the grains are settling. A settling tube is used for medium sized grains (typically 63  $\mu\text{m}$  to 2 mm), and by measuring the weight of sediment settled as a function of time, a grain-size distribution curve is produced. X-ray absorption techniques are used for the finest grains (<63  $\mu\text{m}$ ) which settle very slowly. A beam of X-rays is used to measure particle concentration in terms of the transmitted intensity through the suspended sample relative to the particle-free

suspending fluid. The rate of change in particulate concentration (density of the fluid) as particles settle can be related to the grain-size distribution.

### **Magnetic Susceptibility**

Magnetic susceptibility is a measure of the susceptibility of a material to magnetization in an applied magnetic field (Dearing, 1994; summarized in Blum, 1997). It is expressed as the ratio of the induced magnetization versus the applied magnetic field:

$$k = I/H$$

where (k) is the magnetic susceptibility, (I) is the measured intensity of magnetization, and (H) is the intensity of the applied magnetic field. Magnetic susceptibility is a unitless value usually expressed as  $10^{-6}$  SI units. The value can be either positive or negative, and is largely a function of the amount and type of ferrous minerals present in the sample. Positive values imply that the induced magnetic field is in the same direction as the applied field, and negative values imply that the induced field is in the opposite direction as the applied field. The instrument must be calibrated to account for the background magnetic field, by running blank measurements in air, water, or materials of known susceptibility (Blum, 1997).

### **Resistivity**

Resistivity, or the inverse of conductivity, is a measure of a sediments resistance to the passage of an electric current (Archie, 1942):



$$R_o = V/I C$$

where, ( $R_o$ ) is resistivity in  $\Omega m$  (ohm-meters). In practice, voltage ( $V$ ) and current ( $I$ ) are measured, and ( $C$ ) is a cell constant determined from calibration in standard sea water (Salinity = 0.035). The resistivity of standard seawater is:

$$R_w = [2.803 + 0.0996 (T)]^{-1}$$

$$= 0.209 \Omega m \text{ at } T=20^\circ C$$

where, ( $R_w$ ) is the resistivity of the standard sea water and ( $T$ ) is temperature. The cell constant is then:

$$C = I R_w/V$$

Resistivity is sensitive to temperature, therefore, sample temperature is taken at the same time as the resistivity measurement, and the corrected sample resistivity is then:

$$R_s = R_o[1 + 0.025 (T-20)]$$

Resistivity is sometimes reported as the *resistivity formation factor*, which is the ratio of the sample resistivity ( $R_s$ ) to the resistivity of standard sea water ( $R_w$ ):

$$F = R_s/R_w$$

Since conductivity of pore waters of marine sediments is about 10 orders of magnitude greater than that of the sediment grains, resistivity is essentially a function of porosity (Archie, 1942; Boyce, 1968):

$$F = a\Phi^{-m}$$

where (a) is a proportionality constant and (m) is the geometric factor, which is a constant that is a function of a particular lithology, and ( $\Phi$ ) is the fractional porosity (determined from index property measurements). If resistivity and porosity data are both available from the same sediment sample, then an exponential fit to a plot of formation factor versus porosity can be used to estimate the (a) and (m) parameters:

$$\text{Log } F = \text{log } a - m (\text{log } \Phi)$$

$$\Phi = 10^{[(\text{log } F - \text{log } a)/-m]}$$

### **Velocity**

The velocity of sound in sediment, or acoustic compressional-wave (P-wave) velocity, can be determined by the time it takes for sound to travel between two ultrasonic transducers (reviewed in Blum, 1997; IKB Technologies, 1997):

$$V_0 = d/t$$

where, ( $V_0$ ) is the measured velocity, ( $d$ ) is the distance between transducers (usually a few cm), and ( $t$ ) is the time taken for the signal to pass between the transducers. The instrument, called a velocimeter, is calibrated in distilled water at regular intervals. The measured sediment velocities are corrected for temperature and porosity as follows (Wyllie *et al.*, 1956):

$$V_s = [V_0^{-1} + (\Phi/V_i - \Phi/V_w)]^{-1}$$

where ( $V_s$ ) is the corrected sample velocity, ( $V_0$ ) is the measured velocity, ( $\Phi$ ) is the sediment porosity, ( $V_i$ ) is the velocity of standard seawater at *in situ* (i.e. ocean floor) temperature, and ( $V_w$ ) is the velocity of standard seawater at core temperature. ( $V_i$ ) and ( $V_w$ ) are determined from the empirically derived equation (Wyllie *et al.*, 1956):

$$V = 1449.22 + 4.6233(T) - 0.054585(T^2) + 0.0002822(T^3) - 0.000000507(T^4)$$

### **Shear Strength**

Undrained shear strength is a measure of the sediments resistance to shearing stress. In the miniature vane test, stress is applied through a vane (probe) that is inserted in the sediment. A motorized instrument is used to apply stress by turning a dial connected to the vane through a calibrated spring. A second dial connected directly to the vane begins to turn as the sediment fails, and therefore, measures the strain. The instrument returns values for the degrees of stress rotation and degrees of strain rotation. Shear strength is

determined by the maximum value of strain rotation subtracted from stress rotation via the following relationship (Boyce, 1974; Blum, 1997).

$$S = (X/s) K$$

where, (X) is the degrees of stress rotation minus the degrees of strain rotation, (s) is a spring constant, and (K) is a vane constant. Values for these constants are usually supplied by the manufacturer. The vane constant is a function of the shearing area determined by the size of the vane, and the spring constant is a function of the strength of the spring, which is determined by its response to a known force.

### **Index Properties**

Measurements of wet bulk density and dry bulk density are used as the basis for calculating other properties such as porosity, water content, and grain density (reviewed in Blum, 1997). Wet bulk density is the mass of an undried sediment sample per unit volume:

$$\rho_w = M_w / V$$

where, ( $M_w$ ) is the wet sample mass and (V) is the sample volume. Dry bulk density is the mass of a dried sediment sample per unit volume:

$$\rho_d = M_d / V$$

where, ( $M_d$ ) is the dry sample mass. Porosity is the volume of pore spaces in the sample, reported as a percentage value of the total volume. It is assumed marine sediments have their pore spaces filled with salt water, and therefore, porosity calculations require a salinity correction:

$$\Phi = (M_w - M_d) / [(1-s) \rho_p V]$$

where, ( $\Phi$ ) is the sediment porosity, ( $s$ ) is the salinity, and ( $\rho_p$ ) is the density of the pore water. If the pore water is assumed to be standard seawater then salinity ( $s$ ) and density ( $\rho_p$ ) are 0.035 and 1.024 g/cm<sup>3</sup>, respectively. Water content is the mass of pore water in a sample, and is expressed as a percentage of the total wet bulk mass.

$$W = (M_w - M_d) / M_w(1-s)$$

where, ( $W$ ) is the percent water content. Grain density is the average density of the constituent particles in the sample:

$$\rho_g = [M_w - (M_w - M_d)/(1-s)] / [V - (M_w - M_d)/(1-s) \rho_p]$$

where, ( $\rho_g$ ) is the grain density, and other parameters are as above.